



TUM SCHOOL OF LIFE SCIENCES

TECHNISCHE UNIVERSITÄT MÜNCHEN

PhD Dissertation

**Rain Microstructure in Europe under the
Influence of Large-Scale Weather Types**

Wael Ghada





TECHNISCHE UNIVERSITÄT MÜNCHEN

Wissenschaftszentrum Weihenstephan für Ernährung, Landnutzung und
Umwelt



Professur für Ökologiklimatologie

**Rain Microstructure in Europe under the Influence of
Large-Scale Weather Types**

Wael Ghada

Vollständiger Abdruck der von der Fakultät Wissenschaftszentrum Weihenstephan für Ernährung, Landnutzung und Umwelt der Technischen Universität München zur Erlangung des akademischen Grades eines

Doktor-Ingenieurs (Dr.-Ing.)

genehmigten Dissertation.

Vorsitzender:

Prof. Dr. Axel Göttlein

Prüfer der Dissertation:

1. Prof. Dr. Annette Menzel
2. Prof. Dr.-Ing. Markus Disse
3. Prof. Dr. Harald Kunstmann

Die Dissertation wurde am 27.01.2020 bei der Technischen Universität München eingereicht und durch die Fakultät Wissenschaftszentrum Weihenstephan für Ernährung, Landnutzung und Umwelt am 31.08.2020 angenommen.

Acknowledgments

As this journey approaches its end, I stop to enjoy this moment, look deep into my heart, and breathe in all the memories of three years and a half, try to condense them into a few lines of appreciation for those who were beside me literally and spiritually, those who made it possible, easier, exciting and completely worth it;

To my dear supervisor, Prof. Menzel, I cherish every lesson you taught me on a professional and a personal level. Thank you for accepting that naïve student into your team, for providing him with all the support needed to improve and grow.

To my dear mentor, Prof. Disse, our brief but meaningful encounters were essential to remind me what it means to be an engineer, and to keep that responsibility in my mind.

To Prof. Bech in the University of Barcelona and his team at the Department of Applied Physics and Meteorology, Enric, Maria, Patricia for the nice and productive research stay, and to Anna who made it all possible.

To Prof. Hamann, the one who showed me practically how much more there is still to learn.

To the DAAD who provided me not only with financial support, but with the opportunity for growth and experiencing Germany for more than six years.

To Nicole, Christian, Marvin, Allan, and Nick, you welcomed me since the beginning and provided me with practical, day to day experiences which are not available to read in a book. Thank you for that, and many thanks to Brigitte, the person able to find a solution when no one else can help.

To all the current and the previous members of the scientific team who were or still are a part of life at this department, those with whom I shared greetings in the morning, smiles, coffee breaks, mensa food, stress, small setbacks and successes, small projects, plans which may never come to happen, and many many stories; Sophie, Alissa, Christina, Lydia (sorry for the noisy bell), Gourav, Upasana, Eli, Caryl, Fanxiang, Lars, Stefan H, Michael M, Hannes, and Tobias. Dear Stephan J, thank you for putting up with a noisy office-mate like me. Dear Nils, my first true German friend. Mr. Ye, the wise colleague, the young mentor in this team, I am “predicting” a great future for you ahead. Homa, my little sister and partner in crime, morning coffee, thesis journey, and many heartfelt laughs. You and your Mr. Ali were and will always be my family in Munich.

To all the volunteers at the "Syrian Researchers", especially my fellows and future scientists at the department of Natural and Environmental Science, those who donate their time and effort to give something meaningful to their community.

To the Damascus University family at the Faculty of Civil Engineering, my first mentor, Dr Tajjar, and all the engineers at the Department of Water Engineering, those carrying the responsibility of day to day teaching despite the challenges and the hard times.

To the SRM family, those who are the change they want to see in this world.

To the ones who were my family in Freising, who made me look forward to the weekend for a breakfast or a football game, Ankit, Inge, Toni and Paul.

To the Arab gang, who brought a piece of home into every meeting and warm conversation, Ata, Omar and Osama.

To my old friends who are only one phone call away so we can continue our conversation from last year, Kinan, Muhannad, Ghadeer, and Rabea.

To Ahmed, my best friend, the one who knows all the secrets, the one who makes the best food and the worst jokes, the one to turn to for honest advice and inspiration in every aspect.

And finally to my family, my father who ignites my desire to become a better person. To my mother, the pure love in her smile, voice and eyes. To my siblings, Olla, Roula, Noah and Majd, and the new family members Loor, Ghassan and Leem. Being away from you was the hardest part, but meeting you again motivated me especially in the last few months.

Abstract

A better understanding of rain microstructure variation enables further improvements of the quantitative estimation of rain intensity by remote sensing instruments. This task is of tremendous importance due to the various applications relevant to water supply for humans and natural ecosystems in addition to flood forecasting. Rain microstructure is a product of many processes that influence the shape, size and velocity of drops before reaching the ground. For example, the two rain types (stratiform and convective) are characterized by distinct rain microstructure. This difference has been widely addressed. However, the influence of large scale weather circulations (also types or patterns – hereafter WTs) on rain microstructure has not been sufficiently considered. Especially for central Europe, available studies fail to consider the combined effect of rain type and WTs on rain microstructure.

In this PhD study, data from various measuring devices on the ground were used to demonstrate the influence of WTs, especially the flow direction component, on precipitation properties in central Europe. This involved demonstrating how the diurnal cycle of precipitation, the proportion of convective rain, and the rain microstructure vary with WTs. For this purpose, it was critical to assess and improve the rain type classification methods. Advanced predictive models using machine learning have been constructed for better classification performance. Finally, the potential to improve the rain intensity retrieval algorithm $Z = AR^b$ was demonstrated by assigning A and b values for each combination of weather type and rain type.

The key findings of this study demonstrate that southern circulations in central Europe intensify convection, leading to a higher proportion of convective rain amount and duration. Additionally, southern circulations are associated with a higher afternoon precipitation peak in the diurnal cycle. On the contrary, northern circulations intensify radiative cooling and suppress convection, resulting in a higher morning precipitation peak. Western circulations represent the dominant source of humidity and contribute the highest amount of precipitation. Rain under western circulations is characterized by the highest intensity and the largest drops. Eastern circulations contribute the least to the precipitation amount and duration, and are associated with small drops, low intensities, and high drop concentrations. These distinct properties in rain microstructures lead to significantly different values of the A and b, the rain intensity retrieval parameters.

Zusammenfassung

Ein besseres Verständnis der Variation der Regenmikrostruktur ermöglicht weitere Verbesserungen der quantitativen Abschätzung der Regenintensität durch Fernerkundungsinstrumente. Diese Aufgabe ist aufgrund der verschiedenen Anwendungen, die neben der Hochwasservorhersage auch für die Wasserversorgung von Menschen und natürlichen Ökosystemen relevant sind, von größter Bedeutung. Die Regenmikrostruktur entsteht in unterschiedlichen atmosphärischen Prozessen, die die Form, Größe und Geschwindigkeit der Tropfen beeinflussen, bevor sie den Bodenerreichen. So ist allgemein bekannt, dass die beiden Regenarten (stratiform und konvektiv) durch ihre ausgeprägte Regenmikrostruktur unterschieden werden kann. Der Einfluss von Großwetterlagen (im Folgenden WTs genannt) auf die Regenmikrostruktur ist bisher jedoch nicht ausreichend berücksichtigt worden. Insbesondere für Mitteleuropa wird in den bisherigen Studien der kombinierte Einfluss von Regentypus und WTs auf die Regenmikrostruktur nicht berücksichtigt.

In dieser Doktorarbeit wurden Daten von verschiedenen Messgeräten am Boden verwendet, um den Einfluss von WTs, insbesondere der großräumigen Anströmrichtung, auf die Niederschlagseigenschaften in Mitteleuropa zu demonstrieren. Dabei wurde aufgezeigt, wie der Tagesgang des Niederschlags, der Anteil des konvektiven Regens und der Regenmikrostruktur mit den unterschiedlichen WTs variieren. Hierzu wurden Methoden zur Klassifizierung der Regenarten bewertet und zu verbessert. Um die Klassifizierungsleistung zu verbessern wurden fortgeschrittene Vorhersagemodelle unter Verwendung des maschinellen Lernens erstellt. Abschließend wurde das Potential zur Verbesserung des Regenradaralgorithmus $Z = AR^b$ zur Bestimmung der Regenintensität demonstriert, indem für jede Kombination von Großwetter- und Regentypus separate A- und b-Werte zugewiesen wurden.

Die wichtigsten Ergebnisse dieser Studie zeigen, dass die südlichen Zirkulationen in Mitteleuropa die Konvektion intensivieren, was zu einem höheren Anteil an konvektiver Regenmenge und -dauer führt. Zusätzlich sind die südlichen Zirkulationen mit einem höheren Nachmittagsniederschlagsmaximum im Tageszyklus verbunden. Im Gegensatz dazu verstärken die nördlichen Zirkulationen die Strahlungsabkühlung und unterdrücken die Konvektion, was zu einer höheren morgendlichen Niederschlagspeak führt. Westliche Zirkulationen stellen die dominierende Feuchtigkeitsquelle dar und tragen die höchste Niederschlagsmenge bei. Der Regen aus westlichen Zirkulationen ist durch die höchste Intensität und die größten Tropfen gekennzeichnet. Östliche Zirkulationen tragen am wenigsten zur Niederschlagsmenge und -dauer bei und sind mit kleinen Tropfen, niedrigen Intensitäten und hohen Tropfenanzahl verbunden. Diese ausgeprägten Eigenschaften in den Mikrostrukturen des Regens führen zu signifikant

unterschiedlichen Werten der Regenradarparameter A und b.

Contents

Acknowledgments	iii
Abstract	v
Zusammenfassung	vi
1 Introduction	1
1.1 General weather types	1
1.2 Cloud types	2
1.3 Cloud formation	3
1.3.1 Cold clouds	4
1.3.2 Warm clouds	5
1.4 Rain observation	5
1.4.1 Automated disdrometers	5
1.4.2 Radar based disdrometers	7
1.4.3 Radar	7
1.5 Rain microstructure	8
1.5.1 Rain type classification based on rain microstructure	8
1.5.2 R-Z	9
1.6 Research Idea	9
2 Outline	11
3 Overview of methods	13
3.1 Sites and time scale	13
3.2 Disdrometer data	13
3.2.1 Retrieving rain parameters	13
3.2.2 Filtering disdrometer data	16
3.3 Micro rain radar (MRR)	17
3.4 Weather types	17
3.5 Machine learning predictive models	18
3.5.1 Overview	18
3.5.2 Selecting Features	18
3.5.3 Stratified sampling	20
3.5.4 Choice of machine learning models	20
3.6 Retrieval of R-Z parameters	20
3.6.1 The traditional retrieval procedure	20

3.6.2	The modified retrieval procedure	21
3.7	Measures of performance	21
3.7.1	Performance indicators for classification models	21
3.7.2	Performance indicators for regression models	22
3.8	Software used	23
4	Publications: Summaries and contributions	24
4.1	Precipitation Diurnal Cycle in Germany Linked to Large-Scale Weather Circulations	25
4.2	Machine Learning Approach to Classify Rain Type Based on Thies Dis- drometers and Cloud Observations	26
4.3	Stratiform and convective rain classification using machine-learning mod- els and Micro Rain Radar and PARSIVEL disdrometer data	27
4.4	Rain Microstructure Parameters Vary with Large-Scale Weather Condi- tions in Lausanne, Switzerland	28
4.5	Weather Types Affect Rain Microstructure: Implications for Quantitative Precipitation Estimates	29
5	Discussion	30
5.1	Precipitation diurnal cycle (PDC) in Germany	30
5.2	Classification of rain type into convective and stratiform	31
5.3	Rain microstructure	32
5.3.1	Rain DSD variation	32
5.3.2	Optimizing retrieval algorithms for rain intensity	33
6	Conclusions	36
7	Outlook	38
	References	39
	List of Figures	50
	List of Tables	51

1 Introduction

This chapter contains a brief overview of the main concepts tackled throughout the dissertation. These concepts are introduced starting with the largest scale “General weather types”, followed by cloud types and precipitation formation processes. Additionally, rain observation devices are presented focusing on those able to measure rain microstructure. The smallest scale of rain microstructure is presented along with its use in classifying rain type and its influence on the radar rain retrieval algorithm. Finally a brief statement of the research idea is provided.

1.1 General weather types

Large scale weather types (aka. synoptic types or patterns, hereafter WT) denote atmospheric conditions that remain relatively stable for several days over a large area (Brdossy and Caspary, 1990). These atmospheric conditions comprise elements such as the distribution of high and low pressure systems, the extent and paths of frontal zones, and the existence of cyclonic or anticyclonic situations (Baur et al., 1944). WTs are clustered in such a way that similar conditions within each type are preserved while clear dissimilarities between the different types are obtained. WT classification had been a common practice in meteorology with the purpose of weather forecasting until the rise of weather forecast models which took over in the last few decades (Huth et al., 2008). However, WT classification remains an important part of statistical climatology (Ramos et al., 2015; Huth et al., 2008).

WTs explain the variations in many local weather phenomena, especially because they influence the thermal and humidity content of air masses and their movement. They are linked to the variations of temperature and precipitation (Buishand and Brandsma, 1997; Vallorani et al., 2018; Huth et al., 2016; Broderick and Fealy, 2015; Cortesi et al., 2013), and the occurrence of extreme events and their magnitude (Cony et al., 2010; Cassano et al., 2006; Nowosad and Stach, 2014; Maheras et al., 2018; Planchon et al., 2009). Indirectly, they also influence stream flows (Steirou et al., 2017), floods (Petrow et al., 2007; Jacobeit et al., 2003; Nied et al., 2014), debris-flow events (Nikolopoulos et al., 2015), forest fires (Wastl et al., 2013; Kassomenos, 2010), air quality, and pollen distribution (Russo et al., 2014; Nidzgorska-Lencewicz and Czarnecka, 2015; Grundström et al., 2017). They have been used to assess the performance of global climate models in terms of reproducing past weather conditions, comparing future scenarios, simulating precipitation on local scales, and statistical downscaling of precipitation and extreme events (Sheridan and Lee, 2010), which explains the continuing interest in WT classification.

The classification process of WTs consists usually of two steps, defining the types, then assigning individual cases to corresponding types (Huth et al., 2008). The whole procedure can be subjective when both steps are based on the expertise of trained individuals such as in the classification of “Hess and Brezowsky” (Gerstengarbe et al., 1993). It can be objective when specific algorithms are followed based on the input of particular weather parameters, such as in the “Objective Weather Classification” run by the German Meteorological Service (DWD, Deutscher Wetterdienst). WT classifications have different performances in resolving precipitation. Some objective classifications explain the daily precipitation patterns better than all the manual classification procedures (Schiemann and Frei, 2010). The performance differences depend on the season, the location, and the number of classes in each classification procedure. These differences might also be a result of the different rules in each classification regarding pressure field height and the different time windows assumed for the consistent weather conditions to prevail (Kysely and Huth, 2006). However, WTs should be viewed as purposeful simplifications of reality and there is no single true classification (Huth et al., 2008).

It is possible to track changes in WTs for long periods back in time, which makes them suitable for climate change studies. The overall warming of central Europe was linked to the changes in frequency of daily circulation patterns (Philipp et al., 2007). Specifically in winter in the few decades until the 1990s (Van Oldenborgh and Van Ulden, 2003; Rebetez and Reinhard, 2008), the warming was associated with a strengthening of the zonal flow (Kysely and Huth, 2006), and a positive phase of the North Atlantic Oscillation (Hurrell, 1995; Jones et al., 1999; Hurrell and van Loon, 1997). However, changes in WTs fail to explain the climatic trends in the remaining seasons (Cahynová and Huth, 2016). Additionally, different classification methods produce different results (Huth, 2010; Beck and Philipp, 2010). In general, at least the frequencies of some WTs are sensitive to some aspects of anthropogenic forcing (Corti et al., 1999). However, linking trends in WT to climate change requires caution and the use of a large number of circulation classifications in order to avoid a misinterpretation of results (Cahynová and Huth, 2016). Another approach to avoid the differences emerging from using different WT classification methods is to identify a specific classification that is suitable for the particular region of interest (Beck and Philipp, 2010).

1.2 Cloud types

Clouds have different shapes and extents in the troposphere. The first attempts to classify clouds based on ground observations were done by Jean Baptiste de Monet and Lamarck Luke Howard (Ahrens, 2009, 2015). The current classification of clouds – cloud genera (World Meteorological Organization, 1975) - includes the high altitude / level clouds, usually above 7 km (cirrus, cirrocumulus, and cirrostratus), the mid-troposphere clouds, between 2 – 7 km (altocumulus, altostratus, and nimbostratus), and the low clouds below 2 km (stratocumulus, stratus, cumulus and cumulonimbus), bearing in mind that cumulonimbus tops might extend to the upper troposphere (see Figure 1.1).

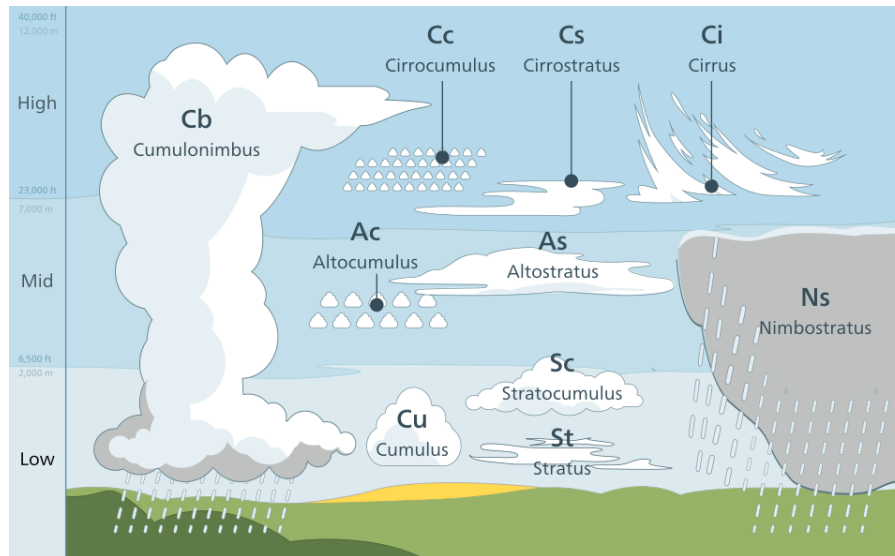


Figure 1.1: Cloud genera shape and level range. Figure By Valentin de Bruyn (CC BY-SA 3.0) (Wikimedia Commons, 2018)

We are mostly interested in low clouds which are the precipitation sources. These have usually two major types: stratiform clouds, including stratocumulus, stratus, and nimbostratus, and the cumuliform (convective) clouds including cumulus and cumulonimbus. In both cases, the formation of clouds is associated with air rising, expanding and cooling. The main mechanisms behind this formation are the surface heating and free convection, the topography, the convergence leading to wide spread ascent, and the weather fronts leading to uplift (Ahrens, 2015).

1.3 Cloud formation

The dominant genera in stratiform clouds are stratus and stratocumulus. They are usually characterized by their thin (less than 1 km) horizontal extent over a large area, and they both cover over 30% of the surface of the earth. Such stratiform clouds form by horizontal advection of warm fronts over cold air masses. Stratiform clouds may also form by the radiative cooling process (Svensson and Jakob, 2002). Near the top of the boundary layer, condensation may initiate when the temperature approaches the dew point. The cooling continues especially during the night at the top of the thin cloud layer (Twardosz, 2007). Other ways of stratiform clouds formation include ascending of moist air near fronts or due to topography, or the advection of warm fronts over cold areas (Wood, 2015). The balance between radiative cooling of these clouds and the flux of energy and moisture controls the stability of stratiform clouds. Additionally, precipitation has a major and complex influence on these fluxes, and therefore the stability of the clouds.

Cumulus and cumulonimbus clouds are the genera of convective clouds. They have limited coverage except for the upper part of the cumulonimbus which takes the shape of an anvil. Cumulus clouds form due to the conversion of air currents and the movement of warm air upward where the temperature decreases rapidly (Rangno, 2015). These clouds have the highest liquid concentration. Precipitating cumulus clouds have 1.5 – 3 km thickness over the ocean and around 3 km over land. Cumulonimbus clouds usually are thicker and could reach a total depth of 20 km. They are also characterized by strong rainshafts and lightning.

When moist air parcels ascend to higher elevations, they expand and cool down. Consequently they become supersaturated with respect to liquid water. This initiates the process of condensation and clouds start to become visible (Wallace and Hobbs, 2006). Condensation starts on the surfaces of small particles called the cloud condensation nuclei (CCN). Their concentration is higher in continental air near the earth's surface compared to the marine air (Hudson, 2002). However, different processes occur and there should be a clear distinction between warm and cold clouds.

1.3.1 Cold clouds

Even well above the 0°C isotherm, small droplets of water exist in the liquid form. It takes very low temperatures to freeze very small droplets. Ice crystals may form in such conditions when ice nuclei are available. These ice nuclei are rare compared to the CCN and they are activated mostly in temperatures below -10°C. There are some uncertainties regarding the sources of ice nuclei. However, it is known that clay minerals, some bacteria and decaying plant materials beside ice particles themselves act as ice nuclei (Ahrens, 2009).

Ice particles in the clouds grow by three processes (Wallace and Hobbs, 2006; Houze, 2014); growth from vapor phase happens in clouds containing a mixture of supercooled droplets and ice particles. Ice particles grow rapidly compared to the growth of droplets and directly from the vapor phase. Growth by rimming happens when supercooled droplets collide into the ice particles and freeze onto them. Growth by aggregation occurs when ice particles collide into each other due to the different falling speed of the particles caused by the variations in drop size and shape. As an ice particle becomes larger, the rimming and aggregation contribute more to its growth and the ice particle start descending. These particles start melting at a certain level. They become coated by a thin film of liquid water. At this stage, a mixture of large volume of ice particles with the coating of liquid water exists. The mixture of ice and water at this melting layer has a higher ability to reflect radar signal. After complete melting, the rain drops have a smaller volume and a higher velocity, which causes a decrease in the reflected radar signal. The melting layer is detected by radars and referred to as the bright band.

1.3.2 Warm clouds

Warm clouds exist beneath the 0°C isotherm. In such clouds, droplets may grow by condensation, colliding and coalescing with other droplets. As the air parcel moves upwards and becomes supersaturated, CCNs are activated and water vapor starts to condensate on the surface of CCNs. Usually small droplets grow faster than larger droplets due to the condensation process. As time passes, the size of droplets becomes relatively uniform. This process is very slow in producing large drops with radii up to 1 mm. However, the growth of one droplet in a million is enough to initiate rain.

The terminal velocity of a droplet is correlated with its size. Consequently, droplets which are larger than average in a cloud will have a higher than average terminal velocity (Hudson, 2002). As they fall they collide with smaller droplets. Depending on the size of the droplets, the velocities, the relative positions and the electrical charge, two droplets may form one larger droplet, bounce, or breakup into several droplets. Other processes which contribute in producing variations in droplet size include the role of giant CCN, the turbulence within the cloud, the stochastic collection of droplets (considering that collision-coalescence process has a probabilistic nature in time and space), and the probability of raindrop breakup due to large size and the fraction with air (Ahrens, 2009).

1.4 Rain observation

In situ measurement of rainfall properties remains an essential practice for scientific research and practical applications such as monitoring water resources, agriculture, erosion, and calibration of remote sensing instruments. Rain gauges continue to provide rainfall intensities and accumulation. They are simple to use and inexpensive. However, errors may occur due to the specific design and principle of measurement. Main sources of error include the effect of wind, evaporation, wetting, splashing, bad choice of location, and calibration issues (Testik and Gebremichael, 2010). Disdrometers provide more details of rain microstructure including the size and velocity of the detected meteors with a very high temporal resolution. This makes disdrometers especially suitable for microphysical studies of precipitation, erosion, and improving remote sensing algorithms for rain intensity estimation.

1.4.1 Automated disdrometers

Measuring rain drop size distribution started with some manual methods such as using stain paper, flour pallets, oil immersion, and photography (Kathiravelu et al., 2016). One of the most frequently used automated disdrometers is the Joss-Waldvogel Disdrometer (Kinnell, 1976). In this impact disdrometer, a rain drop falls on a moving plate which causes a displacement. This displacement is correlated with the size of the drop. One major disadvantage of the Joss-Waldvogel disdrometer is that it is intrusive and alters

the behavior of the falling rain drop. This limitation was overcome by the development of optical disdrometers.

Optical disdrometers, such as PARSIVEL (see Figure 1.2) and Thies disdrometers, generate a laser or light signal in one end of the device. This signal is received by a detector at the other end. Whenever a drop passes this measurement area, the received signal is reduced. The magnitude of this reduction corresponds to the size of the drop. The velocity of the drop is also correlated with the time it needs to pass the measuring area. Such disdrometers have high temporal resolutions which could exceed one minute. The disdrometer output can be used to produce a wide range of precipitation parameters, such as the rain intensity, kinetic energy, mean diameter, mean velocity, visibility and type of precipitation. Disadvantages differ depending on the type of disdrometer used. For example, PARSIVEL1 has an inhomogeneous laser source which affects the accuracy of the device. This led to the second version of the device PARSIVEL2 (Tokay et al., 2014). The disdrometer measuring area is commonly small (Tapiador et al., 2017). Additionally, the measurement errors due to splashing, masking (when one drop is shadowed at least partially by another), birds, pollen, insects and spider webs, need to be filtered away (Friedrich et al., 2013).



Figure 1.2: The PARSIVEL disdrometr (front) and the micro rain radar inside its housing (back) located in Das, north east of Spain. Photo by Ghada, Wael. (2019)

1.4.2 Radar based disdrometers

Radar based disdrometers are vertically pointing radars such as micro rain radars (MRR - see Figure 1.3) and wind profilers. They are able to retrieve the rain drop size distribution (DSD) based on the assumption that vertical air velocity is absent. In this case the terminal fall velocity of drops equals the Doppler radial velocity. These instruments have a larger sampling volume compared to ground disdrometers. They also provide the change in rain DSD as a function of elevation, which allows the study of rain microstructure evolution. However, a main disadvantage especially in the case of MRR is the signal attenuation (Testik and Gebremichael, 2010).



Figure 1.3: Micro rain radar (MRR) located in Das, north east of Spain. Photo by Ghada, Wael. (2019)

1.4.3 Radar

Radio detection and ranging (Radar) has the advantage of wide coverage and reaching areas which were not previously accessible. In these devices, a microwave signal is transmitted by the radar into space. Fractions of this signal are scattered when encountering a target. The scattered signal is received again in the radar and shown on its screen as an echo. The distance to the target determines the time needed for the signal to travel back and forth. Most radars have a wavelength in the range 0.8 - 10 cm. A shorter wavelength (3 - 5 cm or less) enables the radar to detect small targets such as droplets (Markowski and Richardson, 2010). However, attenuation for such short

wavelengths is severe. In case of rain, the higher the intensity, the brighter the echo detected (Ahrens, 2009).

1.5 Rain microstructure

The importance of rain microstructure lays in its ability to give an insight into the rain formation processes behind. The practical applications of this knowledge include erosion studies, telecommunication, and quantitative estimation of rain by remote sensing. Our assumptions regarding rain microstructure play a decisive role in these applications, especially considering the uncertainties in formation mechanisms which lead to the broad distribution of the detected rain parameters that represent the rain DSD (Beard and Ochs, 1993). Exponential distribution has been used widely to represent rain DSD (Marshall and Palmer, 1948) in terms of concentration of raindrops N per diameter interval D as:

$$N(D) = N_0 \times \exp(-\Lambda \times D) \quad (1.1)$$

where N_0 is the intercept parameter, and $-\Lambda$ is the slope parameter.

Gamma distribution alternatively represents the concentration of raindrops as:

$$N(D) = N_0 \times D^\mu \exp(-\Lambda \times D) \quad (1.2)$$

where μ is the shape parameter (Willis, 1984). The parameters of the fitted gamma distribution have been used to demonstrate the variation in rain DSD with different rain types, different meteorological conditions and different geographical locations (Wen et al., 2019; Niu et al., 2010; Fernandez-Raga et al., 2017).

1.5.1 Rain type classification based on rain microstructure

Convective and stratiform rain have different formation processes which contribute to the rain properties as observed on the ground. Classifying rain into these two categories have been proven to improve quantitative estimation of precipitation (QPE) by radars (Thompson et al., 2015). It also fosters the improvement of global climate and circulation models (Steiner and Smith, 1998; Ferrier et al., 1995; Houze, 1997). To classify rain type when cloud observations are absent, rain intensity and its variation have been widely used. When the rain intensity itself or the standard deviation of rain intensity exceeds a threshold, the corresponding interval is classified as convective rain (Bringi et al., 2003; Tang et al., 2014; Marzano et al., 2010). However, when records of rain DSD are available, it is possible to use the distinct microstructure for the classification purpose. Most proposed methods to classify rain based on its microstructure use simply a combination of two parameters. These combinations include for example the rain rate with the intercept parameter (R- N_0) (Tokay and Short, 1996), the slope with the shape parameter (Λ - μ) (Caracciolo et al., 2006), the intercept with the slope parameter (N_0 - Λ) (Caracciolo et al., 2008), or the median drop diameter with the log normalized concentration (N_0 - $\log N_w$) (Bringi et al., 2009). All of these methods include drawing a

line separating two regions in the space of the chosen parameters. This line is affected by the chosen pre-classified cases. Applying any of these classification methods requires careful consideration of the different geographical location (Caracciolo et al., 2006; Uijlenhoet et al., 2003; You et al., 2016) and the used instrument to retrieve rain DSD and its parameters (Bukovčić et al., 2015).

1.5.2 R-Z

As mentioned earlier, radars do not provide a direct measure of rain intensity. Instead they provide measures such as the radar reflectivity Z which represents the efficiency of the radar target in intercepting and returning radio energy (American Meteorological Society, 2020). Z is assumed to have an exponential relation with rain intensity R . The retrieval of rain intensity is based on the equation $Z=AR^b$, where Z has the unit mm^6/m^3 , and R in mm h^{-1} .

Marshall and Palmer (Marshall and Palmer, 1948) determined the values of A and b to be 200 and 1.6 respectively. These values are still used widely despite the fact that variations in A and b values have been found with respect to rain microstructure. The reason behind this variation lays in the different sensitivity of Z and R to changes in rain DSD. Z is the 6th moment of DSD which makes it more sensitive to changes in drop size. On the other hand, R is more sensitive to the drop concentration since it is correlated with the 3.67th moment of DSD. (Chen, 2004). In other words, the same amount of water content distributed over large drops or small drops will result in different values of Z . To determine the values of A and b , independent ground measurements of rain intensity are required. This highlights the importance of combining radars with a network of ground based devices such as rain gauges and disdrometers. These devices are essential to calibrate the radar equations and validate measures over the long term.

1.6 Research Idea

Using different types of disdrometers leads to significant variations in rain microstructure and all bulk precipitation (Angulo-Martínez et al., 2018; Guyot et al., 2019). Similarly, using different disdrometers result in different radar rain retrieval algorithms, which in turn result in significant differences in the amount of accumulated rain measured, especially on the event level (Adirosi et al., 2018). Considering that rain microstructure parameters which are used to classify rain types are derived by different disdrometers types raises the question about the suitability of such rain classification techniques and their performance when using different devices.

Advection and convection are known to have different major precipitation formation processes. These processes lead to distinct rain microstructures, which when considered, can reduce the error in accumulated rain amount by up to 50% (Kirsch et al., 2019). However, weather types influence many aspects of the meteorological conditions. Especially depending on the large-scale wind direction component, these weather types vary in their

humidity, energy, and aerosols content. These distinct properties of the weather types might explain further the variations observed in rain microstructure. Consequently, we hypothesize that rain microstructure varies significantly between weather types in both rain types. Therefore, distinct, weather-type-specific, radar algorithms could be developed with the potential to improve the quantitative estimation of rain. This improvement in particular is of great interest for many hydrological and environmental applications.

2 Outline

Large scale weather types represent a simplification of the meteorological conditions w.r.t. centers of action prevailing over a large area. Especially the flow direction component of these types have a large influence on the humidity and energy transport over the area in focus. This influence is still overlooked when it comes to the variation of rain properties despite the availability of precipitation and meteorological data in Central Europe to address it. The potential impact of weather types on rain microstructure, and consequently, on the remote sensing algorithms that retrieve rain intensity needs to be investigated. This also requires a clear distinction between rain types into convective and stratiform. Currently available rain type classification methods have questionable performance because they were designed based on specific measuring devices. Even when using the same device, performance may drop due to different climatic conditions in different locations.

This work analyses the influence of large-scale weather types on rain properties, namely diurnal cycle of precipitation and rain microstructure. It presents machine learning classification of rain type using two types of devices. It also demonstrates the potential influence of considering weather types on the rain intensity retrieval algorithms which are used by radars as a direct practical application. This is organized in three stages:

1. The influence of flow direction as a component of weather type on the diurnal cycle has been addressed. Daily patterns of precipitation frequency and amount and their variations were investigated under the combined effect of flow direction, seasonality, locations and elevations in Germany. The research questions addressed in this stage were:
 - How do patterns of diurnal precipitation cycles vary with weather types over Germany?
 - How does seasonality and location within Germany influence such a variation?
2. The suitability of the available rain type classification methods for the instruments available was questionable. Therefore, it was necessary to assess this performance and reach a reliable classification procedure in order to move on to the next step of investigating the effect of weather patterns on rain microstructure. With the help of a pre-classification of rain based on cloud observations in Bavaria, several classification methods have been assessed. The use of machine learning predictive models was also investigated. In a follow up study in the north east of Spain, the

suitability of machine learning classification models was investigated for two types of devices. Both of these methodological papers discuss the questions:

- How do the performance of classification methods which are designed for one type of instruments perform on different types of instruments?
- Is it possible to improve the performance of available simple, dual parameters classification methods?
- How do machine learning classification models perform when applied in different locations and using different instruments?

3. Finally, the main aim of the work was to investigate the variation of rain microstructure under the influence of large scale weather types. This has been done in two locations; the first in Lausanne in Switzerland, and the second in Bavaria, Germany. The main differences between the two studies were the time scale, the spatial scale, the disdrometer types, and the rain type classification methods. Both studies addressed the questions:

- Can we observe a consistent pattern of rain microstructure that is associated with the different classes of large scale weather types?
- Can such a pattern influence the rain intensity retrieval algorithms which are used in radars?

3 Overview of methods

A brief overview of the applied methodology is given in this section.

3.1 Sites and time scale

In total, 27 disdrometers in Germany, Switzerland and Spain, and one Micro Rain Radar (MRR) in Spain were involved in studying rain microstructure within this work. Additionally, 136 stations containing a variety of rain collecting devices, mostly pluviometers, were used to demonstrate the influence of weather types over the diurnal precipitation patterns in Germany. These stations included hourly precipitation data for at least 15 years each. Figure 3.1 shows the measurement locations.

The studies of rain type classifications were performed at two sites in Bavaria and one site in the north east of Spain. The sites in Bavaria included Thies measurement and hourly cloud observations for one year in Fürstenzell and seven months in Regensburg. The Spanish site included a PARSIVEL and an MRR with measurements for 27 months.

To demonstrate the influence on WTs on rain microstructure, 16 PARSIVEL disdrometers in Lausanne, Switzerland, and 10 Thies disdrometers at 10 locations in Bavaria were used. The disdrometer data from Switzerland were measured during the EPFL-LTE campaign which spanned over 22 months. The Bavarian disdrometer data was provided by the German Meteorological Service (DWD) and spanned over three full years.

3.2 Disdrometer data

Two types of disdrometers were involved in this study, Thies and PARSIVEL. Both devices have the same measurement principle, but different sensitivities. Thies disdrometers are able to detect drops with a diameter of 0.16 mm or larger (Thies Clima, 2007), while PARSIVEL disdrometers detect drops starting with a diameter of 0.2 mm (OTT Hydromet, 2020). Disdrometer data comprise drop counts for specific ranges (bins) of diameters and velocities. The temporal resolution of all measures in this work was set to an interval of one minute.

3.2.1 Retrieving rain parameters

From the disdrometer output, a large number of parameters can be extracted for each one-minute interval. Therefore, only the most relevant ones for rain microstructure

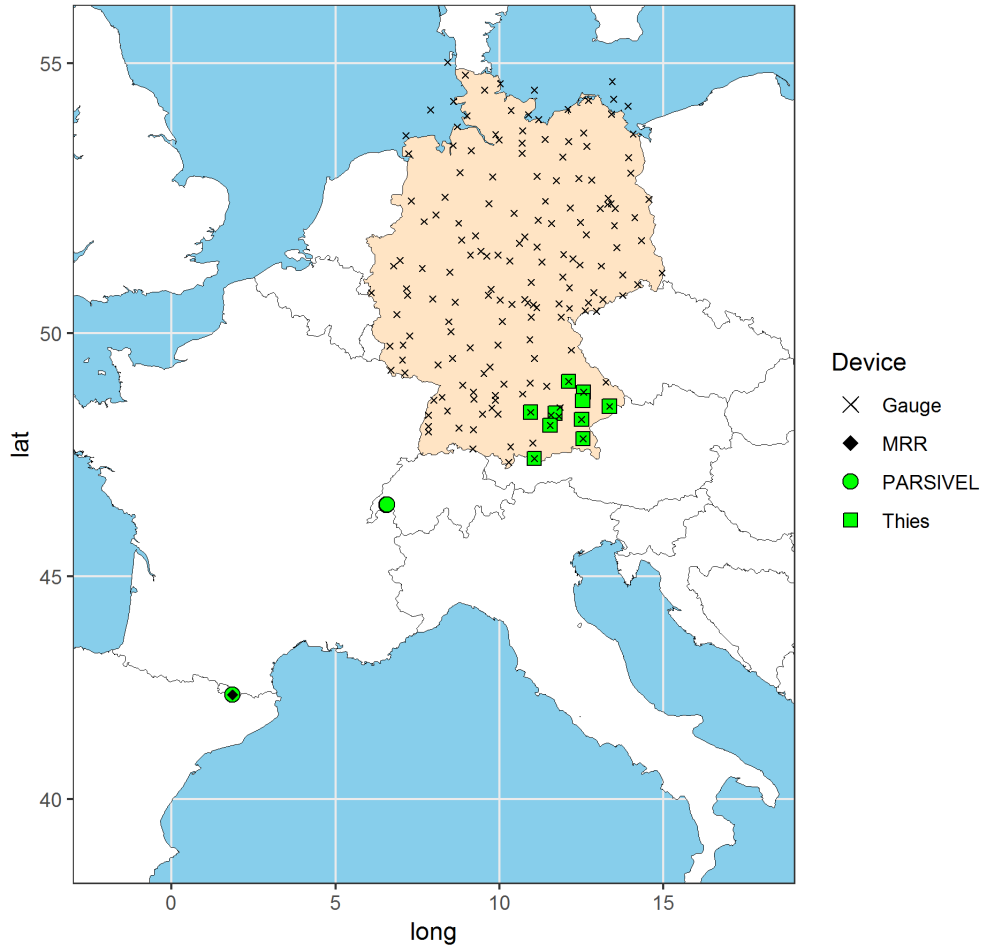


Figure 3.1: Location of measuring devices over the study sites in Germany, Switzerland and Spain. The site in Switzerland includes 16 disdrometers.

studies are presented in the following. The remaining parameters can be found in the publications and the relevant references.

Rain intensity

Rain intensity (R in mm h^{-1}) is defined by the equation (Chen et al., 2016a):

$$R = 60 \times 60 \times \pi \div (6 \times 1000000 \times \Delta T) \sum_{i=1}^{nd} \sum_{j=1}^{nv} (x_{i,j} \times D^3 \div A_i) \quad (3.1)$$

where

$x_{i,j}$: Detected number of drops that fall in diameter range i and velocity range j .

nd : the total number of diameter ranges.

nv : the total number of velocity ranges.

ΔT (s): Temporal resolution = 60 s.

A_i (m²): Corrected detection area:

$$A_i = L_A \times (W_A - D_i/2) \div 1000000$$

L_A (mm): the length of the detection area.

W_A (mm): the width of the detection area.

D_i (mm): Mean diameter of drops that fall in diameter range i.

Reflectivity

Reflectivity (Z in mm⁶ m⁻³) is defined by the equation (Chen et al., 2016a):

$$Z = \sum_{i=1}^{nd} \sum_{j=1}^{nv} x_{i,j} \times D_i^6 \div (A_i \times V_j \times \Delta T) \quad (3.2)$$

where: V_j (m s⁻¹): Mean velocity of drops in velocity range j.

The reflectivity is usually expressed in another unit (dBZ):

$$Z_{dBZ} = 10 \times \log_{10}(Z_{mm^6m^{-3}}) \quad (3.3)$$

Rain microstructure parameters

The total drop concentration (N in m⁻³, i.e. the total number of drops per m³) is defined by the equation (Chen et al., 2016a):

$$N = \sum_{i=1}^{nd} \sum_{j=1}^{nv} (x_{i,j} \div (V_i \times \Delta T \times W_i \times A_i)) \quad (3.4)$$

where:

W_i (mm): the Width of the diameter range i.

The Mass weighted diameter (D_m in mm) is defined by the equation (Marzuki et al., 2010):

$$D_m = \frac{\sum_{i=1}^{nd} \sum_{j=1}^{nv} (x_{i,j} \times D^4)}{\sum_{i=1}^{nd} \sum_{j=1}^{nv} (x_{i,j} \times D^3)} \quad (3.5)$$

The median volume diameter (D_0 in mm) is the diameter that divides the volume of liquid water content in half (Kanofsky and Chilson, 2008):

$$\int_{D=0}^{D_0} (x_D \times D^3 dD) = \int_{D=D_0}^{\infty} (x_D \times D^3 dD) \quad (3.6)$$

Kinetic energy

The kinetic energy (KE in J m⁻² h⁻¹) is defined by the equation (Petrů and Kalibová, 2018):

$$KE = 3600 \times \pi \div (12 \times 1000000 \times \Delta T) \sum_{i=1}^{nd} \sum_{j=1}^{nv} (x_{i,j} \times D_j^3 \times V_i^2 \div A_i) \quad (3.7)$$

Gamma distribution parameters

Gamma distribution parameters are especially of interest for the rain type classification. Assuming that rain DSD follows a gamma distribution (Willis, 1984).

$$N(D) = N_0 \times D^\mu \times \exp(-\Lambda \times D) \quad (3.8)$$

where N_0 ($\text{mm}^{-1-\mu}\text{m}^{-3}$) is the intercept parameter.

λ (mm^{-1}) is the slope parameter

μ (non-dimensional) is the shape parameter

Gamma parameters were calculated using the moments method (Testud et al., 2001) where The k_{th} moment of rain DSD is:

$$M_k = \sum_{i=1}^{nd} \sum_{j=1}^{nv} (x_{i,j} \times D_i^k) = N_0 \times \Gamma(\mu + k + 1) \div \Lambda^{\mu+k+1} \quad (3.9)$$

Using the 3_{rd}, 4_{th}, and 6_{th} moments, we can obtain the gamma parameters:

$$m = (11 \times G - 8 + (G \times (G + 8))^{0.5}) / (2 \times (1 - G)) \quad (3.10)$$

$$G = (M_4)^3 \div ((M_3)^2 \times M_6) \quad (3.11)$$

$$N_0 = \Lambda^{\mu+4} \times M_3 \div \Gamma(\mu + 4) \quad (3.12)$$

$$\Lambda = ((\mu + 4) \times M_3 \div M^4) \quad (3.13)$$

Where $D_m = M_3 \div M^4$ is the Mass weighted diameter (Equation: 3.5). And G is the third moment of the mass spectrum normalized by $(D_m)^3$.

3.2.2 Filtering disdrometer data

Disdrometers provide records of size distribution for each interval regardless of the nature of the object that passes the detection area. An important step in preparing the raw disdrometer data is to identify and exclude non-rain intervals. Another challenge is filtering out non-rain detected objects within rains intervals. The most important criteria for this process is identifying the terminal velocity for each drop diameter range. The filtering process of disdrometer data was based on the suggestions of Friedrich et al. (2013) and adjusted for each disdrometer type. This included the removal of:

- Intervals associated with damaged laser signal,
- Intervals associated with snow, hail, frozen rain, and mixed precipitation as reported by the disdrometer internal classification,
- Intervals with rain intensity below 0.1 mm.h^{-1} ,

- Intervals in which less than four drop diameter ranges were detected,
- Intervals where large drops with a low falling speed were detected as an indicator of high wind speed,
- Drops with a diameter larger than 8 mm, and
- Drops outside the range of $TV \times (1 \pm 60\%)$ for each diameter range, considering the terminal velocity TV (m/ sec) as a function of the drop diameter (mm) (Atlas et al., 1973):

$$TV(D) = 9.65 - 10.3 \times \exp(-0.6 \times D) \quad (3.14)$$

3.3 Micro rain radar (MRR)

MRR was used at one site in Spain in order to test and improve rain type classification procedures. It is a low cost, K band (24 GHz) FM–CW Doppler radar profiler manufactured by METEK (Löffler-Mang et al., 1999). The device was set to provide records with a temporal resolution of one minute for the vertical range between 100 m and 3000 m. The output was post-processed to provide values of the equivalent reflectivity (Z), Doppler velocity (W), and spectral width (SW). The post processing was proposed by Maahn and Kollias (2012) and explained in details by Gonzalez et al. (2019).

The existence of a bright band in radar records is considered to be a clear indicator of the melting layer and stratiform rain type. Regardless of the existence of a melting layer, the level with the highest increase in the Doppler velocity was identified for each interval within the range between 500 m and 2900 m. This level was labeled as the separation level (SL). A five minutes average temporal moving window was used to reduce the noise in identifying SL. The same moving window was used to determine the average values of Z , W , SW , and their standard deviations for the whole column, for the region above the separation level, and for the region below the separation level. The resulting 19 parameters were used as potential classifiers of rain type and were provided as features for machine learning classification models.

3.4 Weather types

Two classifications of weather types were used in this work. Both classifications are performed and provided on a daily basis by the DWD. The Hess and Brezowsky classification includes 30 patterns. Each pattern is based on air mass movement and the direction of rotation around centers of actions. They can be grouped further into five main flow directions (see Table 3.1).

The objective weather type classification is based on the output of a numerical weather analysis and forecast system run by the DWD (currently the operational global model extended or GME). Each day is classified to one out of 40 possible classes of weather types. Each class is a combination of a wind index, a cyclonality index, and

Table 3.1: Summary of the Hess and Brezowsky classification of weather types (C.E.: Central Europe)

Flow Direction	GWL			
W: Westerly	WA	Anticyclonic Westerly	WS	South-Shifted Westerly
	WZ	Cyclonic Westerly	WW	Maritime Westerly
S: Southerly	SWA	Anticyclonic Southwesterly	SZ	Cyclonic Southerly
	SA	Anticyclonic Southerly	TB	Low over the British Isles
	SEA	Anticyclonic Southeasterly	TRW	Trough over Western Europe
	SWZ	Cyclonic Southwesterly	SEZ	Cyclonic Southeasterly
NW-N: Northwesterly, Northerly	NWA	Anticyclonic Northwesterly	NWZ	Cyclonic Northwesterly
	NA	Anticyclonic Northerly	NZ	Cyclonic Northerly
	HNA	Icelandic High, Ridge C.E.	HNZ	Icelandic High, Trough C.E.
	HB	High over the British Isles	TRM	Trough over C.E.
CE: No specific prevailing direction	HM	High over C.E.	BM	Ridge across C.E.
	TM	Low (Cut-Off) over C.E.		
NE-E: Northeasterly, Easterly	NEA	Anticyclonic Northeasterly	NEZ	Cyclonic Northeasterly
	HFA	Scandinavian High, Ridge C.E.	HFZ	Scandinavian High, Trough C.E.
	HNFA	High Scandinavia-Iceland, Ridge C.E.	HNFZ	High Scandinavia-Iceland, Trough C.E.
-	U	Transitional		

humidity index. We only focused on the wind index which takes one of five values: no prevailing direction (XX), northeasterly (NE), southeasterly (SE), southwesterly (SW), and northwesterly (NW).

3.5 Machine learning predictive models

3.5.1 Overview

Machine learning predictive models have been used in this work to classify rain type into convective and stratiform based on disdrometer data or MRR data. The whole process can be summarized by the flow chart in Figure 3.2.

3.5.2 Selecting Features

It is possible to build machine learning predictive models with many features. However, a high number of features comes with high computational costs. Additionally, the model performance might be influenced by the existence of non-informative parameters (Kuhn and Johnson, 2016). This is why it is a common practice to reduce the number of features for such models. In this work, feature selection was performed in two ways, in a heuristic approach, and by forward stepwise selection.

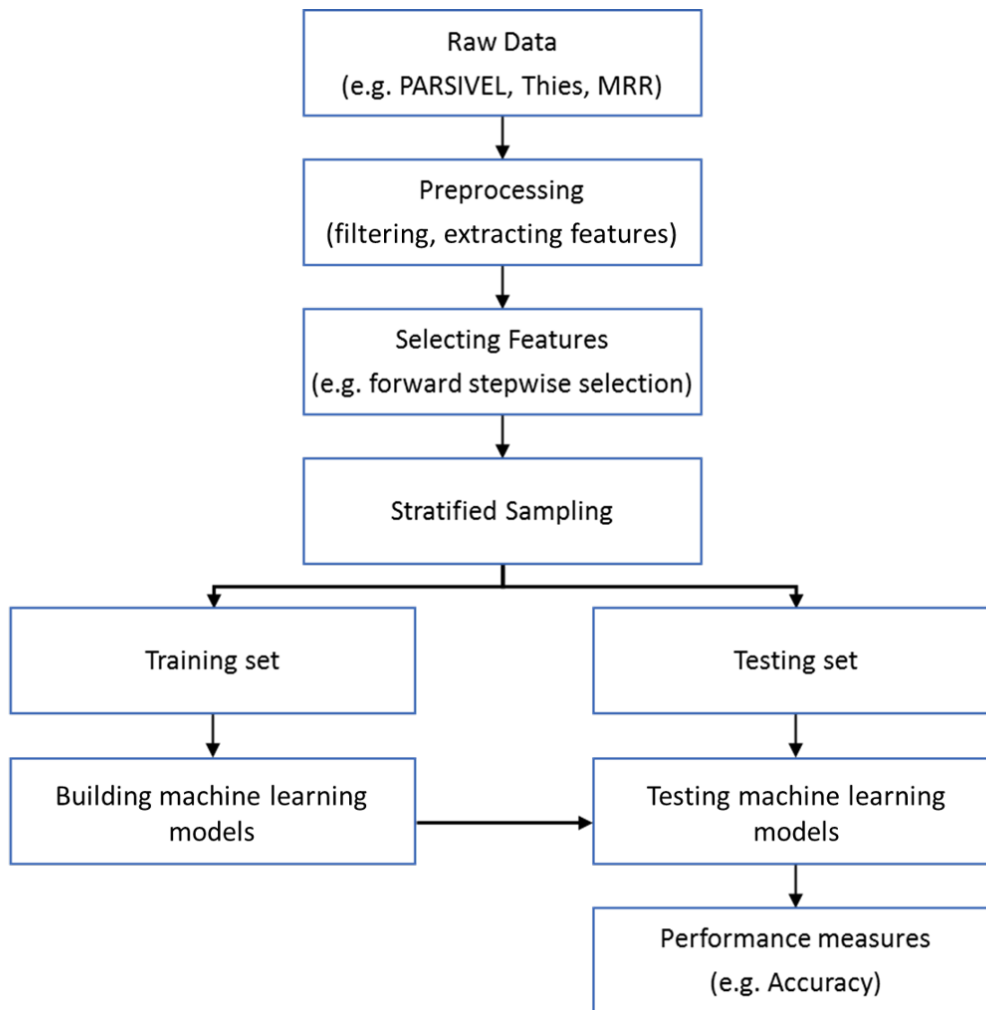


Figure 3.2: A summary of the machine learning model building process

In the heuristic approach, features were clustered based on their correlation coefficients. Out of each group of highly correlated features, one feature was selected based on the value of AUC (the area under the receiver operating characteristic curve), which is a performance measure for each feature when used as a classifier of rain type.

The forward stepwise procedure starts with building predictive models (random forest in this case). Each model uses only one feature out of the available features for classification. The model which achieves the best performance indicates the first feature to be selected. The process is repeated by adding one feature at a time to the model which has been produced in the previous step, and again the added feature is chosen which provides the greatest increase to the performance indicators.

3.5.3 Stratified sampling

Stratified sampling was used to produce a balanced distribution of convective and stratiform rain intervals in the subsets which were used to train and test the classification models. In other words, the proportion of convective rain needs to be the same in the subsets and in the original whole dataset. In most cases the dataset was split into 70% training and 30% testing subsets. The sampling was repeated several hundred times to demonstrate the stability of the results.

3.5.4 Choice of machine learning models

Only five simple machine learning methods were used for the classification of rain types. These methods require no or a minimum amount of adjustment for the hyper parameters. The chosen methods were Linear Discriminate Analysis (LDA), K nearest neighbor (KNN), Naïve Bayes (NB), the Conditional Trees (Ctree), and Random Forests (RF).

3.6 Retrieval of R-Z parameters

3.6.1 The traditional retrieval procedure

The radar reflectivity Z is assumed to be related to rain intensity R by the power law:

$$Z = A \times R^b \quad (3.15)$$

In this equation, Z is expressed in mm^6m^{-3} . By taking the \log_{10} and multiplying by 10:

$$10 \times \log_{10}(Z) = 10 \times \log_{10}(A) + 10 \times b \times \log_{10}(R) \quad (3.16)$$

And based on Equation 3.3:

$$dBZ = 10 \times \log_{10}(A) + 10 \times b \times \log_{10}(R) \quad (3.17)$$

a linear model is fitted to the values of dBZ and $\log R$ which are calculated from the rain DSD. The linear model has the equation:

$$dBZ = intercept + slope \times \log_{10}(R) \quad (3.18)$$

by linking equations 3.17 and 3.18:

$$slope = 10 \times b \Rightarrow b = slope \div 10 \quad (3.19)$$

$$10 \times \log_{10}(A) = intercept \Rightarrow A = 10^{intercept \div 10} \quad (3.20)$$

3.6.2 The modified retrieval procedure

The traditional procedure is commonly used to retrieve the values of A and b. However, the linear model in this case is fitted to minimize the errors on the vertical axis which is dBZ. A more appropriate approach is assuming R as the dependent variable (Jaffrain and Berne, 2012):

$$R = (1 \div A)^{1 \div b} \times Z^{1 \div b} \quad (3.21)$$

By taking the \log_{10} of both sides:

$$\log_{10}(R) = (1 \div b) \times \log_{10}(Z) - (1 \div b) \times \log_{10}(A) \quad (3.22)$$

$$\log_{10}(R) = dBZ \div (10 \times b) - \log_{10}(A) \div b \quad (3.23)$$

The linear model assuming R as the dependent variable:

$$\log_{10}(R) = \text{intercept} + \text{slope} \times dBZ \quad (3.24)$$

by linking equations 3.23 and 3.24 :

$$b = 1 \div (10 \times \text{slope}) \quad (3.25)$$

$$A = 10^{(-b \times \text{intercept})} \quad (3.26)$$

3.7 Measures of performance

The assessment of predictive models was based on performance indicators for two cases.

3.7.1 Performance indicators for classification models

When classifying rain into convective and stratiform, it is important to consider the imbalance between the two classes. Since almost 90% of rain intervals are stratiform, classification procedures could produce high accuracy simply by assigning all intervals to stratiform. Thus, it was important to include beside accuracy additional performance indicators such as the F-measure that focus on the model ability to correctly identify the least occurring rain type. Both the accuracy and the F-measure are based on the classification contingency (Table 3.2).

The accuracy is the percentage of correctly classified intervals out of the total number of intervals:

$$\text{accuracy} = (TP + TN) \div (TP + FP + FN + TN) \quad (3.27)$$

Table 3.2: Rain type classification contingency table

Model prediction of Rain Type	Observed Rain Type (pre-classification)	
	Convective	Stratiform
Convective	True Positive (TP)	False Positive (FP)
Stratiform	False Negative (FN)	True Negative (TN)

The F-measure is the harmonic average between the recall and the precision (Chinchor, 1992):

$$F - measure = (2 \times Recall \times Precesion) \div (Recall + Precesion) \quad (3.28)$$

where recall is the number of correctly identified convective rain intervals divided by the total number of actual convective rain intervals:

$$Recall = TP \div (TP + FN) \quad (3.29)$$

Precision is the number of correctly identified convective rain intervals divided by the total number of convective rain intervals as predicted by the model:

$$Precision = TP \div (TP + FP) \quad (3.30)$$

3.7.2 Performance indicators for regression models

The mean absolute error (MAE) of the rain intensity (R) estimations of each model was used as recommended by Willmott and Matsuura (2005). The R value based on Equation 3.1 is considered to be the accurate observed rain intensity, while the model outputs of R based on Z (as in equations 3.15 and 3.21) was considered to be the prediction. MAE is given as

$$MAE = n^{-1} \sum_{i=1}^n |e_i| \quad (3.31)$$

n is the number of observations,

e_i is the model prediction error:

$$e_i = Vm_i - Vo_i \quad (3.32)$$

Vm_i is the model prediction value.

Vo_i is the observed value.

i is the observation index.

The relative error was also used to assess the overestimation (or underestimation) of the total rain amount by both models for the entire dataset, as well as for each GWL-rain type combination:

$$RE = \sum(e_i) \div \sum(Vo_i) \quad (3.33)$$

3.8 Software used

For data handling, statistical analysis and visual representation of the results, R (R Core Team, 2019) and RStudio (RStudio Team, 2018) were used, in addition to the packages ggplot2 (Wickham, 2016), caret (Kuhn et al., 2018), e1071 (Meyer et al., 2018), MASS (Venables and Ripley, 2002), doSNOW (Microsoft Corporation and Weston, 2017), zoo (Zeileis and Grothendieck, 2005), maptools (Bivand and Lewin-Koh, 2018), reshape2 (Wickham, 2007), dplyr (Wickham et al., 2018), lubridate (Grolemund and Wickham, 2011), IMProToo (Maahn and Kollias, 2012), and pROC (Robin et al., 2011).

4 Publications: Summaries and contributions

The following publications provide the basis for this thesis:

- Wael Ghada, Ye Yuan, Clemens Wastl, Nicole Estrella, and Annette Menzel, “Precipitation Diurnal Cycle in Germany Linked to Large-Scale Weather Circulations”. *Atmosphere* 2019, 10, 545.
- Wael Ghada, Nicole Estrella, and Annette Menzel, “Machine Learning Approach to Classify Rain Type Based on Thies Disdrometers and Cloud Observations”. *Atmosphere* 2019, 10, 251.
- Wael Ghada, Enric Casellas, Joan Bech, Nicole Estrella, and Annette Menzel, “Stratiform and Convective Rain Classification Using Machine-learning Models and Micro Rain Radar and PARSIVEL Disdrometer data”. (under review) *Remote Sensing of Environment*.
- Wael Ghada, Allan Buras, Marvin Lübke, Christian Schunk, and Annette Menzel, “Rain Microstructure Parameters Vary with Large-Scale Weather Conditions in Lausanne, Switzerland”. *Remote Sensing* 2018, 10, 811.
- Wael Ghada, Joan Bech, Nicole Estrella, Andreas Hamman, and Annette Menzel, “Weather Types Affect Rain Microstructure: Implications for Quantitative Precipitation Estimates”. (submitted – *Remote Sensing*)

A summary of the results and details on the contributions are provided in the following pages. In the contributions, authors are abbreviated with their initials, for example, Wael Ghada as W.G. The five papers are attached to the end of the dissertation.

4.1 Precipitation Diurnal Cycle in Germany Linked to Large-Scale Weather Circulations

Ghada, W.; Yuan, Y.; Wastl, C.; Estrella, N.; Menzel, A.; Precipitation Diurnal Cycle in Germany Linked to Large-Scale Weather Circulations. *Atmosphere* 2019, 10, 545.

Abstract

The precipitation diurnal cycle (PDC) varies with the season and location. Its link to large-scale weather circulations has been studied in different regions. However, comparable information is lacking for Central Europe. Two decades of hourly precipitation data were combined with records of objective weather patterns over Germany, focusing on the general atmospheric wind directions (WD). The PDC is characterized by the frequency and the average amount of hourly precipitation. The precipitation frequency generally has two peaks: one in the morning and the other in the afternoon. The morning peak of the precipitation amount is small compared to that of the afternoon peak. Remarkably, WD has a prominent influence on the PDC. Days with southwesterly WD have a high afternoon peak and a lower morning peak, while days with northwesterly WD have a high morning peak and a lower afternoon peak. Furthermore, the seasonal variations of PDC are dominated by the seasonal frequency of WD classes. This study presents a general overview of the PDC in Germany with regard to its variation with seasonality, geographical location, elevation, and WD.

Contributions

W.G., N.E., and A.M. conceptualized the research idea. W.G. and Y.Y. processed the data. W.G. wrote the original draft. W.G. and C.W. interpreted the results. A.M. supervised the work. All coauthors contributed to reviewing and editing.

4.2 Machine Learning Approach to Classify Rain Type Based on Thies Disdrometers and Cloud Observations

Ghada, W.; Estrella, N.; Menzel, A. Machine Learning Approach to Classify Rain Type Based on Thies Disdrometers and Cloud Observations. *Atmosphere* 2019, 10, 251.

Abstract

Rain microstructure parameters assessed by disdrometers are commonly used to classify rain into convective and stratiform. However, different types of disdrometer result in different values for these parameters. This in turn potentially deteriorates the quality of rain type classifications. Thies disdrometer measurements at two sites in Bavaria in southern Germany were combined with cloud observations to construct a set of clear convective and stratiform intervals. This reference dataset was used to study the performance of classification methods from the literature based on the rain microstructure. We also explored the possibility of improving the performance of these methods by tuning the decision boundary. We further identified highly discriminant rain microstructure parameters and used these parameters in five machine-learning classification models. Our results confirm the potential of achieving high classification performance by applying the concepts of machine learning compared to already available methods. Machine-learning classification methods provide a concrete and flexible procedure that is applicable regardless of the geographical location or the device. The suggested procedure for classifying rain types is recommended prior to studying rain microstructure variability or any attempts at improving radar estimations of rain intensity.

Contributions

W.G. and A.M. conceptualized the research idea. W.G. processed the data and wrote the original draft. A.M. supervised the work. All coauthors contributed to reviewing and editing.

4.3 Stratiform and convective rain classification using machine-learning models and Micro Rain Radar and PARSIVEL disdrometer data

Ghada, W.; Casellas, E.; Bech, J.; Estrella, N.; Menzel, A.; “Stratiform and convective rain classification using machine-learning models and Micro Rain Radar and PARSIVEL disdrometer data”. (under review) Remote Sensing of Environment.

Abstract

Rain type classification is an essential step required to improve quantitative rain estimations by remote sensing instruments. It is also necessary to thoroughly understand the mechanisms behind the observed rain microstructure. However, classification procedures depend on the available rain observation instruments. A total of 20,979 min of rain data measured by a collocated PARSIVEL disdrometer and Micro Rain Radar (MRR) at Das in Northeast Spain were used to build and compare five types of machine-learning models for stratiform and convective rain type classification. The feature selection process based on the PARSIVEL parameters yielded similar results to that of a previous study in Bavaria in Southeast Germany using Thies disdrometers. The random forest model performed better than the remaining machine-learning models for both the MRR parameters and the PARSIVEL parameters. Models using PARSIVEL parameters achieved better results than those using MRR parameters when compared to previous simpler schemes of rain type classification. Several mixed rain events were used to assess the agreement between the models based on the two instruments. While only four parameters were sufficient in the case of PARSIVEL, six parameters were needed in the case of MRR to reach a reasonable model performance.

Contributions

W.G. and J.B. conceptualized the research idea. W.G. and E.C. processed the data. W.G. wrote the original draft. J.B. and A.M. supervised the work. All coauthors contributed to reviewing and editing.

4.4 Rain Microstructure Parameters Vary with Large-Scale Weather Conditions in Lausanne, Switzerland

Ghada, W.; Buras, A.; Lüpke, M.; Schunk, C.; Menzel, A.; Rain Microstructure Parameters Vary with Large-Scale Weather Conditions in Lausanne, Switzerland. *Remote Sensing*. 2018, 10, 811.

Abstract

Rain properties vary spatially and temporally for several reasons. In particular, rain types (convective and stratiform) affect the rain drop size distribution (DSD). It has also been established that local weather conditions are influenced by large-scale circulations. However, the effect of these circulations on rain microstructures has not been sufficiently addressed. Based on DSD measurements from 16 disdrometers located in Lausanne, Switzerland, we present evidence that rain DSD differs among general weather patterns (GWLs). GWLs were successfully linked to significant variations in the rain microstructure characterized by the most important rain properties: rain intensity (R), mass weighted rain drop diameter (D_m), and rain drop concentration (N), as well as $Z = AR^b$ parameters. Our results highlight the potential to improve radar-based estimations of rain intensity, which is crucial for several hydrological and environmental applications.

Contributions

W.G. and A.M. conceptualized the research idea. W.G. processed the data. A.B. and M.L. supported the data processing. W.G. wrote the original draft. A.M. supervised the work. All coauthors contributed to reviewing and editing.

4.5 Weather Types Affect Rain Microstructure: Implications for Quantitative Precipitation Estimates

Ghada, W; Bech, J.; Estrella, N.; Hamann, A.; Menzel, A.; Weather Types Affect Rain Microstructure: Implications for Quantitative Precipitation Estimates. (submitted to Remote Sensing)

Abstract

Quantitative precipitation estimation (QPE) through remote sensing has to take rain microstructure into consideration, because it influences the relationship between radar reflectivity Z and rain intensity R . For this reason, separate equations are used to estimate rain intensity of convective and stratiform rain types. Here, we investigate whether incorporating synoptic scale meteorology could yield further QPE improvements. Depending on large-scale weather types, variability in cloud condensation nuclei and the humidity content may lead to variation in rain microstructure. In a case study for Bavaria, we measured rain microstructure at ten locations with laser-based disdrometers, covering a combined 18,600 hours of rain in a period of 36 months. Rain was classified on a temporal scale of one minute into convective and stratiform based on a machine learning model. Large-scale wind direction classes were on a daily scale to represent the synoptic weather types. Significant variations in rain microstructure parameters were evident not only for rain types, but also for wind direction classes. The main contrast was observed between westerly and easterly circulations, with the latter characterized by smaller average size of drops and a higher average concentration. This led to substantial variation in the parameters of the radar rain intensity retrieval equation Z - R . The effect of wind direction on Z - R parameters was more pronounced for stratiform than convective rain types. We conclude that building separate Z - R retrieval equations for regional wind direction classes should improve radar-based QPE, especially for stratiform rain events.

Contributions

W.G. and A.M. conceptualized the research idea. W.G. processed the data and wrote the original draft. All coauthors contributed to reviewing and editing.

5 Discussion

This chapter discusses the major outcomes of the five papers. The questions stated in the introduction are addressed with respect to relevant and recent literature. Additionally, suggestions for potential future research are provided.

5.1 Precipitation diurnal cycle (PDC) in Germany

Hourly precipitation over Germany has a diurnal cycle characterized by two peaks in precipitation occurrence and amount. Those peaks happen near dawn (hereafter morning peak) and in the late afternoon (afternoon peak). They have similar magnitudes when it comes to precipitation frequency. However, the afternoon peak has a larger magnitude when it comes to precipitation amount.

The most remarkable finding of this particular study is the strong variation in PDC under the influence of weather types. This variation is clearly visible in the two most occurring weather types, namely SW and NW. In the case of SW, the morning peak of both precipitation frequency and amount is always smaller than the afternoon peak. The exact opposite is evident in the case of NW, for which the morning peak is larger than the afternoon peak. This finding is consistent regardless of the season and location over Germany.

Two major processes contribute to the observed PDC, radiative cooling and convection. Both processes are influenced by the energy content of moving air parcels. This energy content is in turn dependent on the flow direction, especially NW (SW) circulation is mostly influenced by the cold (warm) polar (subtropical) jet stream.

Radiative cooling is active in stratiform clouds over night when condensation initiates and intensifies as temperatures drop. This intensification continues until dawn when the solar energy suppresses it. The whole process intensifies in the case of NW circulations when the incoming air parcels are cold. In contrast, when the incoming air parcels are warm in the case of SW, the radiative cooling is not as efficient. The morning precipitation peak was reported and discussed for locations in Asia (Li et al., 2008; Oki and Musiak, 1994), North America (Landin and Bosart, 1989), and Europe (Jeong et al., 2011; Twardosz, 2007; Svensson and Jakob, 2002) with focus on the seasonal and spatial variations. Some studies attribute the morning peak to convection in areas adjacent to water bodies (Zheng et al., 2019; Mori et al., 2004; Chen et al., 2016b) or topography (Kubota and Nitta, 2001). Such processes cannot be the main reason for the morning peak over Germany. A similar conclusion has been reported for Austria (Yaqub et al., 2011). This suggests that stratiform precipitation and radiative cooling play the decisive

role in the observed morning peak.

Convection requires sufficient energy input to heat air parcels forcing them to ascend. This happens during the day when energy accumulates as long as the incoming solar radiation is larger than the outgoing longwave radiation, which explains the afternoon peak. Convection is intensified in the case of SW and suppressed in the case on NW because of the energy content of air parcels carried along these circulations. Additionally, cloud formation during the night by radiative cooling blocks solar energy in the beginning of the day which further suppresses convection (Xiao et al., 2018). Such influence might happen more often in NW circulations compared to SW.

The importance of weather circulations in controlling the PDC over Germany was addressed for the first time in this study. However, and despite the fact that no discrimination between convective and stratiform precipitation was performed, the observations suggest a strong influence of the different formation processes associated with both types. This also makes it crucial to classify rain into convective and stratiform prior to addressing the rain microstructure.

5.2 Classification of rain type into convective and stratiform

Classifying rain into convective and stratiform based on the microstructure needs to be adjusted for the variations that originate from using different measuring devices, and the different regions. For example, Bringi et al. (Bringi et al., 2009) used the normalized intercept parameter (NW) and the median volume diameter (D0) to classify rain measured with a Joss disdrometer at Darwin, Australia. You et al. (You et al., 2016) adjusted the separation scheme of Bringi et al. (Bringi et al., 2009) to be suitable for PARSIVEL disdrometer in Korea.

With a few exceptions only, these simple dual classification schemes were designed based on a limited number of events. A separation line was chosen to separate the convective and stratiform regions somehow subjectively. Using a clear pre-classified dataset, and a linear discriminant model, the performance indicators of available classification schemes can be improved significantly. Out of the available simple dual parameters classification schemes, the method of Bringi et al. (Bringi et al., 2009) achieved the highest performance compared to the other simple classification schemes. The Bringi method performed again best when using the linear discriminant model, which implies the importance of the two parameters N_w and D_0 .

Only in one other case, four parameters were used to classify rain using the naïve bays approach (Bukovčić et al., 2015). This model clearly gave a better classification in comparison to all the other simple classification schemes. This was an indicator for the potential of using machine learning predictive models to classify rain.

The top rain type classifiers in each of the two disdrometers were:

- For Thies: sd_N_{10} , sd_D0_{10} , $sd_log_{10}R_{10}$, R .
- For PARSIVEL: R , $sd_log_{10}R_{10}$, sd_Dm_{10} , sd_N_{10} .

Apart from the order of the selected parameters, the only difference in the case of PARSIVEL was choosing `sd_Dm_10` instead of `sd_D0_10`. This difference is negligible, especially because both parameters are highly correlated representations of the drop size variation. Despite the consistency in feature selection for two different types of disdrometers in two locations, this selection should not be taken for granted, especially because it may highly depend on the pre-classification dataset. It might be appropriate to use the same features to classify rain using the same device type for nearby locations. However, a better practice would be to identify for each case the list of appropriate classification parameters based on carefully selected pre-classified dataset, at least until further research confirms the suitability and performance stability of the listed parameters in other locations.

To classify rain based on MRR records, a common step would be to detect the bright band as the echo of the melting layer which is in turn a strong indicator of stratiform rain (White et al., 2003; Sarkar et al., 2015). A peak in Z value is not the only indicator for the bright band, but spectral width (Cifelli et al., 2000) and Doppler velocity (Massmann et al., 2017; Gil-de Vergara et al., 2018) can be used to detect it. However, this detection should not be the sole criteria for classifying rain type. The classification in such cases is based on the records in one interval (one minute in this case). This might produce variations in the melting layer elevation in the adjacent intervals, which in turn allows for subjective interpretation. For our work, the detection of bright band is replaced by determination of a separation level (SL). This level is always available regardless of rain type and represents the level where Doppler velocity increases the most. This separation level was the key factor in generating 18 other parameters which represented the input for the machine learning classification models. The list of the best six MRR parameters to be used as classifiers include `SW_upper`, `Z_lower`, `W_lower`, `SL`, `sd_Z`, `W_upper`. No comparable method could be found in the literature to be discussed here. However the classification performance using these parameters in a random forest model was very similar to the performance of the best classification model using disdrometer output.

The three machine learning models proposed in this work can be easily deployed at the operational level. Each model needs to be trained once using a well-selected pre-classified dataset. The progress in machine learning makes it very realistic to classify rain using other remote sensors with a very high classification quality, especially by applying image recognition techniques.

5.3 Rain microstructure

5.3.1 Rain DSD variation

This work highlighted the difference in rain microstructure between stratiform rain and convective rain for two locations in Central Europe. Generally speaking, convective rain has larger drops, more drops per cubic meter and higher intensities compared to stratiform rain. The key finding in this work is that WTs have consistent patterns of

rain microstructure for stratiform rain. These different patterns can be explained by the variation of available humidity and condensation nuclei in the advecting air in different WTs. However, in the case of convective rain, those patterns do not apply, which implies the larger influence of local meteorological conditions during convective rain events.

Southwestern circulations were associated with a high average rain intensity, a high average drop size and low average drop concentration. Eastern and northeastern circulations had low rain intensities, small drop size, and a low drop concentration. This contrast was evident at both locations in Bavaria and Lausanne. Similar contrasts between southwesterly and northeasterly flows were reported in the Cévennes-Vivarais region, France. (Hachani et al., 2017). Also for the Iberian Peninsula, western and southwestern flows with air masses carrying humidity from the Atlantic cause rain events with large drops, while northern flows tend to have small rain drops (Fernandez-Raga et al., 2017).

To explain the contrast in rain microstructure among WTs, especially in drop size and drop concentrations, we need to consider the variation in humidity and cloud condensation nuclei (CCN) with flow direction. Westerly circulations in Central Europe represent the major carrier of moisture which comes mainly from the Atlantic, in contrast to the easterly circulations which are mainly of a continental dry origin (Van der Ent et al., 2010). On the other hand, anthropogenic activities play a decisive role in the variation of CCN. CCN availability is influenced by aerosols (Lohmann and Feichter, 2005), and especially in stratiform rain, drop concentration is significantly higher in cases of polluted events (Zhang et al., 2019; Cecchini et al., 2014). High concentrations of aerosols were reported at Melpitz, Saxonia, Germany for flows which pass over Russia, Central Europe and Eastern Europe (Birmili et al., 2001). High particle number concentrations in Lithuania were associated with flows over heavily industrialized areas in Germany, the Czech Republic, and Poland (Byčenkienė et al., 2014).

In westerly and southwesterly flows, the smaller CCN numbers do not allow a high drop concentration. However, the high water content in the clouds favor drops to grow in size. In easterly flows, lower humidity makes the growth of drop sizes more difficult. Additionally, the higher abundance of CCN means that the available water content is distributed over a larger number of drops.

There is a complex interaction between rain formation processes and the available energy, water content and CCN. Additionally, drops may undergo many other processes which influence the microstructure as measured on the ground, such as drop breakup, evaporation, and collision-coalescence. However, the provided explanation is a simple overview of observed influence of WTs over rain microstructure in Central Europe. These important findings are summarized in Table 1.

5.3.2 Optimizing retrieval algorithms for rain intensity

The parameters of rain intensity retrieval algorithm by radars $Z=AR^b$ depend on the variability of rain DSD (Uijlenhoet and Pomeroy, 2001; Lee and Zawadzki, 2005). This in turn means that A and b values vary with rain type, geographical location and season

Table 5.1: Summary of the influence of WT on precipitation properties

Flow direction	Drivers	Observed impacts on rain properties
E	High CCN	Higher drop concentration Smaller drops
S	Warm air parcels	Intensified convection, stronger afternoon peak Suppressed radiative cooling, smaller morning peak
W	High humidity	Higher rain intensities Larger drops
N	Cold air parcels	Intensified radiative cooling, stronger morning peak Suppressed convection, smaller afternoon peak

(Jaffrain and Berne, 2012). We hypothesized in this work, because of the associated variability in DSD, that A and b values differ between flow directions. The variation in A and b values across rainfall regimes has been addressed only scarcely so far. For example, distinct A and b values were found for the periods before, during and after the monsoon season for the south China sea (Zeng et al., 2019). The variation in Z-R relation parameters with WTs was also demonstrated for Cévennes-Vivarais, France. (Hachani et al., 2017).

In this work, and following the classical procedure (see section 3.6.1.) A and b values were obtained for Lausanne Switzerland with significant variation between WTs. This variability was evident in both rain types. The variability of A and b values with WTs exceeded the spatial variability which was reported previously for the same dataset (Jaffrain and Berne, 2012). This is an indicator of the potential improvement in retrieving R associated with considering separate equations for each WT. The improvement was particularly high within some WTs, especially the most frequent. Only in one other study in central Europe that Z-R relations were found to vary with WTs (Hachani et al., 2017), however the combined effect of WTs and rain type was not addressed.

Similar conclusions were reached when using the classical and the modified retrieval procedure for A and b for the ten locations in Bavaria (see section 3.6.2.). A and b values which are acquired for each flow direction separately varied substantially. This variation exceeds A and b spatial variation within the addressed regional scale in the case of stratiform rain, and at least is similar to the spatial variation in the case of convective rain. Jaffrain and Berne (Jaffrain and Berne, 2012) quantified an error range in the rain measurement between -2% and $+15\%$ based on the subgrid (less than 1 km^2) spatial variability of rain microstructure. Generally, the spatial variability of rain microstructure is expected to be higher for the addressed regional scale in Bavaria (more than $30,000 \text{ km}^2$). Consequently, the potential for a large improvement in rain estimation when accounting for rain microstructure variability with WD is expected to be high.

The results of both papers must be considered as an indicator for the potential

improvement when considering WTs. A more precise estimation of this needs to be based on actual Z values taken from radar measurements. Only in this case it would be possible to provide a plausible judgement on the practical use of WT-specific R retrieval algorithms. This issue has not been addressed in this work. However, it is the next logical step to take.

6 Conclusions

Precipitation properties vary under the influence of WTs. This variation manifests itself in the precipitation diurnal cycle, the frequency of convective and stratiform rain, and the rain microstructure.

Convection is intensified, and radiative cooling is suppressed in the case of southerly flows, but suppressed, intensified in the northerly flows, respectively. This influences the precipitation diurnal cycle by strengthening (weakening) the afternoon peak in comparison with the morning peak.

WTs associated with southerly flows have higher proportions of convective rain in comparison to northerly flows. The imbalance in convection frequency among WTs, if not considered, may influence the detected variations in rain properties. Consequently, it is essential to address the quality of the available rain type classification methods.

Simple dual parameter classification methods, which use rain microstructure parameters can be improved simply by an objective specification of the decision boundary. However, machine learning models, specifically random forests, provide much higher classification performance. This high performance is achieved regardless of the involved measuring instrument (Thies disdrometer, PARSIVEL disdrometer, or MRR). The choice of best rain microstructure parameters to be used as classifiers is suggested to be spatially stable (Bavaria and northeastern Spain).

In stratiform rain, westerly and southwesterly flows are characterized by high rain intensities and large drops on average because they represent the main direction of humidity transport from the Atlantic and the Mediterranean to Central Europe. Easterly flows have low rain intensities, small drops and high drop concentrations. This is because the easterly flows are typically dry with high aerosol concentrations which act as cloud condensation nuclei. Rain microstructure varies also for the case of convective rain. However, this variation has a different pattern in comparison with stratiform rain, and it is not spatially consistent which might indicate a higher influence of local weather conditions.

The parameters in the rain intensity retrieval equation vary between WTs for both rain types. This variation leads to improvements in rain retrieval performance at least for the most frequent WTs. A plausible judgement on the practical use of WT-specific R retrieval algorithms requires actual radar measurements to be used.

Understanding the influence of WTs on the precipitation diurnal cycle aids in the development of numerical weather models, particularly because the accuracy of a climate model on a daily scale reflects its quality in properly representing the physical processes or in parameterizing them. Additionally, the rain microstructure variation with the large-scale wind direction can be further utilized to investigate the variation in rain

kinetic energy and its influence on soil erosion. Moreover, the potential improvement of the rain retrieval algorithms is of great interest for hydrological and environmental applications.

7 Outlook

Future research may address the following points:

- Precipitation properties associated with advection of cold fronts and warm fronts may carry further insight into the combined effect of precipitation type and WTs. The formation processes controlling the potential variation between cold and warm fronts could be investigated to enrich the knowledge regarding the development of rain microstructure, and consequently the QPE by remote sensing.
- Heavy and extreme rain events are of special interest for flood studies. Investigating the PDC of such events might reveal different patterns opposed to the ones shown in this work. WTs might be associated with distinct probabilities of heavy-short rain events, and events with long durations.
- Additionally, heavy and extreme rain microstructure for each WT, and the spatial and temporal variation of rain properties in such events require long-term measurements using a dense network of devices. Such a dataset is not yet available.
- Machine learning and artificial intelligence are promising tools in the field of meteorology. Rain type classification used in this thesis is one of the simplest successful examples. Image recognition technique might be especially suitable for radar and satellite outputs.
- Mostly, this work focused on the aspect of flow direction of WTs. However, WTs carry further information such as the cyclonality index and humidity index in the case of the objective weather type classification. These indices could have further influence on rain microstructure and the QPE.
- Previous studies have already investigated the influence of climate change on convective rainfall. Other studies tried to identify trends in the frequency of WTs and in meteorological characteristics within each WT. Consideration of trends in frequency and rain properties within each combination of weather type and rain type remains to be clarified.

References

- Adirosi, E., Roberto, N., Montopoli, M., Gorgucci, E., and Baldini, L. (2018). Influence of disdrometer type on weather radar algorithms from measured dsd: Application to italian climatology. *Atmosphere*, 9(9):360.
- Ahrens, C. D. (2009). *Meteorology today: An introduction to weather, climate, and the environment*. Brooks/Cole CengageLearning, Belmont CA, 9th ed. edition.
- Ahrens, C. D. (2015). *Essentials of meteorology: An invitation to the atmosphere*. Cengage Learning, Stamford, CT, seventh edition edition.
- American Meteorological Society (2020). "radar reflectivity". glossary of meteorology.
- Angulo-Martínez, M., Beguería, S., Latorre, B., and Fernández-Raga, M. (2018). Comparison of precipitation measurements by ott parsivel 2 and thies lpm optical disdrometers. *Hydrology and Earth System Sciences*, 22(5):2811–2837.
- Atlas, D., Srivastava, R. C., and Sekhon, R. S. (1973). Doppler radar characteristics of precipitation at vertical incidence. *Reviews of Geophysics*, 11(1):1.
- Baur, F., Hess, P., and Nagel, H. (1944). Kalender der grosswetterlagen europas 1881–1939. *Bad Homburg*, 35.
- Beard, K. V. and Ochs, H. T. (1993). Warm-rain initiation: An overview of microphysical mechanisms. *Journal of Applied Meteorology*, 32(4):608–625.
- Beck, C. and Philipp, A. (2010). Evaluation and comparison of circulation type classifications for the european domain. *Physics and Chemistry of the Earth, Parts A/B/C*, 35(9-12):374–387.
- Birmili, W., Wiedensohler, A., Heintzenberg, J., and Lehmann, K. (2001). Atmospheric particle number size distribution in central europe: Statistical relations to air masses and meteorology. *Journal of Geophysical Research*, 106(D23):32005–32018.
- Bivand, R. and Lewin-Koh, N. (2018). maptools: Tools for handling spatial objects. <https://CRAN.R-project.org/package=maptools> (Accessed on 22 January 2020).
- Brdossy, A. and Caspary, H. J. (1990). Detection of climate change in europe by analyzing european atmospheric circulation patterns from 1881 to 1989. *Theoretical and Applied Climatology*, 42(3):155–167.

- Bringi, V. N., Chandrasekar, V., Hubbert, J., Gorgucci, E., Randeu, W. L., and Schoenhuber, M. (2003). Raindrop size distribution in different climatic regimes from disdrometer and dual-polarized radar analysis. *Journal of the Atmospheric Sciences*, 60(2):354–365.
- Bringi, V. N., Williams, C. R., Thurai, M., and May, P. T. (2009). Using dual-polarized radar and dual-frequency profiler for dsd characterization: A case study from darwin, australia. *Journal of Atmospheric and Oceanic Technology*, 26(10):2107–2122.
- Broderick, C. and Fealy, R. (2015). An analysis of the synoptic and climatological applicability of circulation type classifications for ireland. *International Journal of Climatology*, 35(4):481–505.
- Buishand, T. A. and Brandsma, T. (1997). Comparison of circulation classification schemes for predicting temperature and precipitation in the netherlands. *International Journal of Climatology*, 17(8):875–889.
- Bukovčić, P., Zrnić, D., and Zhang, G. (2015). Convective–stratiform separation using video disdrometer observations in central oklahoma – the bayesian approach. *Atmospheric Research*, 155:176–191.
- Byčenkienė, S., Plauškaitė, K., Dudoitis, V., and Ulevicius, V. (2014). Urban background levels of particle number concentration and sources in vilnius, lithuania. *Atmospheric Research*, 143:279–292.
- Cahynová, M. and Huth, R. (2016). Atmospheric circulation influence on climatic trends in europe: an analysis of circulation type classifications from the cost733 catalogue. *International Journal of Climatology*, 36(7):2743–2760.
- Caracciolo, C., Porcù, F., and Prodi, F. (2008). Precipitation classification at mid-latitudes in terms of drop size distribution parameters. *Advances in Geosciences*, 16:11–17.
- Caracciolo, C., Prodi, F., Battaglia, A., and Porcu', F. (2006). Analysis of the moments and parameters of a gamma dsd to infer precipitation properties: A convective stratiform discrimination algorithm. *Atmospheric Research*, 80(2-3):165–186.
- Cassano, E. N., Lynch, A. H., Cassano, J. J., and Koslow (2006). Classification of synoptic patterns in the western arctic associated with extreme events at barrow, alaska, usa. *Climate Research*, 30:83–97.
- Cecchini, M. A., Machado, L. A., and Artaxo, P. (2014). Droplet size distributions as a function of rainy system type and cloud condensation nuclei concentrations. *Atmospheric Research*, 143:301–312.
- Chen, B., Wang, J., and Gong, D. (2016a). Raindrop size distribution in a midlatitude continental squall line measured by thies optical disdrometers over east china. *Journal of Applied Meteorology and Climatology*, 55(3):621–634.

- Chen, X., Zhang, F., and Zhao, K. (2016b). Diurnal variations of the land–sea breeze and its related precipitation over south china. *Journal of the Atmospheric Sciences*, 73(12):4793–4815.
- Chen, Y. (2004). *GIS and remote sensing in hydrology, water resources and environment*, volume 289 of *IAHS publication*. International Association of Hydrological Sciences, Wallingford.
- Chinchor, N. (1992). Muc-4 evaluation metrics. In *Proceedings of the 4th Conference on Message Understanding, MUC4 '92*, page 22–29, USA. Association for Computational Linguistics.
- Cifelli, R., Williams, C. R., Rajopadhyaya, D. K., Avery, S. K., Gage, K. S., and May, P. T. (2000). Drop-size distribution characteristics in tropical mesoscale convective systems. *Journal of Applied Meteorology*, 39(6):760–777.
- Cony, M., Martán, L., Hernández, E., and Del Teso, T. (2010). Synoptic patterns that contribute to extremely hot days in europe. *Atmósfera*, 23:295–306.
- Cortesi, N., Trigo, R. M., Gonzalez-Hidalgo, J. C., and Ramos, A. M. (2013). Modelling monthly precipitation with circulation weather types for a dense network of stations over iberia. *Hydrology and Earth System Sciences*, 17(2):665–678.
- Corti, S., Molteni, F., and Palmer, T. N. (1999). Signature of recent climate change in frequencies of natural atmospheric circulation regimes. *Nature*, 398(6730):799–802.
- Fernandez-Raga, M., Castro, A., Marcos, E., Palencia, C., and Fraile, R. (2017). Weather types and rainfall microstructure in leon, spain. *International Journal of Climatology*, 37(4):1834–1842.
- Ferrier, B. S., Tao, W.-K., and Simpson, J. (1995). A double-moment multiple-phase four-class bulk ice scheme. part ii: Simulations of convective storms in different large-scale environments and comparisons with other bulk parameterizations. *Journal of the Atmospheric Sciences*, 52(8):1001–1033.
- Friedrich, K., Kalina, E. A., Masters, F. J., and Lopez, C. R. (2013). Drop-size distributions in thunderstorms measured by optical disdrometers during vortex2. *Monthly Weather Review*, 141(4):1182–1203.
- Gerstengarbe, F.-W., Hess, P., and Brezowsky, H. (1993). *Katalog der Grosswetterlagen Europas nach Paul Hess und Helmuth Brezowski: 1881-1992*. Selbstverlag des Deutschen Wetterdienstes, Offenbach am Main, 4. voll. neu bearbeitete aufl. edition.
- Gil-de Vergara, N., Riera, J. M., Pérez-Peña, S., Garcia-Rubia, J., and Benarroch, A. (2018). Classification of rainfall events and evaluation of drop size distributions using a k-band doppler radar. In *EuCAP 2018*, pages 829 (5 pp.)–829 (5 pp.), [S. 1.]. EurAAP = European Association for Antennas and Propagation.

- Gonzalez, S., Bech, J., Udina, M., Codina, B., Paci, A., and Trapero, L. (2019). Decoupling between precipitation processes and mountain wave induced circulations observed with a vertically pointing k-band doppler radar. *Remote Sensing*, 11(9):1034.
- Grolemund, G. and Wickham, H. (2011). Dates and times made easy with lubridate. *Journal of Statistical Software*, 40(3):1–25.
- Grundström, M., Dahl, Å., Ou, T., Chen, D., and Pleijel, H. (2017). The relationship between birch pollen, air pollution and weather types and their effect on antihistamine purchase in two swedish cities. *Aerobiologia*, 33(4):457–471.
- Guyot, A., Pudashine, J., Protat, A., Uijlenhoet, R., Pauwels, V., Seed, A., and Walker, J. P. (2019). Effect of disdrometer type on rain drop size distribution characterisation: a new dataset for south-eastern australia. *Hydrology and Earth System Sciences*, 23(11):4737–4761.
- Hachani, S., Boudevillain, B., Delrieu, G., and Bargaoui, Z. (2017). Drop size distribution climatology in cévennes-vivarais region, france. *Atmosphere*, 8(12):233.
- Houze, J. R. A. (2014). *Cloud Dynamics: International Geophysics*. Academic Press.
- Houze, R. A. (1997). Stratiform precipitation in regions of convection: A meteorological paradox? *Bulletin of the American Meteorological Society*, 78(10):2179–2196.
- Hudson, J. G. (2002). Cloud condensation nuclei spectra and polluted and clean clouds over the indian ocean. *Journal of Geophysical Research*, 107(D19):16,625.
- Hurrell, J. W. (1995). Decadal trends in the north atlantic oscillation: regional temperatures and precipitation. *Science (New York, N.Y.)*, 269(5224):676–679.
- Hurrell, J. W. and van Loon, H. (1997). Decadal variations in climate associated with the north atlantic oscillation. *Climatic Change*, 36(3/4):301–326.
- Huth, R. (2010). Synoptic-climatological applicability of circulation classifications from the cost733 collection: First results. *Physics and Chemistry of the Earth, Parts A/B/C*, 35(9-12):388–394.
- Huth, R., Beck, C., and Kučerová, M. (2016). Synoptic-climatological evaluation of the classifications of atmospheric circulation patterns over europe. *International Journal of Climatology*, 36(7):2710–2726.
- Huth, R., Beck, C., Philipp, A., Demuzere, M., Ustrnul, Z., Cahynová, M., Kyselý, J., and Tveito, O. E. (2008). Classifications of atmospheric circulation patterns: recent advances and applications. *Annals of the New York Academy of Sciences*, 1146:105–152.
- Jacobeit, J., Glaser, R., Luterbacher, J., and Wanner, H. (2003). Links between flood events in central europe since ad 1500 and large-scale atmospheric circulation modes. *Geophysical Research Letters*, 30(4):292.

- Jaffrain, J. and Berne, A. (2012). Influence of the subgrid variability of the raindrop size distribution on radar rainfall estimators. *Journal of Applied Meteorology and Climatology*, 51(4):780–785.
- Jeong, J.-H., Walther, A., Nikulin, G., Chen, D., and Jones, C. (2011). Diurnal cycle of precipitation amount and frequency in sweden: observation versus model simulation. *Tellus A: Dynamic Meteorology and Oceanography*, 63(4):664–674.
- Jones, P. D., Davies, T. D., Lister, D. H., Slonosky, V., Jónsson, T., Barring, L., Jönsson, P., Maheras, P., Kolyva-Machera, F., Barriendos, M., Martin-Vide, J., Rodriguez, R., Alcoforado, M. J., Wanner, H., Pfister, C., Luterbacher, J., Rickli, R., Schuepbach, E., Kaas, E., Schmith, T., Jacobeit, J., and Beck, C. (1999). Monthly mean pressure reconstructions for europe for the 1780–1995 period. *International Journal of Climatology*, 19(4):347–364.
- Kanofsky, L. and Chilson, P. (2008). An analysis of errors in drop size distribution retrievals and rain bulk parameters with a uhf wind profiling radar and a two-dimensional video disdrometer. *Journal of Atmospheric and Oceanic Technology*, 25(12):2282–2292.
- Kassomenos, P. (2010). Synoptic circulation control on wild fire occurrence. *Physics and Chemistry of the Earth, Parts A/B/C*, 35(9):544–552.
- Kathiravelu, G., Lucke, T., and Nichols, P. (2016). Rain drop measurement techniques: A review. *Water*, 8(1):29.
- Kinnell, P. I. A. (1976). Some observations on the joss-waldvogel rainfall disdrometer. *Journal of Applied Meteorology*, 15(5):499–502.
- Kirsch, B., Clemens, M., and Ament, F. (2019). Stratiform and convective radar reflectivity–rain rate relationships and their potential to improve radar rainfall estimates. *Journal of Applied Meteorology and Climatology*, 58(10):2259–2271.
- Kubota, H. and Nitta, T. (2001). Diurnal variations of tropical convection observed during the toga-coare. *Journal of the Meteorological Society of Japan*, 79(3):815–830.
- Kuhn, M. and Johnson, K. (2016). *Applied predictive modeling*. Springer, New York, corrected at 5th printing edition.
- Kuhn, M., Wing, J., Weston, S., Williams, A., Keefer, C., Engelhardt, A., Cooper, T., Mayer, Z., Kenkel, B., the R Core Team, Benesty, M., Lescarbeau, R., Ziem, A., Scrucca, L., Tang, Y., Candan, C., and Hunt, T. (2018). caret: Classification and regression training.
- Kyselý, J. and Huth, R. (2006). Changes in atmospheric circulation over europe detected by objective and subjective methods. *Theoretical and Applied Climatology*, 85(1-2):19–36.

- Landin, M. G. and Bosart, L. F. (1989). The diurnal variation of precipitation in california and nevada. *Monthly Weather Review*, 117(8):1801–1816.
- Lee, G. W. and Zawadzki, I. (2005). Variability of drop size distributions: Time-scale dependence of the variability and its effects on rain estimation. *Journal of Applied Meteorology*, 44(2):241–255.
- Li, J., Yu, R., and Zhou, T. (2008). Seasonal variation of the diurnal cycle of rainfall in southern contiguous china. *Journal of Climate*, 21(22):6036–6043.
- Löffler-Mang, M., Kunz, M., and Schmid, W. (1999). On the performance of a low-cost k-band doppler radar for quantitative rain measurements. *Journal of Atmospheric and Oceanic Technology*, 16(3):379–387.
- Lohmann, U. and Feichter, J. (2005). Global indirect aerosol effects: a review. *Atmospheric Chemistry and Physics*, 5(3):715–737.
- Maahn, M. and Kollias, P. (2012). Improved micro rain radar snow measurements using doppler spectra post-processing. *Atmospheric Measurement Techniques*, 5(11):2661–2673.
- Maheras, P., Tolika, K., Anagnostopoulou, C., Makra, L., Szpirosz, K., and Károssy, C. (2018). Relationship between mean and extreme precipitation and circulation types over hungary. *International Journal of Climatology*, 38(12):4518–4532.
- Markowski, P. and Richardson, Y. (2010). *Mesoscale meteorology in midlatitudes*. Advancing weather and climate science. Wiley-Blackwell, Chichester.
- Marshall, J. S. and Palmer, W. M. K. (1948). The distribution of raindrops with size. *Journal of Meteorology*, 5(4):165–166.
- Marzano, F. S., Cimini, D., and Montopoli, M. (2010). Investigating precipitation microphysics using ground-based microwave remote sensors and disdrometer data. *Atmospheric Research*, 97(4):583–600.
- Marzuki, M., Randeu, W. L., Schönhuber, M., Bringi, V. N., Kozu, T., and Shimomai, T. (2010). Raindrop size distribution parameters of distrometer data with different bin sizes. *IEEE Transactions on Geoscience and Remote Sensing*, 48(8):3075–3080.
- Massmann, A. K., Minder, J. R., Garreaud, R. D., Kingsmill, D. E., Valenzuela, R. A., Montecinos, A., Fults, S. L., and Snider, J. R. (2017). The chilean coastal orographic precipitation experiment: Observing the influence of microphysical rain regimes on coastal orographic precipitation. *Journal of Hydrometeorology*, 18(10):2723–2743.
- Meyer, D., Dimitriadou, E., Hornik, K., Weingessel, A., and Leisch, F. (2018). e1071: Misc functions of the department of statistics, probability theory group (formerly: E1071), tu wien. <https://CRAN.R-project.org/package=e1071>.

-
- Microsoft Corporation and Weston, S. (2017). dosnow: Foreach parallel adaptor for the 'snow' package. <https://CRAN.R-project.org/package=doSNOW>.
- Mori, S., Jun-Ichi, H., Tauhid, Y. I., Yamanaka, M. D., Okamoto, N., Murata, F., Sakurai, N., Hashiguchi, H., and Sribimawati, T. (2004). Diurnal land–sea rainfall peak migration over sumatera island, indonesian maritime continent, observed by trmm satellite and intensive rawinsonde soundings. *Monthly Weather Review*, 132(8):2021–2039.
- Nidzgorska-Lencewicz, J. and Czarnecka, M. (2015). Winter weather conditions vs. air quality in tricity, poland. *Theoretical and Applied Climatology*, 119(3-4):611–627.
- Nied, M., Pardowitz, T., Nissen, K., Ulbrich, U., Hundecha, Y., and Merz, B. (2014). On the relationship between hydro-meteorological patterns and flood types. *Journal of Hydrology*, 519:3249–3262.
- Nikolopoulos, E. I., Borga, M., Marra, F., Crema, S., and Marchi, L. (2015). Debris flows in the eastern italian alps: seasonality and atmospheric circulation patterns. *Natural Hazards and Earth System Sciences*, 15(3):647–656.
- Niu, S., Jia, X., Sang, J., Liu, X., Lu, C., and Liu, Y. (2010). Distributions of raindrop sizes and fall velocities in a semiarid plateau climate: Convective versus stratiform rains. *Journal of Applied Meteorology and Climatology*, 49(4):632–645.
- Nowosad, J. and Stach, A. (2014). Relation between extensive extreme precipitation in poland and atmospheric circulation. *Quaestiones Geographicae*, 33(1):115–129.
- Oki, T. and Musiaka, K. (1994). Seasonal change of the diurnal cycle of precipitation over japan and malaysia. *Journal of Applied Meteorology*, 33(12):1445–1463.
- OTT Hydromet (2020). Operating instructions, present weather sensor: Ott parsivel2. <https://www.ott.com/download/operating-instructions-present-weather-sensor-ott-parsivel2-without-screen-heating/> (Accessed on 22 January 2020).
- Petrow, T., Merz, B., Lindenschmidt, K.-E., and Thielen, A. H. (2007). Aspects of seasonality and flood generating circulation patterns in a mountainous catchment in south-eastern germany. *Hydrology and Earth System Sciences*, 11(4):1455–1468.
- Petrů, J. and Kalibová, J. (2018). Measurement and computation of kinetic energy of simulated rainfall in comparison with natural rainfall. *Soil and Water Research*, 13(No. 4):226–233.
- Philipp, A., Della-Marta, P. M., Jacobeit, J., Fereday, D. R., Jones, P. D., Moberg, A., and Wanner, H. (2007). Long-term variability of daily north atlantic–european pressure patterns since 1850 classified by simulated annealing clustering. *Journal of Climate*, 20(16):4065–4095.

- Planchon, O., Quénol, H., Dupont, N., and Corgne, S. (2009). Application of the hess-brezowsky classification to the identification of weather patterns causing heavy winter rainfall in brittany (france). *Natural Hazards and Earth System Sciences*, 9(4):1161–1173.
- R Core Team (2019). R: A language and environment for statistical computing. <https://www.R-project.org/> (Accessed on 22 January 2020).
- Ramos, A. M., Barriopedro, D., and Dutra, E. (2015). Circulation weather types as a tool in atmospheric, climate, and environmental research. *Frontiers in Environmental Science*, 3.
- Rangno, A. L. (2015). Clouds and fog | classification of clouds. In North, G. R., Zhang, F., and Pyle, J., editors, *Encyclopedia of Atmospheric Sciences (Second Edition)*, pages 141–160. Academic Press.
- Rebetez, M. and Reinhard, M. (2008). Monthly air temperature trends in switzerland 1901–2000 and 1975–2004. *Theoretical and Applied Climatology*, 91(1-4):27–34.
- Robin, X., Turck, N., Hainard, A., Tiberti, N., Lisacek, F., Sanchez, J.-C., and Müller, M. (2011). proc: an open-source package for r and s+ to analyze and compare roc curves. *BMC Bioinformatics*, 12:77.
- RStudio Team (2018). Rstudio: Integrated development environment for r. <http://www.rstudio.com/> (Accessed on 22 January 2020).
- Russo, A., Trigo, R. M., Martins, H., and Mendes, M. T. (2014). No₂, pm₁₀ and o₃ urban concentrations and its association with circulation weather types in portugal. *Atmospheric Environment*, 89:768–785.
- Sarkar, T., Das, S., and Maitra, A. (2015). Assessment of different raindrop size measuring techniques: Inter-comparison of doppler radar, impact and optical disdrometer. *Atmospheric Research*, 160:15–27.
- Schiemann, R. and Frei, C. (2010). How to quantify the resolution of surface climate by circulation types: An example for alpine precipitation. *Physics and Chemistry of the Earth, Parts A/B/C*, 35(9-12):403–410.
- Sheridan, S. C. and Lee, C. C. (2010). Synoptic climatology and the general circulation model. *Progress in Physical Geography: Earth and Environment*, 34(1):101–109.
- Steiner, M. and Smith, J. A. (1998). Convective versus stratiform rainfall: An ice-microphysical and kinematic conceptual model. *Atmospheric Research*, 47-48:317–326.
- Steirou, E., Gerlitz, L., Apel, H., and Merz, B. (2017). Links between large-scale circulation patterns and streamflow in central europe: A review. *Journal of Hydrology*, 549:484–500.
- Svensson, C. and Jakob, D. (2002). Diurnal and seasonal characteristics of precipitation at an upland site in scotland. *International Journal of Climatology*, 22(5):587–598.

- Tang, Q., Xiao, H., Guo, C., and Feng, L. (2014). Characteristics of the raindrop size distributions and their retrieved polarimetric radar parameters in northern and southern china. *Atmospheric Research*, 135-136:59–75.
- Tapiador, F. J., Navarro, A., Moreno, R., Jiménez-Alcázar, A., Marcos, C., Tokay, A., Durán, L., Bodoque, J. M., Martín, R., Petersen, W., and de Castro, M. (2017). On the optimal measuring area for pointwise rainfall estimation: A dedicated experiment with 14 laser disdrometers. *Journal of Hydrometeorology*, 18(3):753–760.
- Testik, F. Y. and Gebremichael, M. (2010). *Rainfall: State of the science*, volume 191 of *Geophysical monograph*. American Geophysical Union, Washington, DC, 1. Aufl. edition.
- Testud, J., Oury, S., Black, R. A., Amayenc, P., and Dou, X. (2001). The concept of “normalized” distribution to describe raindrop spectra: A tool for cloud physics and cloud remote sensing. *Journal of Applied Meteorology*, 40(6):1118–1140.
- Thies Clima (2007). Instructions for use. laser precipitation monitor 5.4110. xx. x00 v2. 4x std. https://www.biral.com/wp-content/uploads/2015/01/5.4110.xx_.xxx_.pdf (Accessed on 22 January 2020).
- Thompson, E. J., Rutledge, S. A., Dolan, B., and Thurai, M. (2015). Drop size distributions and radar observations of convective and stratiform rain over the equatorial indian and west pacific oceans. *Journal of the Atmospheric Sciences*, 72(11):4091–4125.
- Tokay, A. and Short, D. A. (1996). Evidence from tropical raindrop spectra of the origin of rain from stratiform versus convective clouds. *Journal of Applied Meteorology*, 35(3):355–371.
- Tokay, A., Wolff, D. B., and Petersen, W. A. (2014). Evaluation of the new version of the laser-optical disdrometer, ott parsivel 2. *Journal of Atmospheric and Oceanic Technology*, 31(6):1276–1288.
- Twardosz, R. (2007). Diurnal variation of precipitation frequency in the warm half of the year according to circulation types in kraków, south poland. *Theoretical and Applied Climatology*, 89(3-4):229–238.
- Uijlenhoet, R. and Pomeroy, J. H. (2001). Raindrop size distributions and radar reflectivity–rain rate relationships for radar hydrology. *Hydrology and Earth System Sciences*, 5(4):615–628.
- Uijlenhoet, R., Steiner, M., and Smith, J. A. (2003). Variability of raindrop size distributions in a squall line and implications for radar rainfall estimation. *Journal of Hydrometeorology*, 4(1):43–61.
- Vallorani, R., Bartolini, G., Betti, G., Crisci, A., Gozzini, B., Grifoni, D., Iannuccilli, M., Messeri, A., Messeri, G., Morabito, M., and Maracchi, G. (2018). Circulation type classifications for temperature and precipitation stratification in italy. *International Journal of Climatology*, 38(2):915–931.

- Van der Ent, R. J., Savenije, H. H. G., Schaefli, B., and Steele-Dunne, S. C. (2010). Origin and fate of atmospheric moisture over continents. *Water Resources Research*, 46(9):61.
- Van Oldenborgh, G. J. and Van Ulden, A. A. (2003). On the relationship between global warming, local warming in the netherlands and changes in circulation in the 20th century. *International Journal of Climatology*, 23(14):1711–1724.
- Venables, W. N. and Ripley, R. B. (2002). *Modern Applied Statistics with S*. Springer, New York, fourth edition.
- Wallace, J. M. and Hobbs, P. V. (2006). *Atmospheric science: An introductory survey / John M. Wallace, Peter V. Hobbs*, volume v. 92 of *International geophysics series*. Academic, Oxford, 2nd ed. edition.
- Wastl, C., Schunk, C., Lüpke, M., Cocca, G., Conedera, M., Valesse, E., and Menzel, A. (2013). Large-scale weather types, forest fire danger, and wildfire occurrence in the alps. *Agricultural and Forest Meteorology*, 168:15–25.
- Wen, L., Zhao, K., Wang, M., and Zhang, G. (2019). Seasonal variations of observed raindrop size distribution in east china. *Advances in Atmospheric Sciences*, 36(4):346–362.
- White, A. B., Neiman, P. J., Ralph, F. M., Kingsmill, D. E., and Persson, P. O. G. (2003). Coastal orographic rainfall processes observed by radar during the california land-falling jets experiment. *Journal of Hydrometeorology*, 4(2):264–282.
- Wickham, H. (2007). Reshaping data with the reshape package. *Journal of Statistical Software*, 21(12):1–20.
- Wickham, H. (2016). *ggplot2: Elegant Graphics for Data Analysis*. Springer-Verlag New York.
- Wickham, H., François, R., Henry, L., and Müller, K. (2018). *dplyr: A grammar of data manipulation*.
- Wikimedia Commons (2018). File: Cloud types en.svg - wikimedia commons, the free media repository. https://commons.wikimedia.org/wiki/File:Cloud_types_en.svg (Accessed on 22 January 2020).
- Willis, P. T. (1984). Functional fits to some observed drop size distributions and parameterization of rain. *Journal of the Atmospheric Sciences*, 41(9):1648–1661.
- Willmott, C. J. and Matsuura, K. (2005). Advantages of the mean absolute error (mae) over the root mean square error (rmse) in assessing average model performance. *Climate Research*, 30:79–82.
- Wood, R. (2015). Clouds and fog | stratus and stratocumulus. In North, G. R., Zhang, F., and Pyle, J., editors, *Encyclopedia of Atmospheric Sciences (Second Edition)*, pages 196–200. Academic Press.

-
- World Meteorological Organization (1975). *International cloud atlas*, volume no. 407 [etc.] of WMO (Collection). Secretariat of the World Meteorological Organization, Geneva, rev. ed. edition.
- Xiao, C., Yuan, W., and Yu, R. (2018). Diurnal cycle of rainfall in amount, frequency, intensity, duration, and the seasonality over the uk. *International Journal of Climatology*, 38(13):4967–4978.
- Yaquub, A., Seibert, P., and Formayer, H. (2011). Diurnal precipitation cycle in austria. *Theoretical and Applied Climatology*, 103(1-2):109–118.
- You, C.-H., Lee, D.-I., Kang, M.-Y., and Kim, H.-J. (2016). Classification of rain types using drop size distributions and polarimetric radar: Case study of a 2014 flooding event in korea. *Atmospheric Research*, 181:211–219.
- Zeileis, A. and Grothendieck, G. (2005). zoo: S3 infrastructure for regular and irregular time series. *Journal of Statistical Software*, 014(i06).
- Zeng, Q., Zhang, Y., Lei, H., Xie, Y., Gao, T., Zhang, L., Wang, C., and Huang, Y. (2019). Microphysical characteristics of precipitation during pre-monsoon, monsoon, and post-monsoon periods over the south china sea. *Advances in Atmospheric Sciences*, 36(10):1103–1120.
- Zhang, Y., Wu, Z., Zhang, L., Xie, Y., Lei, H., Zheng, H., and Ma, X. (2019). Modelling the effects of aerosol on mei-yu frontal precipitation and physical processes. *Applied Sciences*, 9(18):3802.
- Zheng, Y., Gong, Y., Chen, J., and Tian, F. (2019). Warm-season diurnal variations of total, stratiform, convective, and extreme hourly precipitation over central and eastern china. *Advances in Atmospheric Sciences*, 36(2):143–159.

List of Figures

1.1	Cloud genera shape and level range. Figure By Valentin de Bruyn (CC BY-SA 3.0) (Wikimedia Commons, 2018)	3
1.2	The PARSIVEL disdrometr (front) and the micro rain radar inside its housing (back) located in Das, north east of Spain. Photo by Ghada, Wael. (2019)	6
1.3	Micro rain radar (MRR) located in Das, north east of Spain. Photo by Ghada, Wael. (2019)	7
3.1	Location of measuring devices over the study sites in Germany, Switzerland and Spain. The site in Switzerland includes 16 disdrometers.	14
3.2	A summary of the machine learning model building process	19

List of Tables

3.1	Summary of the Hess and Brezowsky classification of weather types (C.E.: Central Europe)	18
3.2	Rain type classification contingency table	22
5.1	Summary of the influence of WT on precipitation properties	34

Publications

The following publications are open-access and the links are provided:

- Wael Ghada, Ye Yuan, Clemens Wastl, Nicole Estrella, and Annette Menzel, “Precipitation Diurnal Cycle in Germany Linked to Large-Scale Weather Circulations”. <https://www.mdpi.com/2073-4433/10/9/545>
- Wael Ghada, Nicole Estrella, and Annette Menzel, “Machine Learning Approach to Classify Rain Type Based on Thies Disdrometers and Cloud Observations”. <https://www.mdpi.com/2073-4433/10/5/251>
- Wael Ghada, Allan Buras, Marvin Lübke, Christian Schunk, and Annette Menzel, “Rain Microstructure Parameters Vary with Large-Scale Weather Conditions in Lausanne, Switzerland”. <https://www.mdpi.com/2072-4292/10/6/811>

The following manuscripts are still not published. The current manuscript of each is provided and might change due to the review process:

- Wael Ghada, Enric Casellas, Joan Bech, Nicole Estrella, and Annette Menzel, “Stratiform and Convective Rain Classification Using Machine-learning Models and Micro Rain Radar and PARSIVEL Disdrometer data”. (in preparation)
- Wael Ghada, Joan Bech, Nicole Estrella, Andreas Hamman, and Annette Menzel, “Weather Types Affect Rain Microstructure: Implications for Quantitative Precipitation Estimates”. (Under review – Remote Sensing).

1 **Stratiform and convective rain classification using machine-learning models and Micro Rain Radar and**
2 **PARSIVEL disdrometer data**

3

4 Wael Ghada ^{a*}, Enric Casellas ^b, Joan Bech ^b, Nicole Estrella ^a, and Annette Menzel ^{a,c}

5 ^a Department of Ecology and Ecosystem Management - Ecoclimatology, Technical University of Munich,
6 Hans-Carl-von-Carlowitz-Platz 2, D-85354 Freising, Germany; estrella@wzw.tum.de (N.E.);
7 annette.menzel@tum.de (A.M.)

8 ^b Department of Applied Physics - Meteorology, University of Barcelona, Barcelona, Spain;
9 enric.casellas@meteo.ub.edu (E.C.); joan.bech@ub.edu (J.B.)

10 ^c Institute for Advanced Study, Technical University of Munich, Lichtenbergstraße 2a, D-85748 Garching,
11 Germany

12 * Correspondence: ghada@wzw.tum.de; Tel.: +49-81-6171-4743

13

14 **Abstract**

15 Rain type classification is an essential step required to improve quantitative rain estimations by remote
16 sensing instruments. It is also necessary to thoroughly understand the mechanisms behind the observed
17 rain microstructure. However, classification procedures depend on the available rain observation
18 instruments. A total of 20,979 min of rain data measured by a collocated PARSIVEL disdrometer and Micro
19 Rain Radar (MRR) at Das in Northeast Spain were used to build and compare five types of machine-learning
20 models for stratiform and convective rain type classification. The feature selection process based on the
21 PARSIVEL parameters yielded similar results to that of a previous study in Bavaria in Southeast Germany
22 using Thies disdrometers. The random forest model performed better than the remaining machine-

23 learning models for both the MRR parameters and the PARSIVEL parameters. Models using PARSIVEL
24 parameters achieved better results than those using MRR parameters when compared to previous simpler
25 schemes of rain type classification. Several mixed rain events were used to assess the agreement between
26 the models based on the two instruments. While only four parameters were sufficient in the case of
27 PARSIVEL, six parameters were needed in the case of MRR to reach a reasonable model performance.

28 Keywords: Micro Rain Radar; MRR; PARSIVEL; disdrometer; convective; stratiform; rain microstructure;
29 classification; machine learning; random forest.

30

31 **Highlights**

- 32 • Four disdrometer parameters are enough to classify rain type using random forest.
- 33 • The chosen parameters are identical for different disdrometer types and locations.
- 34 • Six Micro Rain Radar parameters are needed to reach a comparable performance.
- 35 • The disdrometer and Micro Rain Radar models agreed for 87% of the test dataset.

36

37 **1 Introduction**

38 Convective and stratiform rain formations result in different rain microstructures. This has been observed
39 in different climatological regions (Dolan et al., 2018); however, the proportions of convective and
40 stratiform rain depend on the season (Sreekanth et al., 2019; Wen et al., 2019) and the geographical
41 location (Dai, 2001). Temporal changes in these proportions have recently been linked to global warming
42 (Chernokulsky et al., 2019). Further, it is indispensable to take into account the differences between
43 convective and stratiform rain when characterizing rain microstructure (Ghada et al., 2018). A better
44 understanding of rain microstructure is needed for remote sensing data processing to improve

45 quantitative rain estimations (Arulraj and Barros, 2019; Kühnlein et al., 2014; Steiner and Houze, 1997;
46 Thompson et al., 2015) which in turn are needed for water management, hydrology, flash flood warnings,
47 and (extreme) precipitation forecasting and to improve the representation of precipitation processes in
48 numerical weather and climate models.

49 Rain type classification and the quality of the classification depend on the available instruments. Cloud
50 observations have been used for classification (Berg et al., 2013; Langer and Reimer, 2007), where cumulus
51 and cumulonimbus (stratus and nimbostratus) are considered to be the sources of convective (stratiform)
52 rain. Combining rain intensity with rain duration provides another approach to classify rain events (Llasat,
53 2001). However, different thresholds of and variations in the rain intensity are commonly used and a
54 variety of precipitation measurement devices can be utilized for this purpose (Bringi et al., 2003; Testud
55 et al., 2000). Satellite imagery and ground-based weather radar observations have the advantage of wider
56 spatial coverage and consequently provide alternative methods to classify rain. This includes analyses of
57 the vertical structure of the radar reflectivity (Z) and the hydrometeor fall speed, horizontal structure, and
58 variation in Z , as well as the spatial extension of the cloud and the temporal variations in its structure.

59 Micro Rain Radars (MRRs) provide vertical profiles of several precipitation parameters. MRRs are typically
60 used to detect the melting layer, which is the atmospheric region where snow and ice particles melt into
61 liquid raindrops as they fall toward the ground. This region is typically identified in radar observations by
62 a local increase in the radar reflectivity, and is usually referred to as the bright band (BB). BB detection
63 supports the classification of rain types because BBs usually appear in stratiform rain (Fabry and Zawadzki,
64 1995), while turbulence and vertical motions, which are typically present in convective rain, do not allow
65 BB formation or its clear detection.

66 Williams et al. (1995) classified precipitation clouds by the existence of a melting layer signature,
67 turbulence, and hydrometeors above the melting level. They also tested the sensitivity of the melting layer
68 detection using different thresholds of the Doppler velocity gradients. Later, the vertical air motion

69 spectral width was found to be a better indicator than the local peak in Z (Cifelli et al., 2000). Rain events
70 have also been classified into BB and non-BB depending on the presence of this feature in the precipitation
71 column (White et al., 2003), which is indicated by a simultaneous decrease in the radar reflectivity and an
72 increase in the Doppler velocity. However, the local maxima in the reflectivity are potentially affected by
73 the use of attenuated radar frequencies (such as the K band), which justifies using only the change in the
74 Doppler velocity as a signal of the BB (Gil-de-Vergara et al., 2018; Massmann et al., 2017). The existence
75 of the BB has also been proposed as a simple criterion to classify rain into convective and stratiform types
76 (Sarkar et al., 2015). In other cases, additional conditions have been taken into consideration, such as the
77 BB sharpness (Cha et al., 2009), the depth of the atmosphere where the hydrometeors exist, and a high
78 value of the signal-to-noise ratio (Kunhikrishnan et al., 2006), as well as the use of specific thresholds for
79 the differences between the reflectivity at the BB and the reflectivity above and below it (Thurai et al.,
80 2016).

81 For more than three decades, disdrometers have been used on the ground to observe the drop size
82 distributions (DSDs) of rain and to classify rain based on different combinations of their retrieved
83 parameters. This is possible because different rain microphysical formation processes lead to either
84 stratiform or convective rain and consequently produce distinct DSDs (Dolan et al., 2018). Different
85 combinations of rain DSD parameters have been applied as type classifiers (Bringi et al., 2009; Caracciolo
86 et al., 2006; Caracciolo et al., 2008; Thurai et al., 2016; Tokay and Short, 1996). The majority of
87 classification methods are based on only two parameters; however, a better classification performance
88 has been achieved when using naïve Bayes and four parameters (Bukovčić et al., 2015). Other machine-
89 learning models, especially random forest, performed better with four parameters when using Thies
90 disdrometers in Bavaria (Ghada et al., 2019).

91 Rain type classification methods for both MRR and disdrometers have been widely reported in the
92 literature. However, despite their identical goals of differentiating between convective and stratiform rain,

93 no systematic comparison of the performances of the two types of methods has yet been provided. When
94 considering this comparison, it is important to take into account the differences between the instruments
95 and, therefore, the potential inconsistencies in the measured parameters between MRRs and
96 disdrometers, for example, during heavy rain conditions (Jash et al., 2019). Major sources of these
97 inconsistencies are, in addition to the different measuring principles between the two instruments, the
98 inhomogeneities in the disdrometer laser and the attenuation of the MRR signal. Methods that first
99 identify the stratiform category and then assign the remainder to convective rain might misclassify
100 stratiform rain within convective regions (Houze, 1997). In the case of disdrometers, single or dual
101 separation methods may not be adequate, as discussed by Bukovčić et al. (2015). In addition, the choice
102 of the best parameters as classifiers and, consequently, the classification performance might be influenced
103 by the disdrometer type and the geographical location (Ghada et al., 2019).

104 In this study, we use a collocated MRR and PARSIVEL disdrometer at Das in Northeast Spain to answer the
105 following questions.

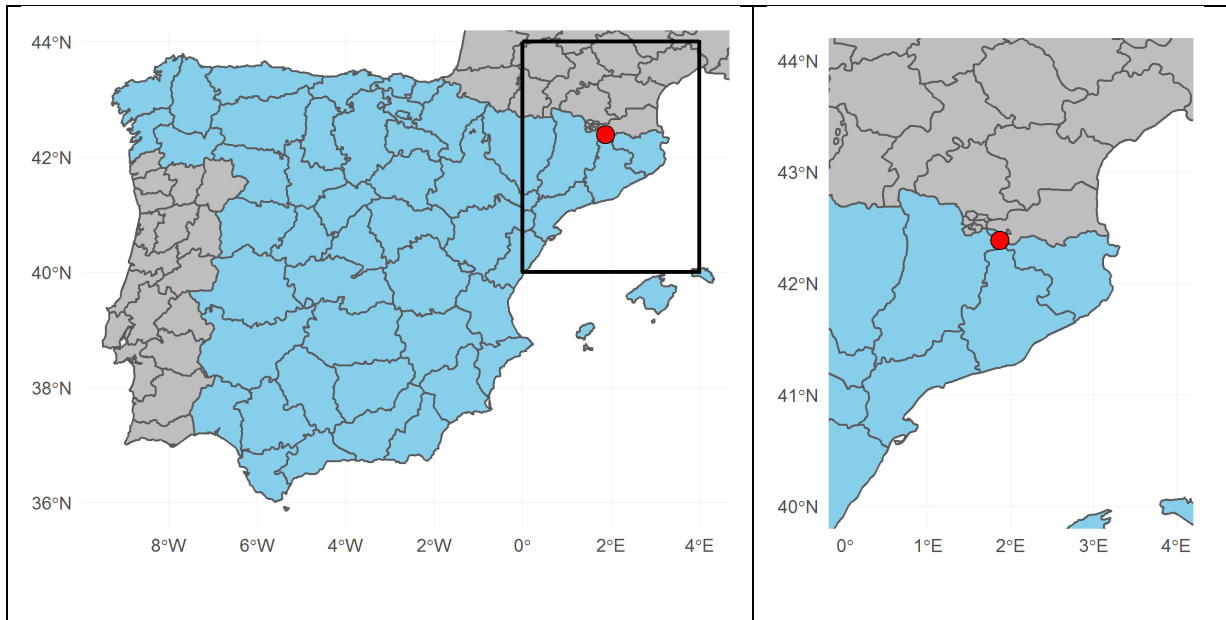
- 106 • Which parameters perform best as rain type classifiers for the PARSIVEL disdrometer and the MRR?
- 107 • Is there a machine-learning method that is suitable for both instruments?
- 108 • Do MRR- and PARSIVEL-based models provide consistent and comparable classification
109 performances?

110 In this study, we build two types of machine-learning models, one based on MRR parameters and the other
111 based on disdrometer parameters. For each type, we provide a list of the best parameters to use as rain
112 type classifiers. We compare the performances of the best models in both cases. Building such machine-
113 learning models is a practical procedure, assuming that either an MRR or a disdrometer and a pre-classified
114 dataset for the training phase are available.

115

116 **2 Data and methods**

117 Precipitation was recorded using a PARSIVEL2 disdrometer and an MMR (model MRR-2), both located at
118 the Das aerodrome at 42.386451° N 1.866562° E, 1100 m above sea level (a.s.l.), and approximately 110
119 km north of Barcelona in Northeast Spain (Figure 1). The study area is relatively flat and surrounded by
120 mountain ranges with elevations of up to 2900 m a.s.l.; see Udina et al. (2019) for more details. Previous
121 disdrometric studies in Barcelona indicated the predominance of convective precipitation in the region
122 (Cerro et al., 1997; Cerro et al., 1998). The precipitation records used in this study spanned from January
123 2017 to March 2019 with a temporal resolution of 1 min. Rain events were defined as continuous records
124 of at least 5 min where the disdrometer detected rain with an intensity greater than 0.1 mm/h. Events
125 may contain dry periods but not exceeding 15 min; otherwise, a new event was recorded. We excluded
126 events where no MRR data were available and non-rain events as detected by the disdrometer. The
127 available dataset contained a total of 293 events spanning over 20,979 min.



128 *Figure 1: Measurement location at the Das aerodrome in Northeast Spain.*

129

130 For data handling, calculations, feature selection, model training, performance estimation, and visual and
131 statistical results analyses, we used R (R Core Team, 2019), RStudio (RStudio Team, 2018), and the reader
132 (Cooper, 2017), reshape2 (Wickham, 2007), ggplot2 (Wickham, 2016), caret (Kuhn, 2018), e1071 (Meyer
133 et al., 2018), zoo (Zeileis and Grothendieck, 2005), MASS (Venables and Ripley, 2002), IMProToo (Maahn
134 and Kollias, 2012), and pROC (Robin et al., 2011) packages.

135

136 **2.1 PARSIVEL2 Disdrometer**

137 Disdrometers detect the number, size, and fall speed of hydrometeors that fall through the layer between
138 the laser transmitter end and the receiver end of the disdrometer. The size measurement is based on the
139 reduction of the received signal. The velocity of each particle corresponds to the time needed for the signal
140 to pass the laser beam and the size of the particle (Löffler-Mang and Joss, 2000). This measurement may
141 be affected by different sources of errors. Consequently, to correctly identify rain events, a filtering
142 process is needed to remove high wind speed intervals, snow, hail, frozen rain, graupel, intervals with very
143 low rain intensity periods, margin fallers, unrealistically large drops, and the splashing effect (Friedrich et
144 al., 2013). We applied the filtering described by Ghada et al. (2018), which is primarily based on the
145 procedure developed by Friedrich et al. (2013).

146 Many parameters can be extracted from measurements of the raindrop size distribution. The PARSIVEL
147 rain microstructure parameters included in this study are listed in Table 1 with their corresponding
148 references.

149

150 *Table 1: Rain microstructure parameters from the PARSIVEL2 disdrometer.*

Abbreviation	Unit	Parameter name
R	mm.h ⁻¹	Rain intensity (Chen et al., 2016)

LWC	g.m^{-3}	Liquid water content (Chen et al., 2016)
Z	dBZ	Radar reflectivity (Chen et al., 2016)
KE	$\text{J.m}^{-2}.\text{h}^{-1}$	Kinetic energy (Jan and Jana, 2018)
Dm	mm	Mass weighted diameter (Mizukami et al., 2013)
D0	mm	Median volume diameter (Marzuki et al., 2010)
sd_D	mm	Instantaneous standard deviation in the drop size (Niu et al., 2010)
sd_V	m.h^{-1}	Instantaneous standard deviation in the drop velocity (Niu et al., 2010)
Nt	drop.m^{-3}	Total number of drops per cubic meter (Chen et al., 2016)
Log_10_Nt	-	$\text{Log}_{10_Nt} = \log_{10}(\text{Nt})$
Nw_Tes	$\text{mm}^{-1}.\text{m}^{-3}$	Normalized number of drops (Testud et al., 2001)
Nw_Br	$\text{mm}^{-1}.\text{m}^{-3}$	Normalized number of drops (Bringi et al., 2009)
logNw	$\text{Nw: mm}^{-1}.\text{m}^{-3}$	$\log\text{Nw} = \log_{10}(\text{NW_Br})$
Lambda_TS	mm^{-1}	Slope of the fitted gamma distribution (Tokay and Short, 1996)
mu_TS	-	Shape of the fitted gamma distribution (Tokay and Short, 1996)
NO_TS	$\text{mm}^{-1}.\text{m}^{-3}$	Intercept of the fitted gamma distribution (Tokay and Short, 1996)
Lambda_Ca06	mm^{-1}	Slope of the fitted gamma distribution (Caracciolo et al., 2006)
mu_Ca06	-	Shape of the fitted gamma distribution (Caracciolo et al., 2006)
NO_Ca06	$\text{mm}^{-1}.\text{m}^{-3}$	Intercept of the fitted gamma distribution (Caracciolo et al., 2006)
A.St	-	The parameters of $Z = A.R^b$ (Steiner et al., 2004)
b.St	-	
sd_Dm_10	mm	} sd_XX_YY: Standard deviations of XX over YY minutes (Bukovčić et al., 2015)
sd_D0_10	mm	
sd_Nt_10	drop.m^{-3}	
sd_log ₁₀ (Nt)_10	-	
sd_log ₁₀ (R)_10	-	

152 **2.2 MRR**

153 The MRR is a low-cost, K band (24 GHz) FM–CW Doppler radar profiler manufactured by METEK (Löffler-
154 Mang et al., 1999). For the purpose of this study, the MRR was set to provide records with a vertical
155 resolution from 100 m to 3000 m above ground level (a.g.l.). The data were aggregated in one-minute
156 intervals and post-processed according to Maahn and Kollias (2012) to provide values of the equivalent
157 reflectivity, Doppler velocity, and spectral width, as explained by Gonzalez et al. (2019).

158 Most rain type classification methods that use MRR contain a step detecting the melting layer level as an
159 important feature for identifying the stratiform rain type. This level is considered to be the one with the
160 highest increase in the Doppler velocity. However, the existence of vertical air motion and turbulence
161 associated with convection does not allow a clear melting layer to form in convective rain profiles. In our
162 approach, we call the level with the highest increase in the Doppler velocity the “separation level (SL)”.
163 This level was identified for each interval within the range between 500 m and 2900 m. The second step
164 consisted of moving a five-minute temporal window to detect the average height of SL. Then, within the
165 same five-minute window, for the area above SL (the upper region), the area below it (the lower region),
166 and the combination of the two (the entire column), the parameters radar reflectivity (Z), hydrometeor
167 vertical velocity (W), spectral width (SW), and their standard deviations were calculated. These 18
168 parameters and the height of SL in meters were used as the MRR parameters to classify the rain. The
169 motivation behind seeking this separation level and splitting the column of MRR data is based on the
170 assumption that the two regions have distinct properties in the cases of convective and stratiform rain.

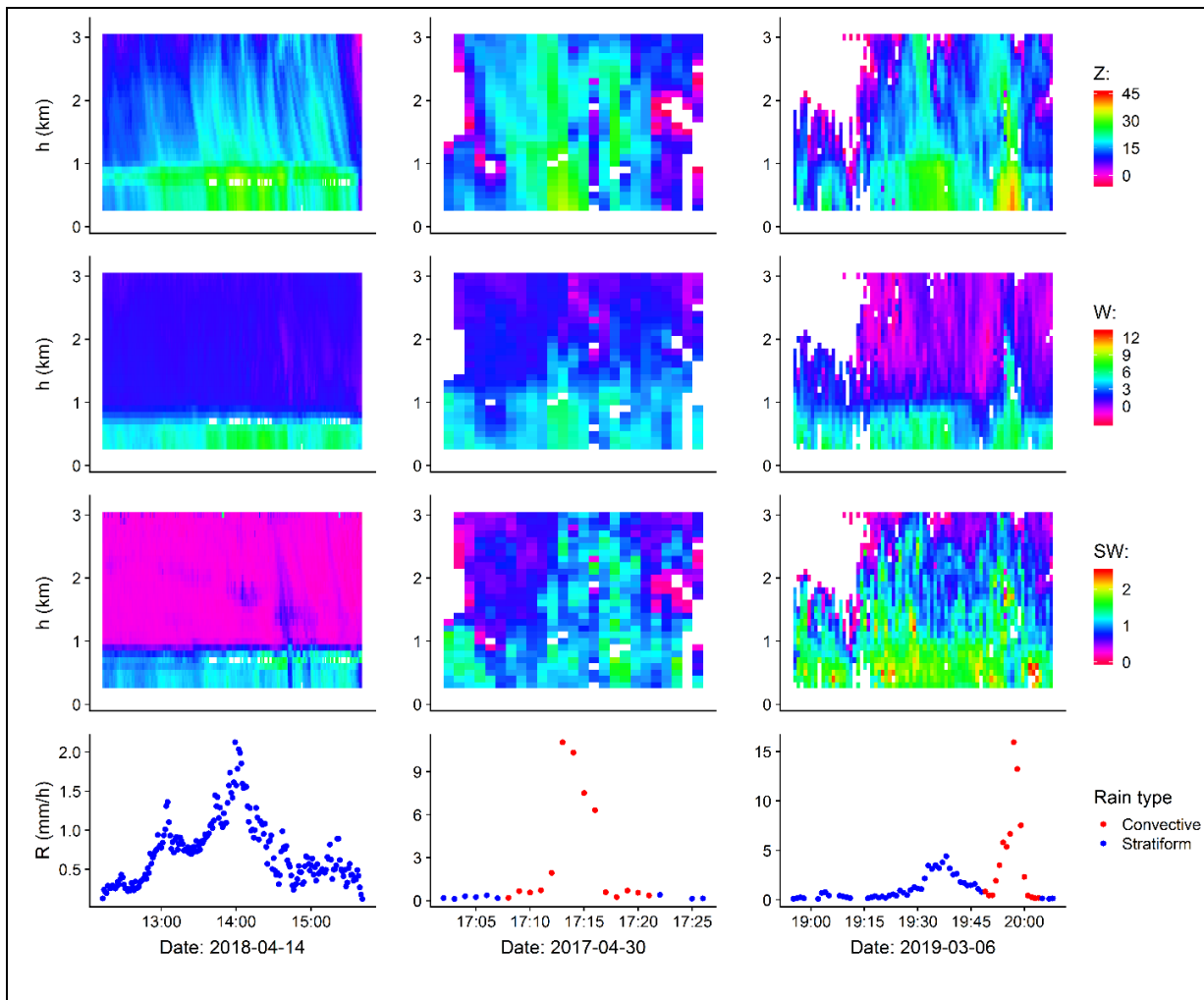
171

172 **2.3 Pre-classification**

173 Two steps were used to create the pre-classified dataset. Each interval was classified based on the method
174 of Bringi et al. (2003) hereafter BR_03. This method takes into account the rain intensity R and its standard

175 deviation over 10 min as measured by PARSIVEL. Each event was then visually classified into convective,
176 stratiform, or mixed based on the values of Z, SW, and W from the MRR (Figure 2). We excluded events
177 with stratiform rain where the melting layer was captured at the edges of the MRR measuring range
178 (higher than 2800 m or lower than 500 m a.g.l.). For the interval to be included in the pre-classified dataset,
179 it had to be either a stratiform interval within a stratiform event or a convective interval within a
180 convective or mixed event. In other words, stratiform intervals detected within convective or mixed events
181 were not included in the pre-classified dataset. The dataset after pre-classification contained 169 events
182 and a total of 10,513 min of data. An additional four mixed events with a total of 494 min of data were
183 used only to check the classification discrepancies between the final models.

184



185 Figure 2: Examples of radar reflectivity (Z , in dBZ, top row), hydrometeor vertical velocity (W , in m/s, second row), spectral width
 186 (SW , in m/s, third row), and rainfall rate (R , in mm/h, bottom row) derived from disdrometer records in pre-classified events: a
 187 stratiform event, a convective event, and a mixed event (from left to right). Only stratiform intervals in the stratiform events and
 188 convective intervals in the convective and mixed events were included in the pre-classified set.

189

190 2.4 Machine-learning model selection

191 A number of supervised machine-learning models are available for rain type classification. Based on a rain
 192 classification study using Thies disdrometer data by Ghada et al. (2019), where random forest proved to
 193 be the best of the tested models for classifying rain type, the random forest method was the only method
 194 used in the feature selection phase (see Section 2.6).

195 To achieve results comparable to those of Ghada et al. (2019), we used the same five suggested machine-
 196 learning models: linear discriminate analysis (LDA), k-nearest neighbor (KNN), naïve Bayes (NB),
 197 conditional trees (Ctree), and random forest (RF). For each model, 200 repetitions of stratified sampling
 198 were performed. In each repetition, 70% randomly selected intervals of the pre-classified dataset were
 199 used to train the model and the remaining 30% were used to test the performance.

200 With the aim of a better view of the performance, we trained the RF models using the entire pre-classified
 201 dataset and used the four best disdrometer parameters (PAR_4), the four best MRR parameters (MRR_4),
 202 and the six best MRR parameters (MRR_6). The models were then tested on four mixed events. We also
 203 included a classification method using the two parameters logNw and D0 based on the method of Thurai
 204 et al. (2010)), hereafter TH_10, which is a modified version of the method of Bringi et al. (2009).

205

206 **2.5 Indicators of the classification performance**

207 To assess the performance of the rain type classification models, a contingency table (confusion matrix)
 208 was built considering a dichotomous binary classification forecast of the convective and stratiform
 209 intervals and observations, the latter based on the pre-classification described above (Section 2.3). Table
 210 2 contains all four possible cases: true positive (TP), false positive (FP), false negative (FN), and true
 211 negative (TN).

212

213

214 *Table 2. Rain type classification contingency table.*

Prediction of Rain Type	Observed Rain Type (according to the pre-classification)	
	Convective	Stratiform
Convective	True Positive (TP)	False Positive (FP)

Stratiform	False Negative (FN)	True Negative (TN)
------------	---------------------	--------------------

215

216 Two indicators, the accuracy and the F-measure, were used to assess and compare the performances of
 217 the models. The accuracy is easy to interpret as the percentage of correctly classified intervals out of the
 218 total number of intervals in the testing set:

$$219 \text{ Accuracy} = \frac{TP + TN}{TP + FP + FN + TN} \quad (1)$$

220 However, the accuracy is not sufficient on its own for unbalanced applications. A high accuracy might
 221 equally be achieved when a model classifies the entire testing set as stratiform, which justifies using the
 222 F-measure:

$$223 \text{ F - measure} = \frac{2 * \text{Recall} * \text{Precision}}{\text{Recall} + \text{Precision}}, \quad (2)$$

224 where the recall is the number of correctly detected convective rain intervals divided by the total number
 225 of actual convective rain intervals (according to the pre-classification):

$$226 \text{ Recall} = \frac{TP}{TP + FN} \quad (3)$$

227 The precision is the number of correctly detected convective rain intervals divided by the total number of
 228 predicted convective rain intervals:

$$229 \text{ Precision} = \frac{TP}{TP + FP} \quad (4)$$

230 The F-measure is therefore the harmonic average between the recall and the precision (Eq. (2)). It
 231 guarantees a higher score for classification methods that increase both the recall and precision values
 232 compared to those that increase just one of the two values (Chinchor, 1992).

233

234 2.6 Feature selection

235 For both the disdrometer and the MRR, several parameters were available to train the machine-learning
236 models. It is a common practice to choose the smallest number of parameters that can achieve the desired
237 level of performance. We built RF models for this purpose. Each model was trained on 70% of the pre-
238 classified dataset and tested on the remaining 30%. A total of 50 repetitions of stratified sampling were
239 used for each model, with the final performance indicator being the average. We used the mean values of
240 the accuracy and the F-measure as the performance indicators in the feature selection process.

241 The step-forward selection algorithm was used to identify the best parameters. This algorithm starts with
242 a model containing no parameters. In each subsequent step, the algorithm finds the parameter from the
243 available parameter pool that, when added to the model, achieves the greatest increase in the
244 performance indicator. This parameter is then added to the model and removed from the parameter pool.
245 This process was repeated until we reached eight parameters.

246

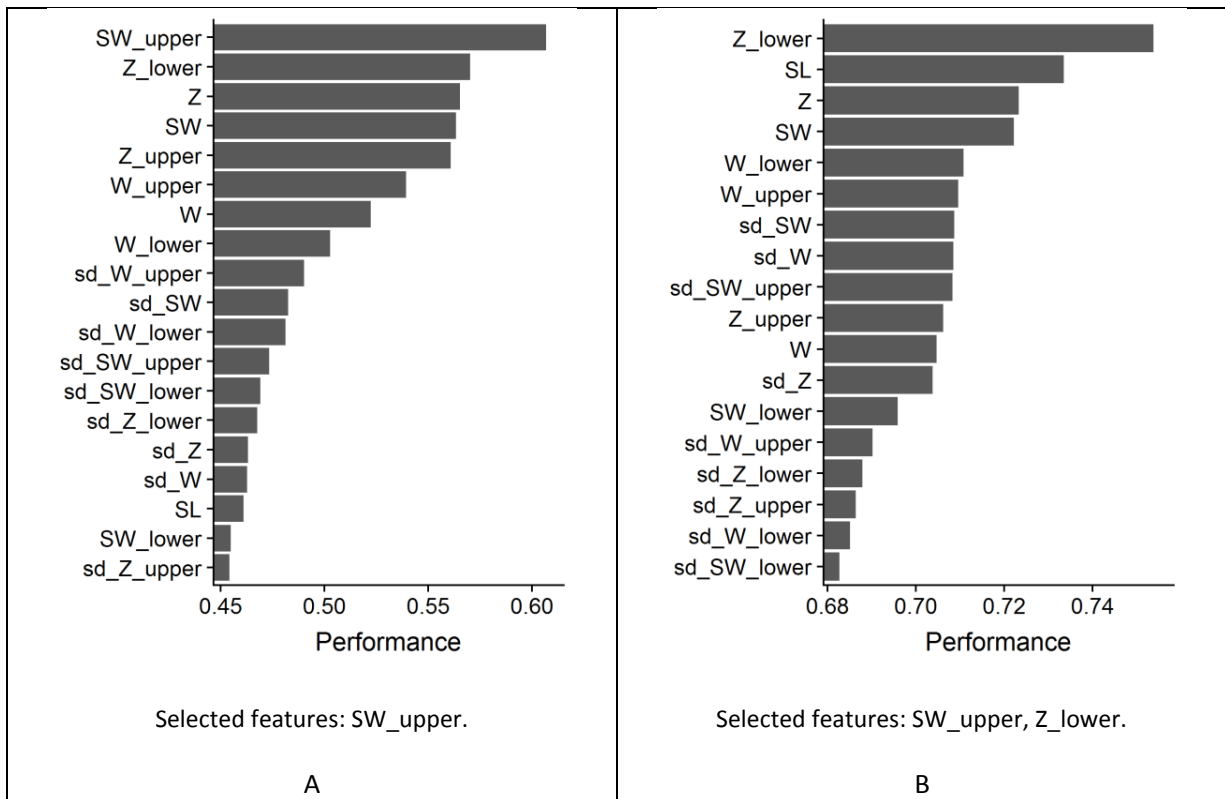
247 **3 Results and discussion**

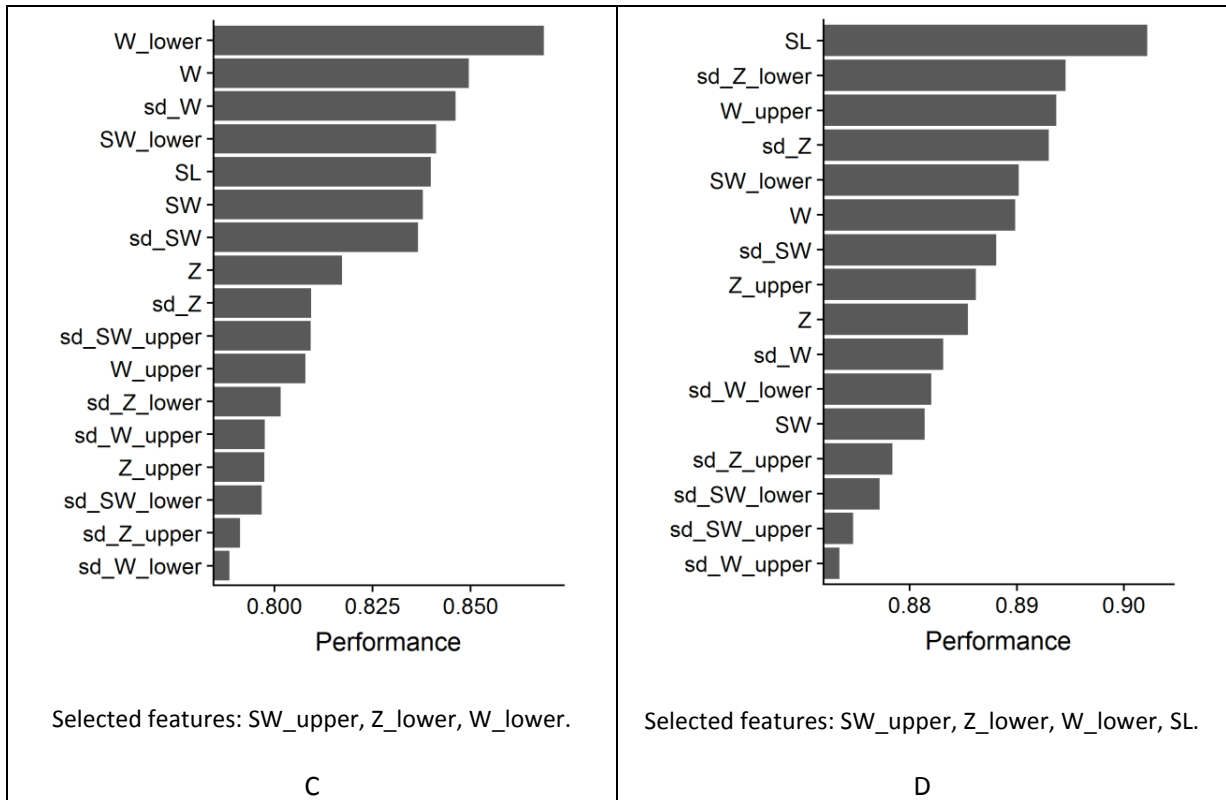
248 The total amount of rain as measured by the disdrometer was 527 mm over the entire 20,979 min. Based
249 on the simple classification method, BR_03, 2364 of these minutes (11%) were convective and contributed
250 246 mm (47%) of the rain amount. In comparison to this site in Northeast Spain, the convective rain
251 duration (amount) proportion was reported to be 11% (40%) in Lausanne, Switzerland (Ghada et al., 2018),
252 and 6% (55%) in Beijing, Northern China (Ji et al., 2019). These differences can be explained due to the
253 different geographical locations and the different seasonal extents of the used datasets. A previous study
254 in the Barcelona region reported that 59% of the annual rainfall amount is of a convective origin (Llasat
255 and Puigcerver, 1997). However, in a later study covering Catalonia (Northeast Spain), convective rain was
256 reported to form 35.5% of the total rain amount and 8% of the rain duration (Llasat et al., 2005).
257 Considering the different methods of classifying rain and the different rain measurement devices, we

258 believe that the proportions of the convective rain duration and the rain amount in our study are
 259 reasonable.

260 After applying the step-forward selection process, the best eight parameters for the MRR models were
 261 SW_upper, Z_lower, W_lower, SL, sd_Z, W_upper, SW_lower, and W. The best eight parameters in the
 262 case of the PARSIVEL models were R, sd_log10_R_10, sd_Dm_10, sd_N_10, sd_log10_N_10, sd_D0_10,
 263 V_avr, and N0.Ca06. We present the first four steps for selecting the MRR features and PARSIVEL features
 264 in Figures 3 and 4, respectively. To improve the readability, instead of showing the full list of 26 PARSIVEL
 265 features, we limited the number of parameters shown in Figures 4 to 8.

266

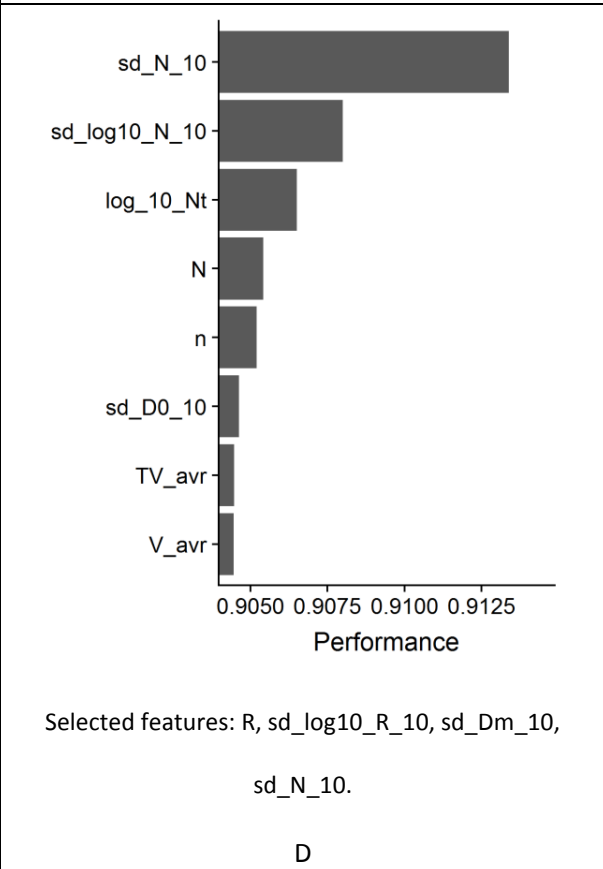
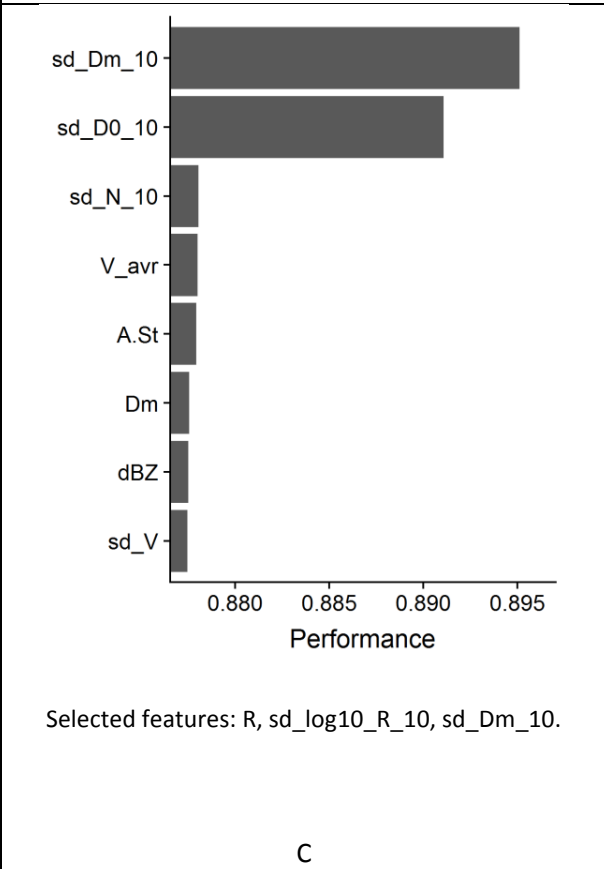
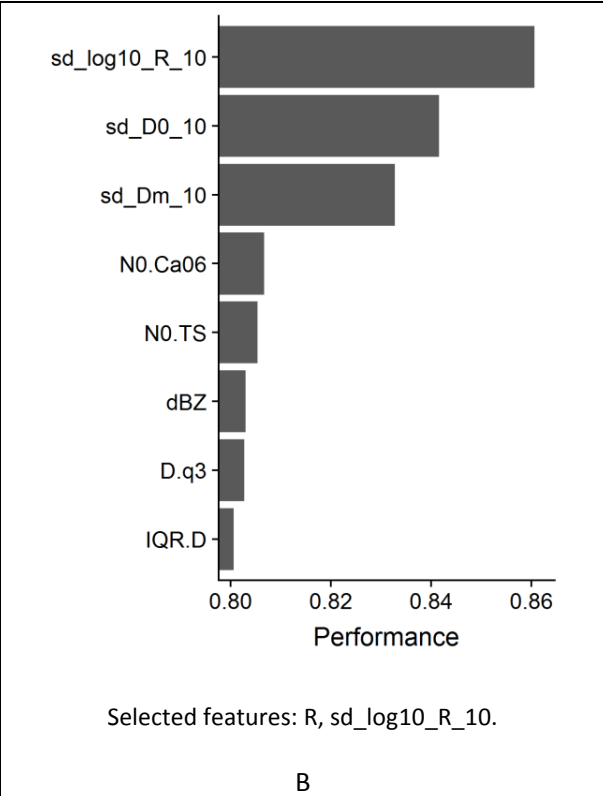
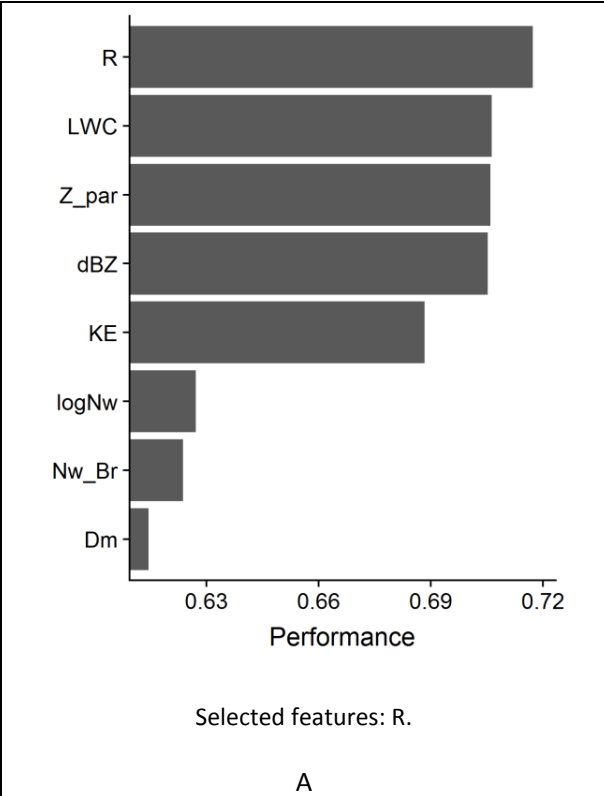




267 *Figure 3: Performance as mean values of the accuracy and F-measure for RF model classification using the MRR parameters.*

268 *Each panel represents one stage of the step-forward feature selection process. The parameters in each step are ordered by their*
 269 *performance value. The selected features are reported in the panels up to and including the respective step.*

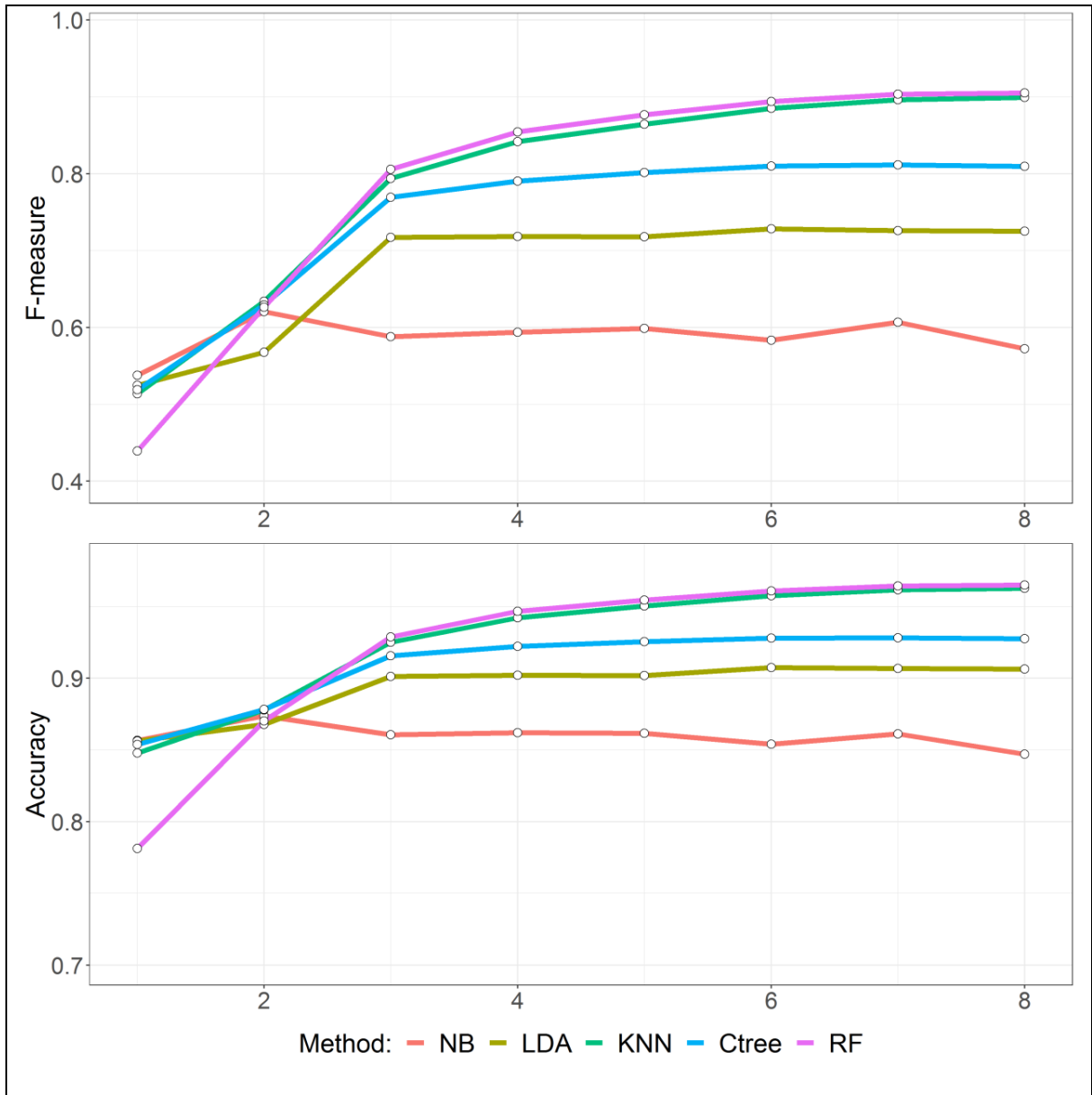
270



271 *Figure 4: Performance as mean values of the accuracy and F-measure for RF model classification using the PARSIVEL parameters.*
272 *Each panel represents one stage of the step-forward feature selection process. The parameters in each step are ordered by their*
273 *performance value. The selected features are reported in the panels up to and including the respective step. We only included the*
274 *eight best parameters (out of the 26 available) in each step to improve the readability of the figure.*

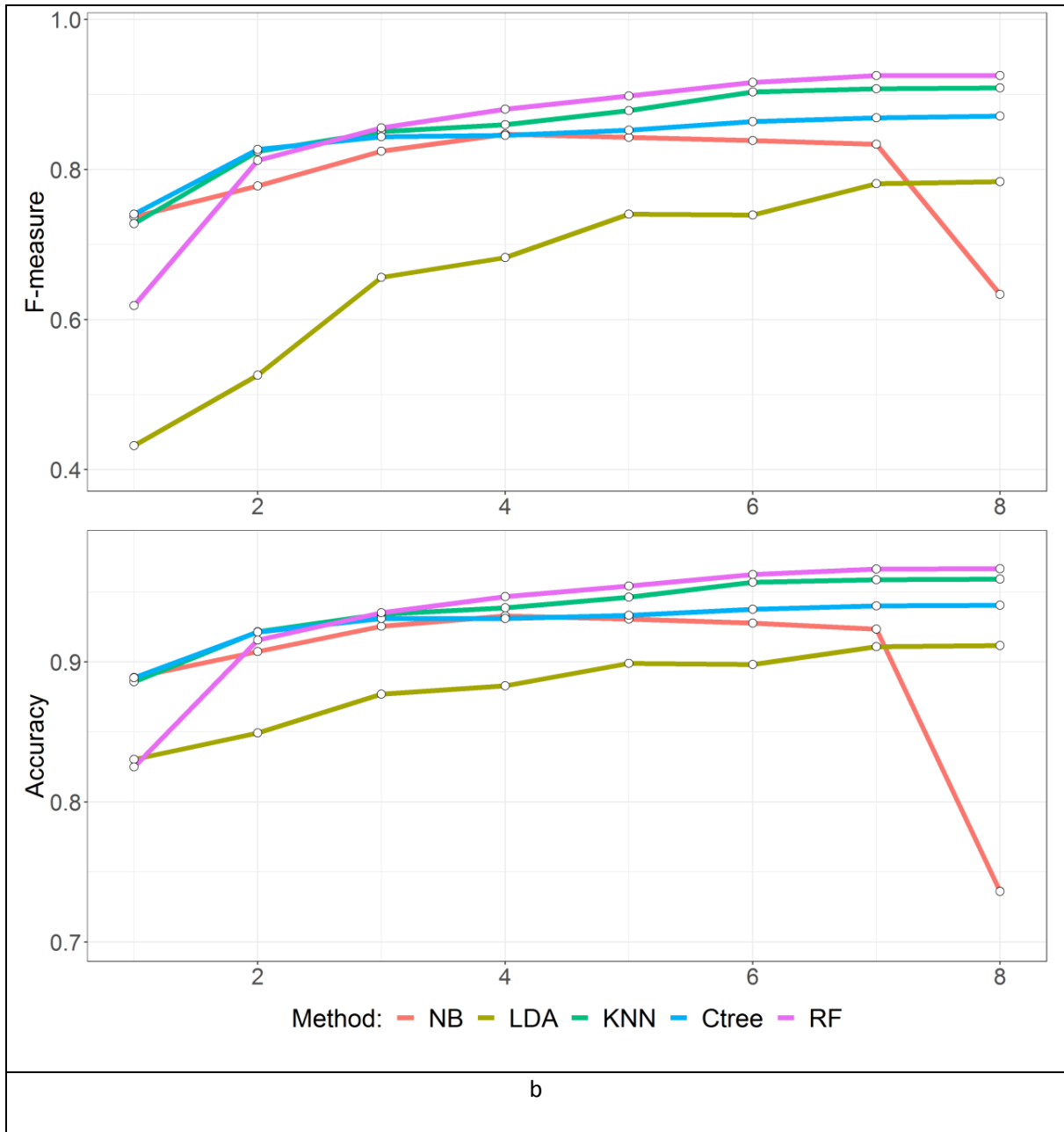
275
276 Note that the range in the model performance decreased with each step of the feature selection
277 procedure. This indicates that, after including a certain number of parameters, the improvement achieved
278 in each additional step became marginal. Remarkably, the four best parameters in the case of the
279 disdrometer were similar to those reported in Ghada et al. (2019); only sd_Dm_10 was replaced by
280 sd_D0_10. These two parameters were highly correlated and appeared to have very similar effects on the
281 performance of the RF model, as shown in Figure 4C. This result, in particular, emphasizes the suitability
282 of the four disdrometer parameters for classifying the rain type despite the different disdrometer types
283 and different geographical locations.

284 When training and testing machine-learning models and increasing the number of parameters, RF models
285 performed better than the remaining machine-learning models in nearly all cases, followed closely by KNN
286 models (Figures 5 and 6). The worst performance was achieved by LDA in the case of disdrometer models
287 and NB in the case of MRR models. The accuracies exceeded 90% even when using only two features in
288 the case of the disdrometer and three features in the case of the MRR. The F-measure was also high and
289 reached 90% close to the sixth parameter. The performance improvement was marginal after including
290 the sixth parameter for both cases. Only in the case of the NB models did the performance drop when
291 including particular parameters, most likely because NB models assume that the parameters included as
292 classifiers are independent; however, this assumption is not true for most DSD parameters.



293 Figure 5: Performance indicators of the five machine-learning classification methods with different numbers of MRR parameters.

294

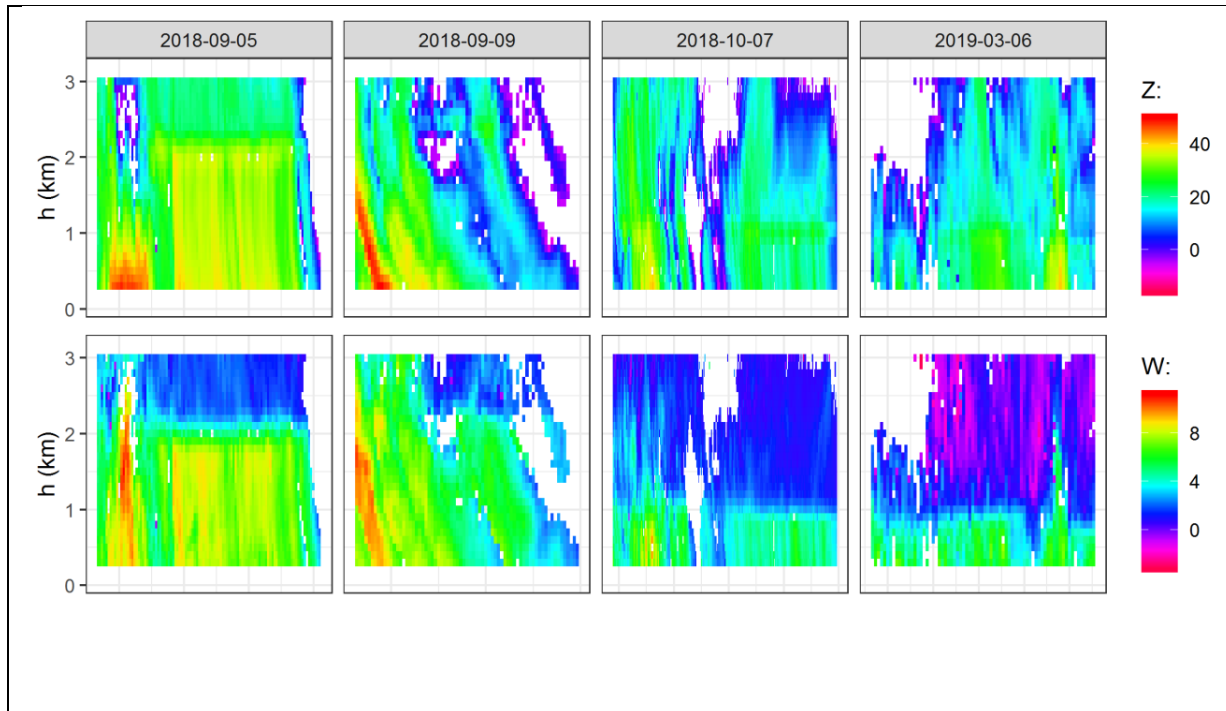


295 Figure 6: Performance indicators of the five machine-learning classification methods with different numbers of PARSIVEL
 296 parameters.

297
 298 Of all the models in this comparison, RF proved to be the best choice when including three or more
 299 parameters as predictors. Four parameters were sufficient in the case of PARSIVEL; however, for MRR
 300 models, it was not clear whether a noticeable improvement could be achieved by including more
 301 parameters. To solve this issue, we present a comparison of the PAR_4, MRR_4, MRR_6, TH_10, and BR_03

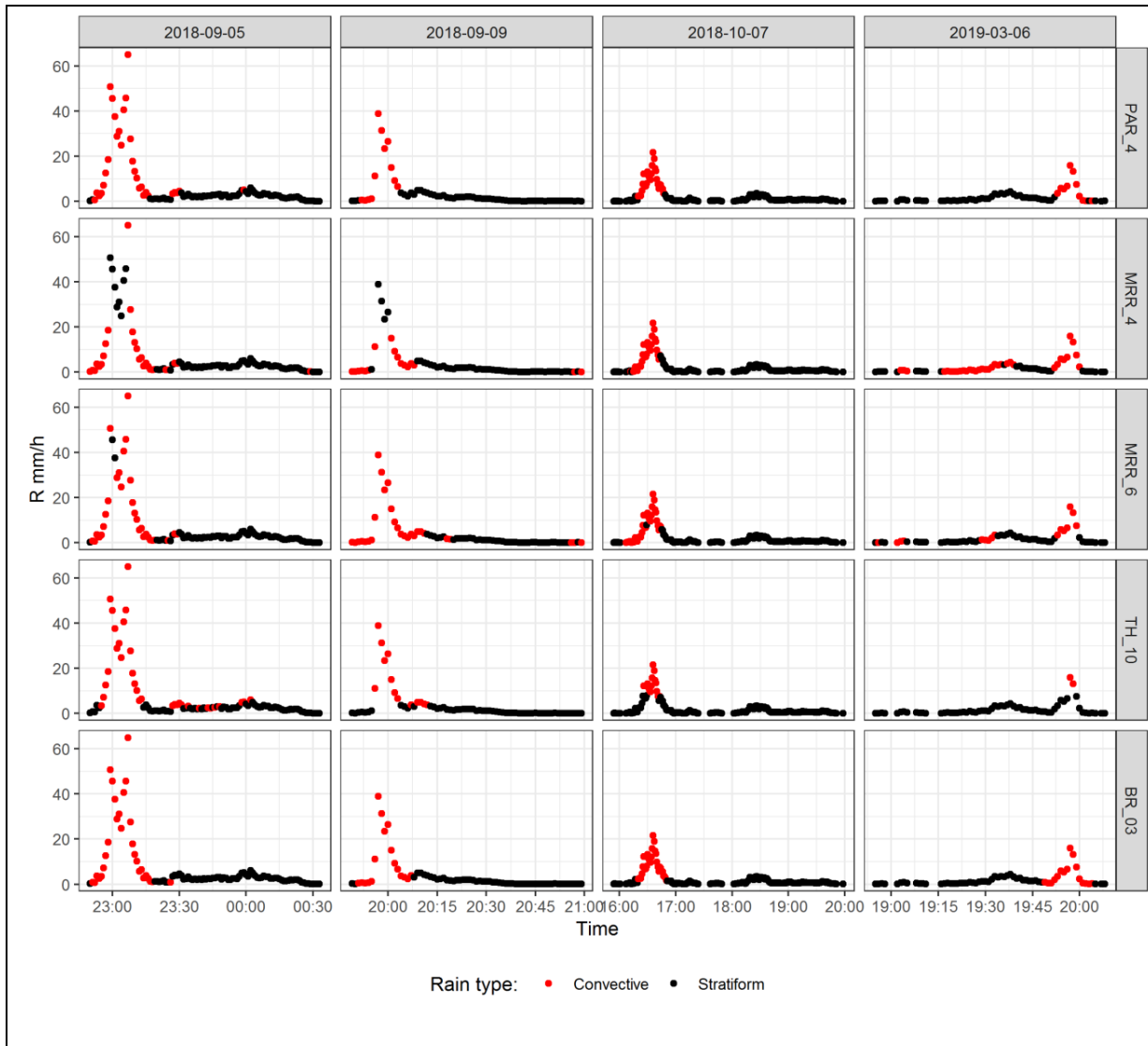
302 models. The Z and W profiles from MRR are presented for the four selected mixed events in Figure 7, and
303 the associated classification results are presented in Figure 8. The events are chronologically ordered in
304 the figures from left to right.

305



306 *Figure 7: Radar reflectivity (Z, in dBZ) and the hydrometeor vertical velocity (W, in m/s) profiles as observed by MRR for a*
307 *selection of four mixed events.*

308



309 *Figure 8: Classification of four mixed events based on the five different classification models. The color indicates the rain type.*

310 *The date of each event is indicated at the top, and the classification method for the rain type is indicated on the right.*

311

312 Both the MRR 6 and PARSIVEL 4 models were able to capture the rain intensity peaks where the convective
 313 cells were noticeable while correctly classifying the stratiform phase of the events with only a few
 314 misclassified intervals. MRR 4 misclassified a number of points in the peak of the convective phase for the
 315 two events in September 2018. It also classified a large portion of the last event in March 2019 as
 316 convective, disagreeing with the other models. The TH_10 method gave a correct classification in most

317 cases despite its low sensitivity to convection, as seen in the last two events. In addition, it misclassified a
318 portion of the stratiform intervals in the first event as convective.

319 The agreement between the five classification methods is also shown in Table 3. The highest agreement
320 appeared between the PARSIVEL model and the simple classification BR_03. There was also very high
321 agreement between the TH_10 and PARSIVEL methods. MRR_4 has the lowest agreement with all the
322 other models except MRR_6. This is to be expected because both models use MRR features, which
323 designate the column above the ground as predictors; in addition, they shared four of these predictors.

324

325 *Table 3: Agreement between the classification methods. The numbers in brackets refer to the absolute number of intervals where*
326 *the respective classification methods agree.*

	PAR_4	MRR_4	MRR_6	TH_10	BR_03
PAR_4	100% (494)				
MRR_4	83% (410)	100% (494)			
MRR_6	87% (430)	89% (440)	100% (494)		
TH_10	89% (440)	77% (380)	82% (405)	100% (494)	
BR_03	95% (469)	84% (415)	88% (435)	85% (420)	100% (494)

327

328 Based on this simple comparison of the model performance at the event level, it appears that using six
329 parameters gives more stable and reasonable results compared to using four parameters in the case of
330 MRR. The PAR_4 model appears to be the most reliable with only a few misclassification intervals. A few
331 discrepancies between the MRR_6 and PAR_4 models are expected, especially when MRR observes
332 precipitation and turbulence up to 3000 m a.g.l., which might or might not produce a signal detectable by
333 the disdrometer on the ground.

334 The advantage of using machine-learning models in comparison to other simple classification methods is
335 their ability to use the increasing amount of available data and parameters in different forms, especially
336 given further developments in machine-learning models and computational power. Special attention

337 needs to be paid to the selection of the training set and the initial evaluation to achieve a reasonable
338 classification performance before moving such models to the operational phase.

339

340 **4. Conclusions**

341 Rain can be observed by a variety of instruments, which may provide complementary information about
342 its characteristics and formation processes. We investigated the possibility of classifying rain into
343 convective and stratiform using two types of instruments, a PARSIVEL disdrometer and an MRR. This led
344 to the construction of a procedure for each instrument and the identification of the best parameters for
345 rain type classification.

346 Classifying rain type using disdrometers gave reasonable results even when the parameters used were
347 limited to four, namely R, sd_log10_R_10, sd_Dm_10, and d_N_10. These parameters, in particular, have
348 already been proven to be the best classifiers for rain type in a different location in central Europe using a
349 different type of disdrometer.

350 Machine-learning models were also able to classify rain based on the MRR output when including six
351 parameters in the model: SW_upper, Z_lower, W_lower, SL, sd_Z, and W_upper.

352 Few discrepancies were observed between the MRR- and PARSIVEL-based classification models. These
353 differences, however, are expected, especially considering the differences in the measuring principles and
354 the parameters used in these models. However, the overall classification performance supports the use of
355 such models in the future.

356 Further developments in the field of machine learning might provide better models for such classification
357 problems. For example, it might be possible to use image classification algorithms to provide reliable
358 performance.

359

360 **Author Contributions**

361 Conceptualization of the study by W.G. and J.B; formal analysis by W.G. and E.C.; supervision by J.B. and
362 A.M.; writing of the original draft by W.G.; and review and editing by all co-authors.

363

364 **Funding**

365 The MRR and PARSIVEL data were acquired and processed thanks to the Spanish projects CGL2015-65627-
366 C3-2-R (MINECO/FEDER), CGL2016-81828-REDT (AEI), RTI2018-098693-B-C32 (AEI/FEDER), and 2017-DI-
367 053.

368

369 **Acknowledgements**

370 The first author thanks the Deutscher Akademischer Austauschdienst (DAAD) for financial support.

371

372 **Declarations of interest**

373 None.

374

375 **References**

376 Arulraj, M., & Barros, A.P. (2019). Improving quantitative precipitation estimates in mountainous regions
377 by modelling low-level seeder-feeder interactions constrained by Global Precipitation Measurement
378 Dual-frequency Precipitation Radar measurements. *Remote Sensing of Environment*, 231, 111213.
379 Berg, P., Moseley, C., & Haerter, J.O. (2013). Strong increase in convective precipitation in response to
380 higher temperatures. *Nature Geoscience*, 6, 181–185.

- 381 Bringi, V.N., Chandrasekar, V., Hubbert, J., Gorgucci, E., Randeu, W.L., & Schoenhuber, M. (2003).
382 Raindrop Size Distribution in Different Climatic Regimes from Disdrometer and Dual-Polarized Radar
383 Analysis. *Journal of the Atmospheric Sciences*, 60, 354–365.
- 384 Bringi, V.N., Williams, C.R., Thurai, M., & May, P.T. (2009). Using Dual-Polarized Radar and Dual-
385 Frequency Profiler for DSD Characterization: A Case Study from Darwin, Australia. *Journal of*
386 *Atmospheric and Oceanic Technology*, 26, 2107–2122.
- 387 Bukovčić, P., Zrnić, D., & Zhang, G. (2015). Convective–stratiform separation using video disdrometer
388 observations in central Oklahoma – the Bayesian approach. *Atmospheric Research*, 155, 176–191.
- 389 Caracciolo, C., Porcù, F., & Prodi, F. (2008). Precipitation classification at mid-latitudes in terms of drop
390 size distribution parameters. *Advances in Geosciences*, 16, 11–17.
- 391 Caracciolo, C., Prodi, F., Battaglia, A., & Porcu', F. (2006). Analysis of the moments and parameters of a
392 gamma DSD to infer precipitation properties: A convective stratiform discrimination algorithm.
393 *Atmospheric Research*, 80, 165–186.
- 394 Cerro, C., Bech, J., Codina, B., & Lorente, J. (1998). Modeling Rain Erosivity Using Disdrometric
395 Techniques. *Soil Science Society of America Journal*, 62, 731.
- 396 Cerro, C., Codina, B., Bech, J., & Lorente, J. (1997). Modeling Raindrop Size Distribution and Z (R)
397 Relations in the Western Mediterranean Area. *Journal of Applied Meteorology*, 36, 1470–1479.
- 398 Cha, J.-W., Chang, K.-H., Yum, S.S., & Choi, Y.-J. (2009). Comparison of the bright band characteristics
399 measured by Micro Rain Radar (MRR) at a mountain and a coastal site in South Korea. *Advances in*
400 *Atmospheric Sciences*, 26, 211–221.
- 401 Chen, B., Wang, J., & Gong, D. (2016). Raindrop Size Distribution in a Midlatitude Continental Squall Line
402 Measured by Thies Optical Disdrometers over East China. *Journal of Applied Meteorology and*
403 *Climatology*, 55, 621–634.

404 Chernokulsky, A., Kozlov, F., Zolina, O., Bulygina, O., Mokhov, I.I., & Semenov, V.A. (2019). Observed
405 changes in convective and stratiform precipitation in Northern Eurasia over the last five decades.
406 *Environmental Research Letters*, 14, 45001.

407 Chinchor, N. (1992). MUC-4 evaluation metrics. In Unknown (Ed.), *Message understanding. 4th*
408 *Conference : Papers* (p. 22). Morristown, NJ, USA: Association for Computational Linguistics.

409 Cifelli, R., Williams, C.R., Rajopadhyaya, D.K., Avery, S.K., Gage, K.S., & May, P.T. (2000). Drop-Size
410 Distribution Characteristics in Tropical Mesoscale Convective Systems. *Journal of Applied*
411 *Meteorology*, 39, 760–777.

412 Cooper, N. (2017). reader: Suite of Functions to Flexibly Read Data from Files. [https://CRAN.R-](https://CRAN.R-project.org/package=reader)
413 [project.org/package=reader](https://CRAN.R-project.org/package=reader).

414 Dai, A. (2001). Global Precipitation and Thunderstorm Frequencies. Part I: Seasonal and Interannual
415 Variations. *Journal of Climate*, 14, 1092–1111.

416 Dolan, B., Fuchs, B., Rutledge, S.A., Barnes, E.A., & Thompson, E.J. (2018). Primary Modes of Global Drop
417 Size Distributions. *Journal of the Atmospheric Sciences*, 75, 1453–1476.

418 Fabry, F., & Zawadzki, I. (1995). Long-Term Radar Observations of the Melting Layer of Precipitation and
419 Their Interpretation. *Journal of the Atmospheric Sciences*, 52, 838–851.

420 Friedrich, K., Kalina, E.A., Masters, F.J., & Lopez, C.R. (2013). Drop-Size Distributions in Thunderstorms
421 Measured by Optical Disdrometers during VORTEX2. *Monthly Weather Review*, 141, 1182–1203.

422 Ghada, W., Buras, A., Lüpke, M., Schunk, C., & Menzel, A. (2018). Rain Microstructure Parameters Vary
423 with Large-Scale Weather Conditions in Lausanne, Switzerland. *Remote Sensing*, 10, 811.

424 Ghada, W., Estrella, N., & Menzel, A. (2019). Machine Learning Approach to Classify Rain Type Based on
425 Thies Disdrometers and Cloud Observations. *Atmosphere*, 10, 251.

426 Gil-de-Vergara, N., Riera, J.M., Pérez-Peña, S., Garcia-Rubia, J., & Benarroch, A. (2018). Classification of
427 rainfall events and evaluation of drop size distributions using a k-band doppler radar. In 12th

428 *European Conference on Antennas and Propagation (EuCAP 2018)* (829 (5 pp.)-829 (5 pp.)):
429 Institution of Engineering and Technology.

430 Gonzalez, S., Bech, J., Udina, M., Codina, B., Paci, A., & Trapero, L. (2019). Decoupling between
431 Precipitation Processes and Mountain Wave Induced Circulations Observed with a Vertically Pointing
432 K-Band Doppler Radar. *Remote Sensing*, *11*, 1034.

433 Houze, R.A. (1997). Stratiform Precipitation in Regions of Convection: A Meteorological Paradox? *Bulletin*
434 *of the American Meteorological Society*, *78*, 2179–2196.

435 Jan, P., & Jana, K. (2018). Measurement and computation of kinetic energy of simulated rainfall in
436 comparison with natural rainfall. *Soil and Water Research*, *13*, 226–233.

437 Jash, D., Resmi, E.A., Unnikrishnan, C.K., Sumesh, R.K., Sreekanth, T.S., Sukumar, N., & Ramachandran,
438 K.K. (2019). Variation in rain drop size distribution and rain integral parameters during southwest
439 monsoon over a tropical station: An inter-comparison of disdrometer and Micro Rain Radar.
440 *Atmospheric Research*, *217*, 24–36.

441 Ji, Chen, Li, Xiao, & Zhang (2019). Raindrop Size Distributions and Rain Characteristics Observed by a
442 PARSIVEL Disdrometer in Beijing, Northern China. *Remote Sensing*, *11*, 1479.

443 Kuhn, M. (2018). caret: Classification and Regression Training. [https://CRAN.R-](https://CRAN.R-project.org/package=caret)
444 [project.org/package=caret](https://CRAN.R-project.org/package=caret).

445 Kühnlein, M., Appelhans, T., Thies, B., & Nauss, T. (2014). Improving the accuracy of rainfall rates from
446 optical satellite sensors with machine learning — A random forests-based approach applied to MSG
447 SEVIRI. *Remote Sensing of Environment*, *141*, 129–143.

448 Kunhikrishnan, P.K., Sivaraman, B.R., Kiran Kumar, N.V.P., & Alappattu, D.P. (2006). Rain observations
449 with micro rain radar (MRR) over Thumba. In S.-C. Tsay, T. Nakajima, R.P. Singh, & R. Sridharan (Eds.),
450 *Remote Sensing of the Atmosphere and Clouds* (64080L): SPIE.

451 Langer, I., & Reimer, E. (2007). Separation of convective and stratiform precipitation for a precipitation
452 analysis of the local model of the German Weather Service. *Advances in Geosciences*, *10*, 159–165.

453 Llasat, M.C., & Puigcerver, M. (1997). Total rainfall and convective rainfall in Catalonia, Spain.
454 *International Journal of Climatology*, 17, 1683–1695.

455 Llasat, M.C., Rigo, T., Ceperuelo, M., & Barrera, A. (2005). Estimation of convective precipitation: the
456 meteorological radar versus an automatic rain gauge network. *Advances in Geosciences*, 2,
457 <https://www.adv-geosci.net/2/103/2005/>.

458 Llasat, M.-C. (2001). An objective classification of rainfall events on the basis of their convective features:
459 application to rainfall intensity in the northeast of Spain. *International Journal of Climatology*, 21,
460 1385–1400.

461 Löffler-Mang, M., & Joss, J. (2000). An Optical Disdrometer for Measuring Size and Velocity of
462 Hydrometeors. *Journal of Atmospheric and Oceanic Technology*, 17, 130–139.

463 Löffler-Mang, M., Kunz, M., & Schmid, W. (1999). On the Performance of a Low-Cost K-Band Doppler
464 Radar for Quantitative Rain Measurements. *Journal of Atmospheric and Oceanic Technology*, 16,
465 379–387.

466 Maahn, M., & Kollias, P. (2012). Improved Micro Rain Radar snow measurements using Doppler spectra
467 post-processing. *Atmospheric Measurement Techniques*, 5, 2661–2673.

468 Marzuki, M., Randeu, W.L., Schönhuber, M., Bringi, V.N., Kozu, T., & Shimomai, T. (2010). Raindrop Size
469 Distribution Parameters of Distrometer Data With Different Bin Sizes. *IEEE Transactions on*
470 *Geoscience and Remote Sensing*, 48, 3075–3080.

471 Massmann, A.K., Minder, J.R., Garreaud, R.D., Kingsmill, D.E., Valenzuela, R.A., Montecinos, A., Fults, S.L.,
472 & Snider, J.R. (2017). The Chilean Coastal Orographic Precipitation Experiment: Observing the
473 Influence of Microphysical Rain Regimes on Coastal Orographic Precipitation. *Journal of*
474 *Hydrometeorology*, 18, 2723–2743.

475 Meyer, D., Dimitriadou, E., Hornik, K., Weingessel, A., & Leisch, F. (2018). e1071: Misc Functions of the
476 Department of Statistics, Probability Theory Group (Formerly: E1071), TU Wien. [https://CRAN.R-](https://CRAN.R-project.org/package=e1071)
477 [project.org/package=e1071](https://CRAN.R-project.org/package=e1071).

478 Mizukami, N., Koren, V., Smith, M., Kingsmill, D., Zhang, Z., Cosgrove, B., & Cui, Z. (2013). The Impact of
479 Precipitation Type Discrimination on Hydrologic Simulation: Rain–Snow Partitioning Derived from
480 HMT-West Radar-Detected Brightband Height versus Surface Temperature Data. *Journal of*
481 *Hydrometeorology*, *14*, 1139–1158.

482 Niu, S., Jia, X., Sang, J., Liu, X., Lu, C., & Liu, Y. (2010). Distributions of Raindrop Sizes and Fall Velocities in
483 a Semiarid Plateau Climate: Convective versus Stratiform Rains. *Journal of Applied Meteorology and*
484 *Climatology*, *49*, 632–645.

485 R Core Team (2019). R: A Language and Environment for Statistical Computing. Vienna, Austria.
486 <https://www.R-project.org/>.

487 Robin, X., Turck, N., Hainard, A., Tiberti, N., Lisacek, F., Sanchez, J.-C., & Müller, M. (2011). pROC: an
488 open-source package for R and S+ to analyze and compare ROC curves. *BMC bioinformatics*, *12*, 77.

489 RStudio Team (2018). RStudio: Integrated Development Environment for R. Boston, MA.
490 <http://www.rstudio.com/>.

491 Sarkar, T., Das, S., & Maitra, A. (2015). Assessment of different raindrop size measuring techniques:
492 Inter-comparison of Doppler radar, impact and optical disdrometer. *Atmospheric Research*, *160*, 15–
493 27.

494 Sreekanth, T.S., Varikoden, H., Resmi, E.A., & Mohan Kumar, G. (2019). Classification and seasonal
495 distribution of rain types based on surface and radar observations over a tropical coastal station.
496 *Atmospheric Research*, *218*, 90–98.

497 Steiner, M., & Houze, R.A. (1997). Sensitivity of the Estimated Monthly Convective Rain Fraction to the
498 Choice of Z – R Relation. *Journal of Applied Meteorology*, *36*, 452–462.

499 Steiner, M., Smith, J.A., & Uijlenhoet, R. (2004). A Microphysical Interpretation of Radar Reflectivity–Rain
500 Rate Relationships. *Journal of the Atmospheric Sciences*, *61*, 1114–1131.

501 Testud, J., Oury, S., & Amayenc, P. (2000). The concept of “normalized” distribution to describe raindrop
502 spectra: A tool for hydrometeor remote sensing. *Physics and Chemistry of the Earth, Part B:
503 Hydrology, Oceans and Atmosphere*, 25, 897–902.

504 Testud, J., Oury, S., Black, R.A., Amayenc, P., & Dou, X. (2001). The Concept of “Normalized” Distribution
505 to Describe Raindrop Spectra: A Tool for Cloud Physics and Cloud Remote Sensing. *Journal of Applied
506 Meteorology*, 40, 1118–1140.

507 Thompson, E.J., Rutledge, S.A., Dolan, B., & Thurai, M. (2015). Drop Size Distributions and Radar
508 Observations of Convective and Stratiform Rain over the Equatorial Indian and West Pacific Oceans.
509 *Journal of the Atmospheric Sciences*, 72, 4091–4125.

510 Thurai, M., Bringi, V.N., & May, P.T. (2010). CPOL Radar-Derived Drop Size Distribution Statistics of
511 Stratiform and Convective Rain for Two Regimes in Darwin, Australia. *Journal of Atmospheric and
512 Oceanic Technology*, 27, 932–942.

513 Thurai, M., Gatlin, P.N., & Bringi, V.N. (2016). Separating stratiform and convective rain types based on
514 the drop size distribution characteristics using 2D video disdrometer data. *Atmospheric Research*,
515 169, 416–423.

516 Tokay, A., & Short, D.A. (1996). Evidence from Tropical Raindrop Spectra of the Origin of Rain from
517 Stratiform versus Convective Clouds. *Journal of Applied Meteorology*, 35, 355–371.

518 Udina, M., Bech, J., González, S., Soler, M.R., Paci, A., Miró, J.R., Trapero, L., Donier, J.M., Douffet, T.,
519 Codina, B., & Pineda, N. (2019). Multi-sensor observations of an elevated rotor during a mountain
520 wave event in the Eastern Pyrenees. *Atmospheric Research*, 104698.

521 Venables, W.N., & Ripley, B.D. (2002). *Modern applied statistics with S*. (4th ed.). New York: Springer.

522 Wen, L., Zhao, K., Wang, M., & Zhang, G. (2019). Seasonal Variations of Observed Raindrop Size
523 Distribution in East China. *Advances in Atmospheric Sciences*, 36, 346–362.

524 White, A.B., Neiman, P.J., Ralph, F.M., Kingsmill, D.E., & Persson, P.O.G. (2003). Coastal Orographic
525 Rainfall Processes Observed by Radar during the California Land-Falling Jets Experiment. *Journal of*
526 *Hydrometeorology*, 4, 264–282.

527 Wickham, H. (2007). Reshaping Data with the reshape Package. *Journal of Statistical Software*, 21.
528 <http://www.iostatsoft.org/v21/i12/>.

529 Wickham, H. (2016). *ggplot2: Elegant Graphics for Data Analysis*: Springer-Verlag New York.

530 Williams, C.R., Ecklund, W.L., & Gage, K.S. (1995). Classification of Precipitating Clouds in the Tropics
531 Using 915-MHz Wind Profilers. *Journal of Atmospheric and Oceanic Technology*, 12, 996–1012.

532 Zeileis, A., & Grothendieck, G. (2005). zoo : S3 Infrastructure for Regular and Irregular Time Series.
533 *Journal of Statistical Software*, 14.

534

1 Article

2 Weather Types Affect Rain Microstructure: 3 Implications for Quantitative Precipitation Estimates

4 Wael Ghada^{1*}, Joan Bech², Nicole Estrella¹, Andreas Hamann³ and Annette Menzel^{1,4}

5 ¹ Department of Ecology and Ecosystem Management, Technical University of Munich, Hans-Carl-von-
6 Carlowitz-Platz 2, D-85354 Freising, Germany; estrella@wzw.tum.de (N.E.), amenzel@wzw.tum.de,
7 <https://orcid.org/0000-0002-7175-2512> (A.M.)

8 ² Department of Applied Physics - Meteorology, University of Barcelona, Barcelona, Spain;
9 joan.bech@ub.edu (J.B.)

10 ³ University of Alberta, Department of Renewable Resources, 733 General Services Building, Edmonton,
11 Alberta, T6G 2H1, andreas.hamann@ualberta.ca, <https://orcid.org/0000-0003-2046-4550> (A. H.).

12 ⁴ Institute for Advanced Study, Technical University of Munich, Lichtenbergstraße 2a, D-85748 Garching,
13 Germany.

14 * Correspondence: ghada@wzw.tum.de; Tel.: +49-81-6171-4743

15 Received: date; Accepted: date; Published: date

16 Abstract:

17 Quantitative precipitation estimation (QPE) through remote sensing has to take rain microstructure
18 into consideration, because it influences the relationship between radar reflectivity Z and rain
19 intensity R . For this reason, separate equations are used to estimate rain intensity of convective and
20 stratiform rain types. Here, we investigate whether incorporating synoptic scale meteorology could
21 yield further QPE improvements. Depending on large-scale weather types, variability in cloud
22 condensation nuclei and the humidity content may lead to variation in rain microstructure. In a case
23 study for Bavaria, we measured rain microstructure at ten locations with laser-based disdrometers,
24 covering a combined 18,600 hours of rain in a period of 36 months. Rain was classified on a temporal
25 scale of one minute into convective and stratiform based on a machine learning model. Large-scale
26 wind direction classes were on a daily scale to represent the synoptic weather types. Significant
27 variations in rain microstructure parameters were evident not only for rain types, but also for wind
28 direction classes. The main contrast was observed between westerly and easterly circulations, with
29 the latter characterized by smaller average size of drops and a higher average concentration. This
30 led to substantial variation in the parameters of the radar rain intensity retrieval equation Z - R . The
31 effect of wind direction on Z - R parameters was more pronounced for stratiform than convective
32 rain types. We conclude that building separate Z - R retrieval equations for regional wind direction
33 classes should improve radar-based QPE, especially for stratiform rain events.

34 **Keywords:** Thies; disdrometer; weather circulations, convective; stratiform; rain spectra; radar
35 reflectivity–rain rate relationship
36

37 1. Introduction

38 Understanding rain microstructure can provide us with an insight of the rain formation
39 processes behind it. This understanding can be employed in improving quantitative estimation of
40 rain intensity by remote sensing [1–3]. Furthermore, the parametrization of the microphysical
41 processes in numerical weather and climate models can be improved [4,5]. The variation in rain
42 microstructure has been reported on different spatial scales ranging from few meters [6], to few
43 hundreds of meters [7], to regional [8] and global extents [9,10]. This variation also appears with
44 seasons [11], rain types [12], and large-scale weather types [13–15].

45 A very clear example of the different rain formation processes leading to variations in rain drop
46 size distribution is the discrepancy between convective and stratiform rain. This has been quantified
47 in a number of studies [4,12,16,17]. The reason for the difference is the relative importance of cold
48 and warm rain formation processes [18]. Stratiform rain forms primarily by processes involving ice
49 crystals and interactions of ice with liquid water, while convective rain formation comprises both
50 warm and cold processes. Factors and processes that influence the rain drop size distribution as
51 observed on the ground include rimming and aggregation (above the 0°C isotherm), condensation
52 (below the 0°C isotherm), collision, coalescence, turbulence, cloud thickness, electric field,
53 evaporation, and drop fragmentation [19,20]. The difference in rain drop size distribution between
54 convective rain and stratiform rain has been used for the classification of both rain types on the
55 ground. Most of these methods use two rain drop size distribution parameters and a linear
56 discrimination between the regions of rain types [16,21–24]. Recent methods employed machine
57 learning and reached higher performance levels when using four rain drop size distribution
58 parameters [25,26].

59 Large-scale weather types denote atmospheric conditions such as the high and low pressure
60 distribution, the position and paths of frontal zones, and the existence of cyclonic or anticyclonic
61 circulation types over a sequence of days [27]. Indirectly, they also influence stream flows [28], floods
62 [29,30], debris-flow events [31], forest fires [32,33], air quality, and pollen distribution [34–36].
63 Weather type classification is an important part of statistical climatology [37,38], because these types
64 explain many local weather phenomena. Weather types influence local near-surface temperatures
65 and precipitation [39–43]. They also affect the diurnal cycle of precipitation in terms of frequency and
66 amount [44–46], and they impact the occurrence and the magnitude of meteorological extreme events
67 [47–51]. Large-scale weather types may therefore also influence rain microstructure by different rain
68 formation processes being more prevalent under different synoptic scale conditions.

69 Quantifying rain microstructure under different large-scale weather types may have practical
70 applications for radar based estimation of rain intensity. Quantitative precipitation estimation (QPE)
71 has to take rain microstructure into consideration, because it influences the relationship between
72 radar reflectivity Z and rain intensity R . For this reason, separate equations are used to estimate rain
73 intensity of convective and stratiform rain type [8,52], instead of using one equation that fits both rain
74 types. A similar improvement of the radar estimation of rain might be possible when considering
75 specific Z - R relation for each weather type case. We previously reported weather type specific Z - R
76 models with lower errors in estimating rain intensity in Lausanne, Switzerland [15]. However,
77 parameterizing Z - R equations for many weather types requires large amounts of data to represent
78 each class. Influence of weather types on Z - R relationships was also reported for the Cévennes-
79 Vivarais Region, France [14].

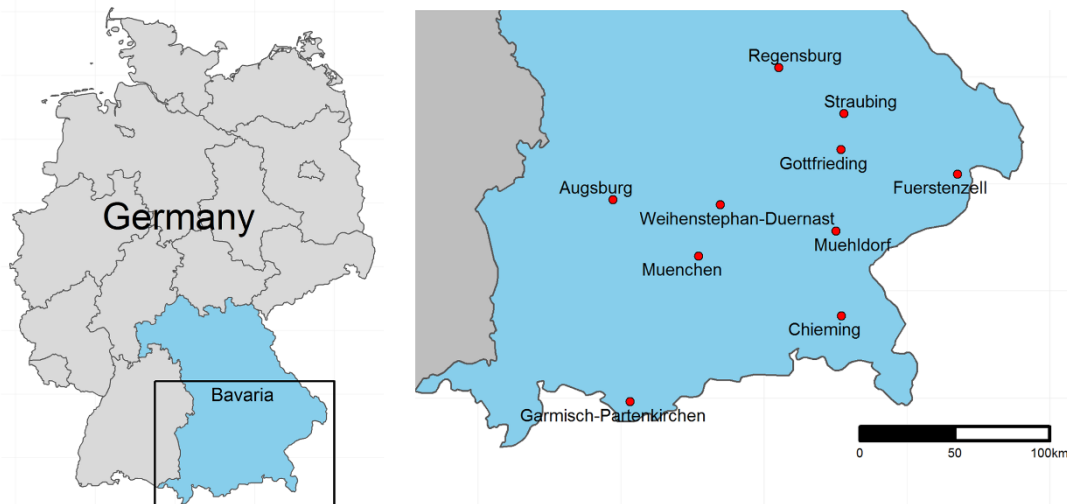
80 Here, we contribute an analysis of the relationship between Z - R parameters and weather types
81 in Central Europe, based on a comprehensive regional dataset of rain microstructure measurements
82 at 10 sites in the province of Bavaria, Germany. We ask: (1) what is the effect and the relative
83 importance of weather type and rain type on rain microstructure? and (2) is there consistent variation
84 between the Z - R parameters between weather types that would imply opportunities to improve QPE
85 with radar-based methods? To address these questions, we investigate disdrometer records under
86 different large-scale wind direction patterns at a daily scale, and rain type classifications at one
87 minute intervals over a period of three years.

88 2. Materials and Methods

89 2.1. Data sources and tools

90 We obtained raw rain drop size distribution measurements from the German Meteorological
91 Service (Deutscher Wetterdienst, DWD), operating a network of Thies disdrometers in Bavaria, in the
92 southeast of Germany (Figure 1). We analyzed measurements at ten sites spanning a period of three
93 years (Jan. 2014 – Dec. 2016) with a temporal resolution of one minute. The disdrometers locations
94 cover a distance of 167 km from north to south and 185 km from east to west (Figure 1). Raw

95 disdrometer data requires some statistical data cleaning procedures to remove erroneous readings.
 96 We follow the filtering procedure of Friedrich et al. [53] and the additional steps of Ghada et al. [15]
 97 to remove unrealistically large particles, margin fallers, splashing effects, or readings of insect and
 98 spider webs. The filtering procedure also removes non-rain intervals, intervals indicating very high
 99 wind speed, and intervals with rain intensity lower than 0.1 mm/h. After filtering, the dataset
 100 contained a total of 21,705 mm of accumulated rain over a period of 18,633 hours.
 101



102 **Figure 1.** Disdrometer locations in Bavaria (SE Germany) that were used to measure rain
 103 microstructure, covering a combined 18,600 hours of rain in a period of 36 months.

104 The DWD classifies large-scale synoptic weather patterns into 40 classes of weather types. The
 105 weather type is provided on a daily time scale, and is applicable to all of Germany and its
 106 surroundings. The classification is based on an operational numerical weather model that represents
 107 the geopotential, temperature, relative humidity, and the zonal and meridional components of the
 108 wind for several elevations [54]. In order to simplify the classification for the purpose of this study,
 109 we grouped all possible classes into according to their prevailing circulation patterns and wind
 110 directions. Five classes of wind direction are possible; northeasterly (NE), southeasterly (SE),
 111 southwesterly (SW), northwesterly (NW), and no prevailing direction (XX). A detailed explanation
 112 of the classification procedure is available online [54], and the full record of weather types is provided
 113 by the DWD [55].

114 For data filtering, analysis, and production of visual and statistical results, we used R [56],
 115 RStudio [57], and the packages caret [58], e1071 [59], reshape2 [60], raster [61], Rmisc [62], ggplot2
 116 [63], and rnatualearth [64].

117 2.2. Drop size distribution parameters

118 Thies disdrometers are laser-based instruments that provide high temporal records of rain
 119 microstructure. When a precipitation particle passes between the transmitter and the receiver, the
 120 strength of the laser beam is reduced. Based on the magnitude and duration of this reduction, it is
 121 possible to estimate the size and velocity of the passing precipitation particle. The Thies disdrometers
 122 raw data output represents one-minute summaries of the number of particles in 22 non-linear size
 123 classes and 20 non-linear velocity classes. From the raw output, a number of parameters can be
 124 obtained. This study is focused particularly on rain intensity R , radar reflectivity Z , total number of
 125 drop concentration N , and median volume drop diameter D_0 .
 126

127 Rain rate R (mm/h) is given by:
 128

$$R = 60 \times 60 \times \frac{\pi}{6 \times 10^6 \times \Delta T} \times \sum_{i=1}^{22} \sum_{j=1}^{20} \left(x_{i,j} \frac{D_i^3}{A_i} \right), \quad (1)$$

129 where

130 $x_{i,j}$: Detected number of drops that fall in diameter range i and velocity range j ,

131 ΔT (s): Temporal resolution (60 s in this case),

132 A_i (m²): Corrected detection area: $A_i = 228 \times (20 - \frac{D_i}{2})/10^6$,

133 D_i (mm): Mean diameter of drops that fall in diameter range i .

134

135 The radar reflectivity Z (dBZ) is calculated with the following expression:

136

$$Z = 10 * \log_{10} \left(\sum_{i=1}^{22} \sum_{j=1}^{20} \left(x_{i,j} \frac{D_i^6}{(A_i V_j \Delta T)} \right) \right), \quad (2)$$

137

138 where V_j (m/s): Mean velocity of drops that fall in the velocity range j .

139

140 The total number of drops N (m⁻³) is computed according to:

141

$$N = \sum_{i=1}^{22} \sum_{j=1}^{20} \left(\frac{x_{i,j}}{A_i V_j W_i \Delta T} \right), \quad (3)$$

142 where W_i (mm): the width of the diameter range i .

143 Finally, the median volume diameter D_0 (mm) is calculated considering that the volume of all

144 drops with diameters smaller than D_0 equals the volume of all drops with a diameter greater than

145 D_0 . It can be specified by solving the equation:

146

$$\int_{D=0}^{D=D_0} D^3 N(D) dD = \int_{D=D_0}^{D=inf} D^3 N(D) dD, \quad (4)$$

147 where $N(D)$ is the number of drops with the specific diameter D in 1 m³.

148 Additionally, the classification of rain type into convective and stratiform requires the use of the

149 following parameters: sd_N_10 , $sd_D_0_10$, and $sd_log_{10}R_10$, where sd_XX_10 is the standard

150 deviation of the values of XX (XX being N , D_0 and R respectively) over a time window of 10 minutes.

151 2.3. Rain type classification

152 Rain type classification uses an ensemble classifier to predict stratiform versus convective rain

153 based on cloud type, rain intensity and the standard deviation of rain intensity over a ten minute

154 time interval.

155 To create a training set for the machine learning model that classifies rain type into convective

156 and stratiform, we obtained records of cloud genera from the DWD [65]. These ground observations

157 were available between July 2013 and August 2014 at Fürstzell and between July 2013 and January

158 2014 at Regensburg. The cloud genera were used to create a training set for the machine learning

159 model that classifies rain type into convective and stratiform.

160 A random forest classification model was trained on the available data from two locations in this

161 dataset. A combination of two criteria was used for the prior classification, the observation of cloud

162 genus, and the values of R and its standard deviation over five minutes. The model was trained based

163 on the intervals where the prior classification was feasible. It was then used to classify rain in the

164 whole dataset. More details about the classification procedure are given by Ghada et al [26].

165 2.4. Retrieving the parameters of the Z–R Relation

166 Weather radars usually provide the reflectivity Z which is transformed into rain intensity R

167 using an exponential equation. In our case, R and Z are provided by the disdrometer, therefore it is

168 possible to get the values of A and b by fitting a linear model to the values of $\log_{10}(R)$ and Z .

169 The radar reflectivity Z is assumed to be related to rain intensity R by the power law:

$$Z = A \times R^b \quad (5)$$

170 In this equation, Z is expressed in mm^6m^{-3} . However, Z is usually expressed in the unit decibel
171 relative to Z (dBZ):

$$Z_{[\text{dBZ}]} = 10 \times \log_{10}(Z_{[\text{mm}^6 \text{m}^{-3}]}) \quad (6)$$

172 By taking the log of equation (5) and multiplying by 10:

$$10 \times \log_{10}(Z) = 10 \times \log_{10}(A) + 10 \times b \times \log_{10}(R) \quad (7)$$

173 And based on equation (6):

$$\text{dBZ} = 10 \times \log_{10}(A) + 10 \times b \times \log_{10}(R) \quad (8)$$

174 a simple linear model is fitted to the values of dBZ and log R which are calculated from the rain drop
175 size distribution. This linear model has the equation:

$$\text{dBZ} = \text{intercept} + \text{slope} \times \log_{10}(R) \quad (9)$$

176 so by comparing equations (8) and (9) the A and b parameters can be readily found:

$$b = \frac{\text{slope}}{10} \quad (10)$$

$$A = 10^{\frac{\text{intercept}}{10}} \quad (11)$$

177 Equations 5 – 11 represent the conventional way of retrieving A and b. An alternative method is
178 to consider R as the dependent variable [66]. This method is more appropriate because the main
179 purpose is to reduce errors in estimating R:

$$R = (1/A)^{1/b} \times Z^{1/b} \quad (12)$$

180 By taking the \log_{10} of both sides of equation (12):

$$\log_{10}(R) = \frac{1}{b} \times \log_{10}(Z) - \frac{1}{b} \times \log_{10}(A) \quad (13)$$

$$\log_{10}(R) = \frac{\text{dBZ}}{10 \times b} - \frac{\log_{10}(A)}{b} \quad (14)$$

$$\log_{10}(R) = \text{intercept} + \text{slope} \times \text{dBZ} \quad (15)$$

181 by comparing equations (14) and (15):

$$b = \frac{1}{\text{slope} \times 10} \quad (16)$$

$$A = 10^{-b \times \text{intercept}} \quad (17)$$

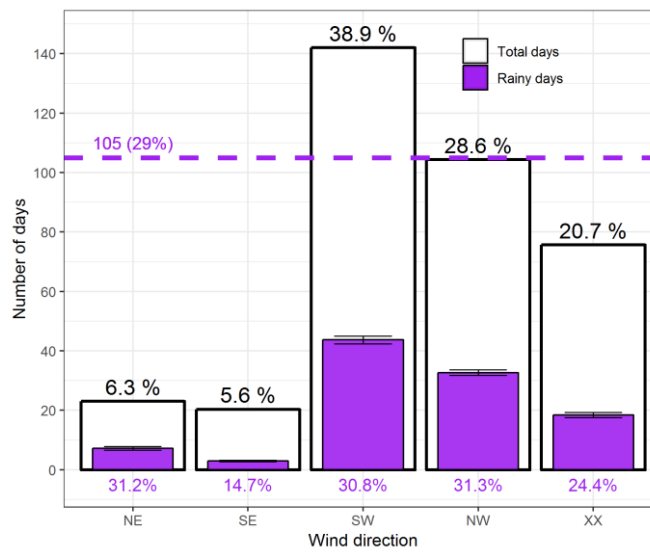
182 The values of A and b based on the conventional way are presented and discussed in the main
183 body of the text. The values using the alternative method are provided in the Appendix.

184 3. Results

185 3.1. Duration and amount variation with rain type and wind direction

186 Over the 1096 days included in the study period, rain was recorded at least at one station in 515
187 days. The five wind directions had different frequencies and the most frequent wind directions were
188 the westerly circulations SW and NW with a total of 739 days or two thirds of the time (Figure 2).
189 More than half of these days included rain in at least one station. The easterly circulations accounted
190 for less than 12% of the total number of days. SE had the lowest occurrence and the lowest percentage
191 of rainy days. Each of XX and NE had more than 40% rainy days (Figure 2).

192

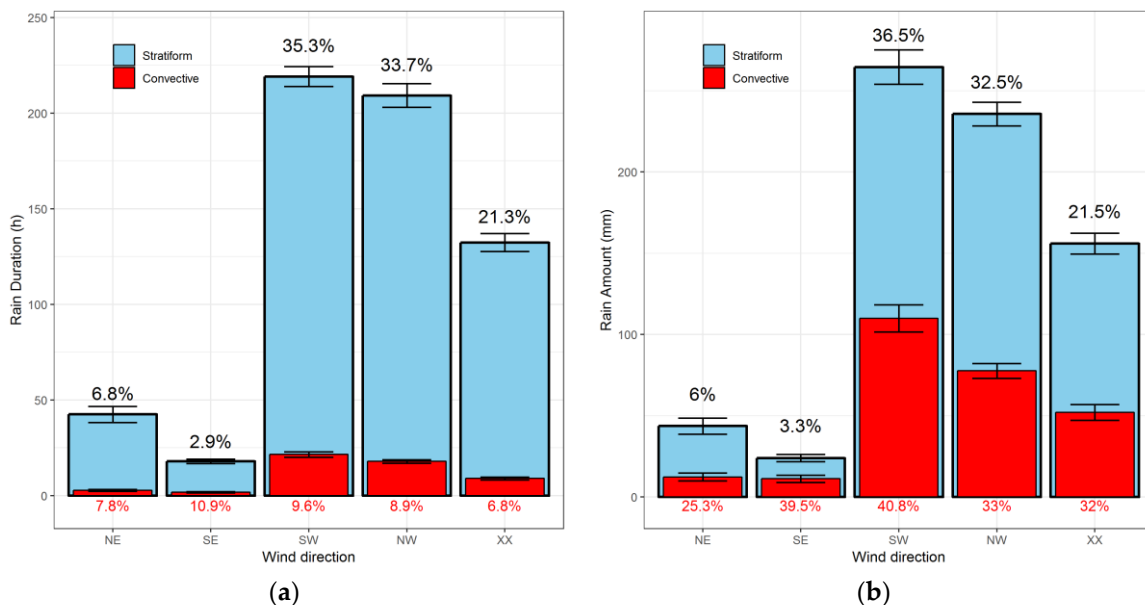


193
194
195
196
197
198

Figure 2. Frequency of rainy days under different wind direction classes that represent large-scale weather types. Rainy days are days where five minutes of rain with intensities exceeding 0.2 mm/h occurred at one station at least. Error bars represent the 95% confidence intervals. Percentages above the white columns represent the portion of each wind direction occurrence and percentages below the columns represent the portion of rainy days in the total number of days within a specific wind direction. The dashed line represents the mean number of rainy days per year.

199
200
201
202
203
204
205
206

When examining the accumulated rain amount and duration, westerly circulations were the dominant wind directions with a contribution reaching 69% of the total rain duration (18633 h) and total rain amount (21705 mm) accumulated over all stations (Figure 3). Easterly circulations contributed less than 10% of both rain duration and amount. Convection contributed 36% of the total rain amount and occupied only 8.5% of rain duration. Southerly circulations had the highest proportion of convective rain with around 10% of the total rain duration and more than 40% of the total rain amount, while northerly, and especially northeasterly circulations had a low proportion of convective rain.



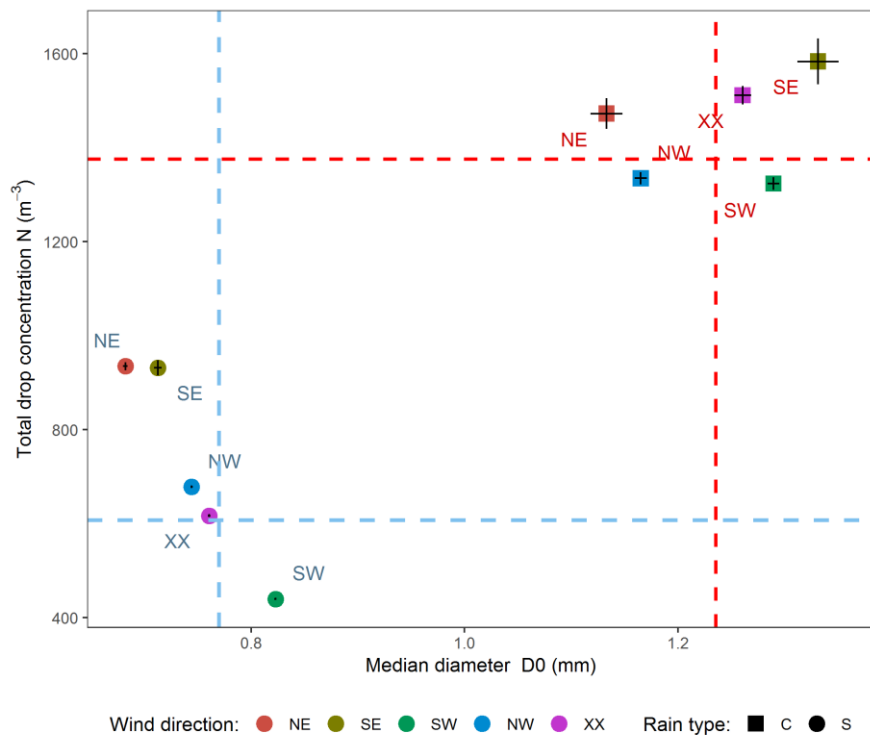
207
208
209
210

Figure 3. Prevalence of convective and stratiform rain types. Accumulated rain duration (a), and rain amount (b) per wind direction averaged over the stations and years. Error bars represent the 95% confidence intervals. The percentages on top of each column represent the proportion of accumulated rain within the respective wind direction to the accumulated rain in the whole year. The percentages

211 below the columns represent the proportion of convective rain to total rain within the respective wind
 212 direction.

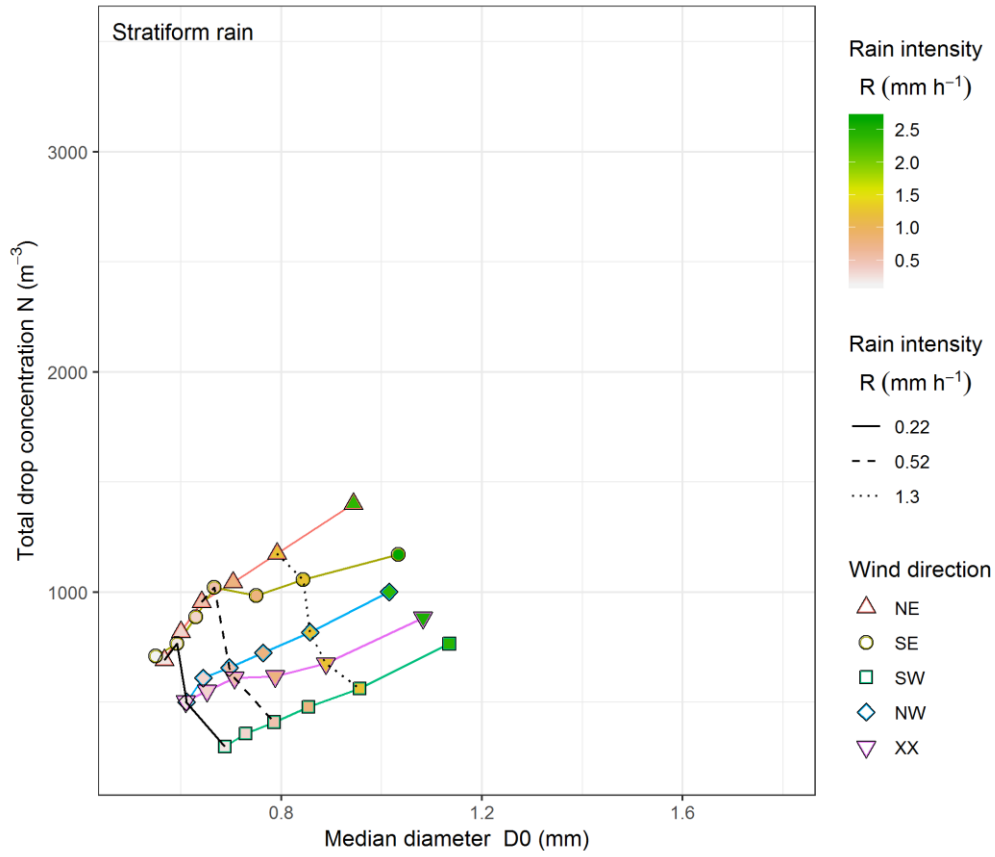
213 3.2. Rain microstructure variation with rain type and wind direction

214 Stratiform rain had smaller drops and lower concentration compared to convective rain (Figure
 215 4). The average D0 for stratiform rain was 0.77 mm compared to 1.24 mm in convective rain. Drop
 216 concentration in stratiform rain was slightly more than 600 drops m^{-3} , while convective rain had an
 217 average of 1375 drops m^{-3} . The overall average D0 (0.81 mm) and N (672 m^{-3}) were closer to the values
 218 of stratiform rain since most rain intervals were of the stratiform type.
 219

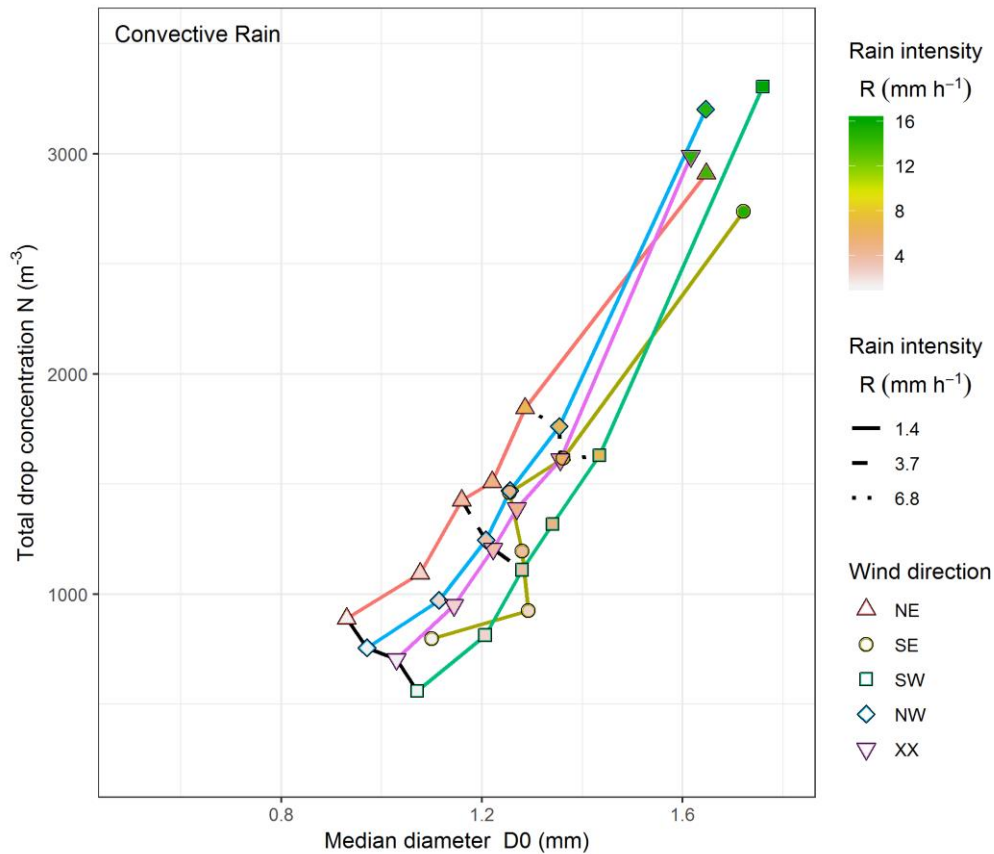


220 **Figure 4.** Summary of rain microstructure for stratiform and convective rain. Each point represents
 221 the mean total concentrations N (y axis) and mean median diameter D0 (x axis) of rain drops per wind
 222 direction and rain type. Horizontal dashed blue (red) line represents the stratiform (convective) mean
 223 rain drop concentration regardless of wind direction. Vertical dashed blue (red) line represents the
 224 stratiform (convective) mean D0 regardless of wind direction. Error bars on the horizontal and vertical
 225 axis represent the 95% confidence intervals.

226 For stratiform rain, westerly circulations had larger drops and lower drop concentration
 227 compared to easterly circulations. Especially SW had the largest mean of D0 and the least N. NE had
 228 clearly the smallest drops and the greatest N. The same pattern appears even when inspecting
 229 different classes of rain intensity within stratiform rain (Figure 5). As rain intensity increases, so does
 230 both D0 and N. For convective rain (Figure 6), only few differences in the previously described
 231 patterns appear especially when examining the rain microstructure for different ranges of rain
 232 intensities. The median diameter D0 was the largest for SW and decreased in values by XX, NW then
 233 NE while N increased in the same order for most cases. The highest range of rain intensities did not
 234 follow this pattern, possibly due to high stochasticity of rare extreme rain events. The wind direction
 235 SE also did not show a consistent pattern across the different rain intensity ranges.



236 **Figure 5.** Rain microstructure for different rain intensities in stratiform rain. Symbol on each colored
 237 line represent summary statistics for a wind direction. Each symbol represents the average median
 238 drop size and drop concentration for a rain intensity interval. The intervals were chosen to represent
 239 six equal sample sizes and were colored by mean rain intensity. Selected symbols that represent equal
 240 rain intensity were connected with black lines for comparison.



241 **Figure 6.** Rain microstructure for different rain intensities in convective rain. Symbol on each colored
 242 line represent summary statistics for a wind direction. Each symbol represents the average median
 243 drop size and drop concentration for a rain intensity interval. The intervals were chosen to represent
 244 six equal sample sizes and were colored by mean rain intensity.

245
 246 The mean stratiform rain intensity was 0.81 mm/h with only marginal variation with wind
 247 directions. On the other hand, convective rain intensity varied around the mean value of 5 mm/h.
 248 The highest mean intensity was associated with SE circulations and the lowest with the NW
 249 circulations. Statistical data for each wind direction and rain type including standard deviation (SD)
 250 and standard error (SE) are summarized in Table 1.

251
 252 **Table 1.** Summary of rain intensities for wind directions in convective and stratiform rain.

Rain type	Wind direction	Duration (h)	Mean R (mm/h)	Median R (mm/h)	SD (mm/h)	SE (mm/h)
Convective	NE	82.5	4.51	3.65	4.90	0.070
	SE	50.7	6.23	4.83	6.41	0.116
	SW	645.6	5.11	3.72	6.09	0.031
	NW	538.1	4.33	3.36	4.89	0.027
	XX	269.6	5.80	4.54	5.79	0.046
Stratiform	NE	1191.9	0.79	0.50	0.79	0.003
	SE	486.2	0.80	0.46	0.92	0.005
	SW	5928.4	0.78	0.49	0.79	0.001
	NW	5740.0	0.83	0.54	0.80	0.001
	XX	3700.8	0.84	0.52	0.89	0.002

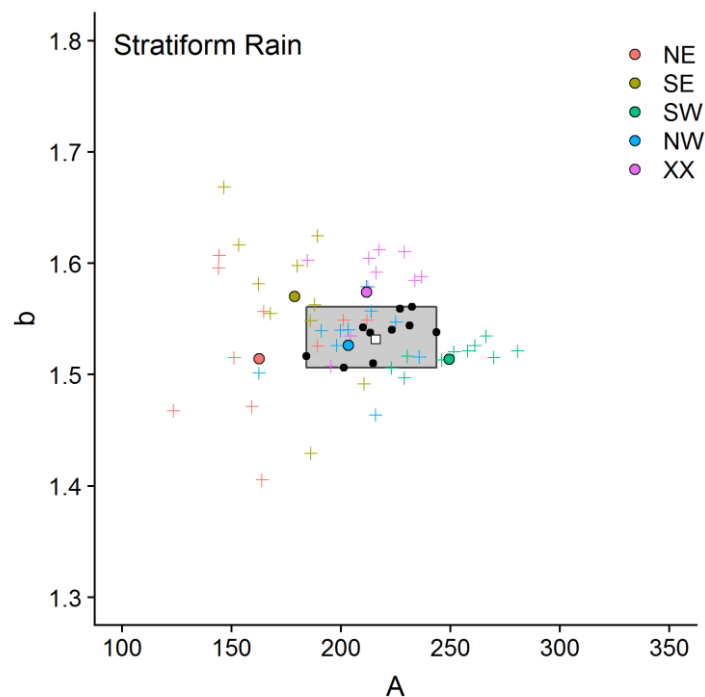
254 3.3. Z-R parameter variation with location, rain type and wind direction

255 To demonstrate the influence of rain microstructure variability with wind direction on the rain
 256 intensity retrieval equation Z-R, the values of A and b were obtained for both rain types (the general
 257 model), then for the combinations of rain types and locations (the location model), then for rain types
 258 and wind directions (the wind direction model), and finally for the rain type, locations and wind
 259 direction combinations (the factorial model).

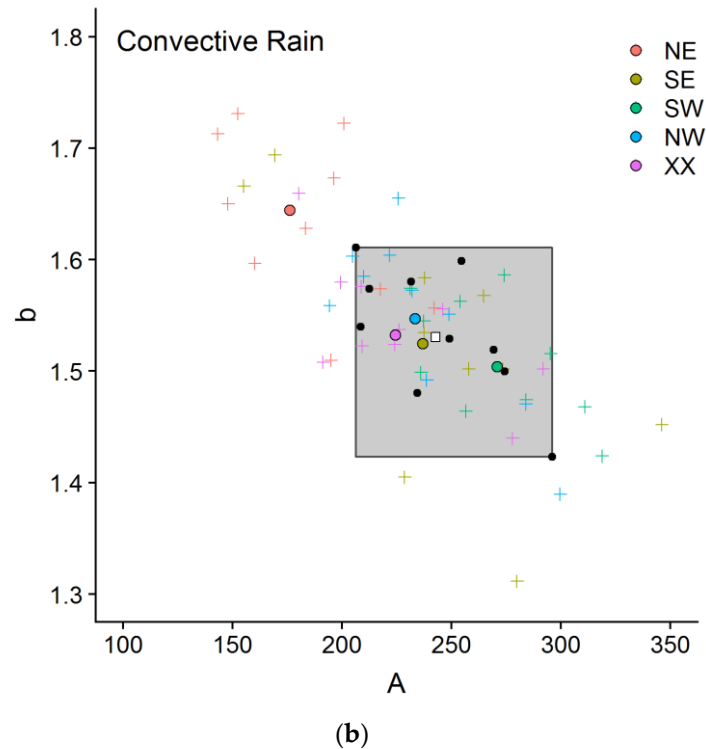
260 The value of the prefactor A was clearly larger in convective rain (216) compared to its value in
 261 stratiform rain (243) for the general model, while the exponent b value (1.53) was similar for both rain
 262 types (Figure 7, white box). In the case of the location model (Figure 7, black points and grey area), A
 263 had a smaller range and values in stratiform rain (184-244) compared to convective rain (206-296). B
 264 on the other hand had similar average value but a smaller range in stratiform rain (1.51-1.56)
 265 compared to its values in convective rain (1.42-1.61).

266 Remarkably for stratiform rain, the range of A values in the wind direction model (162-249,
 267 Figure 7.a colored circles) exceeded the range of A values for the location model (black points), with
 268 SW circulations scoring the highest A values, and the easterly circulations scoring the least. On the
 269 other hand, b values had a range in the wind direction model very close to the location model, with
 270 the smallest values associated with the three wind direction classes SW, NW and NE, and the highest
 271 values associated with XX and SE. A and b values in the factorial model had a similar pattern to the
 272 one observed in the wind direction model with a higher variability; A value is large for SW, close to
 273 the mean for NW and XX, and small for NE and SE, while b value is large for XX and SE, and small
 274 for SW, NW and NE.

275
 276



(a)



277 **Figure 7.** The parameters of the radar rain intensity retrieval equation ($Z=AR^b$) for the general model
 278 (white square), the location model (black dots), the wind direction model (colored circles), and the
 279 factorial model (colored crosses) for stratiform rain (a) and convective rain (b). The grey area
 280 represents the range of A and b for the location model.

281 In convective rain (Figure 7.b), the patterns of A and b for the wind direction model differed
 282 compared to the stratiform rain; A values were close to value of A for the general model, while SW
 283 had the largest and NE had the smallest values. All b values in the wind direction model were close
 284 to that in the general model except for NE circulations which had higher value. The same pattern
 285 appeared again with higher variability in the case of the factorial model, with the exception of SE
 286 circulation which did not follow a particular pattern in this case.

287 4. Discussion

288 Our data indicate high frequency and high contribution of westerly and especially SW
 289 circulations to the rainy days over Bavaria, Germany. Easterly circulations have the least frequency
 290 and especially SE has the lowest share of rainy days. This is in agreement with the frequency of wind
 291 directions and proportions of rainy days of long-term studies for Germany for the period between
 292 1995 and 2017 [44]. The high frequency and high contribution of westerly and southwesterly
 293 circulations to the number of rainy days is expected for this region since the main moisture flux is
 294 westerly [67].

295 Convection is responsible for 40% of rain amount in this region despite occupying only 10% of
 296 rain duration. Similar contributions of convective rain were reported in the Czech Republic [68] and
 297 in Switzerland [15]. Convective rain has typically higher rain rates and distinct microstructure
 298 compared to stratiform rain. This makes it essential to separate convective and stratiform rain prior
 299 to addressing rain microstructure, especially considering the variation in convective rain proportion
 300 with wind directions [15]. Southerly circulations generally have a higher proportion of convective
 301 rain compared to northerly circulations. A possible explanation is the strengthening and inhibition
 302 of convection and radiative cooling under different wind directions, which in turn has a major
 303 influence on the precipitation diurnal cycle over Germany [44]. Southerly circulations carry along
 304 warm air masses which intensify convection in the afternoon and inhibit radiative cooling in the

305 morning. Northerly circulations, in contrast, transport cold air masses and therefore suppress
306 convection and intensify radiative cooling.

307 Westerly circulations need special attention when addressing rain and microstructure, especially
308 with the reported high contribution to rain duration and rain amount, and the expected increase in
309 frequency over Europe [69,70]. Westerly circulations have larger rain drops than easterly circulations
310 in stratiform rain, while easterly circulations have higher number of drops. This pattern is consistent
311 for both stratiform and convective rain and across the ranges of rain intensity, except for SE
312 circulations in convective rain, which was not well represented by data, accounting only for 0.6% of
313 convective rain amount observed in this study.

314 Rain microstructure dependence on synoptic weather patterns have previously been reported
315 for other locations in Europe. Northerly circulations in Leon Spain were associated with smaller drop
316 sizes, while westerly and southerly circulations have larger drops of rain [13]. This pattern was
317 explained by the location of Leon to the south of the Cantabrian Mountains. Northerly circulation air
318 masses precipitate prior to reaching Leon, leaving less humidity, lower rain intensities and smaller
319 drops. Westerly and southerly circulations carry along higher humidity, leading to higher rain
320 intensities and larger drops. For Cévennes-Vivarais region in France, easterly circulations were
321 associated with lower number of rain drops and larger drop size while most of the westerly
322 circulations had the opposite traits [14]. The associations of rain microstructure with large-scale
323 weather patterns observed in this and other studies are therefore not generally consistent, but region-
324 specific. Different regions have different associated general air-mass characteristics, for example
325 influenced by proximity to the sea or the presence of mountain massifs nearby.

326 The rain microstructure patterns in Bavaria have more in common with the patterns reported
327 for Lausanne, Switzerland. Despite using different disdrometer types, having different schemes for
328 rain type classification, using different weather type classifications, and the geographical locations at
329 different sides of the Alps, easterly circulations in both locations have higher number of drops per
330 interval and smaller drop size compared to westerly circulations [15]. A plausible explanation for this
331 is the variation of humidity and aerosol content in air masses between these wind direction clusters.
332 Aerosols are particularly abundant in air masses which pass over Russia and Eastern Europe,
333 especially heavy industrialized areas [71,72]. These aerosols act as cloud condensation nuclei [73].
334 High cloud condensation nuclei availability increases the number of rain drops in the case of
335 stratiform rain, increases the size of drops in local convection, and have no significant influence on
336 rain microstructure in organized convection [74].

337 Differences in the load of cloud condensation nuclei under different circulations appear to be a
338 plausible explanation for the rain microstructure differences observed in this study, especially in
339 stratiform rain. The abundance on cloud condensation nuclei in easterly circulations in comparison
340 with westerly circulations leads to higher number of rain drops. This in combination with the high
341 (low) available humidity in westerly (easterly) circulations leads to larger (smaller) size of rain drops.
342 For convective rain, easterly circulations are clustered in two wind directions, NE which has the
343 smallest mean D_0 , and SE which has the largest mean D_0 compared to the remaining wind directions.
344 The rain type classification method used in this study does not differentiate local and organized
345 convection, which makes it impossible to thoroughly compare with the findings of Cecchini et al.
346 [74].

347 Regarding applications of our results for radar-based quantitative precipitation estimates (QPE),
348 Jaffrain et al. [66] demonstrated that the variation of A and b values of the Z-R retrieval equation
349 should be accounted for. In their case study for Lausanne, Switzerland, they showed that spatial
350 subgrid variability of rain microstructure was present, and then assessed the influence of this
351 variation on the quality of the estimation of rain rate. Using the same dataset, Ghada et al. [15] showed
352 that the variability of A and b is larger than the subgrid spatial variability (in an area less than 1 km²)
353 when weather types are considered. In this study, variation of rain microstructure parameters with
354 wind directions in Bavaria led to significant variation in the values of Z-R parameters. The variation
355 in the values of the prefactor A and the exponent b exceeds their spatial variation within the

356 addressed regional scale in the case of stratiform rain, and at least is similar to the spatial variation
357 in the case of convective rain.

358 Assessing potential benefits of accounting for variation in Z-R parameters, Jaffrain and Berne
359 [66] concluded that the subgrid spatial variability in rain microstructure caused rain measurement
360 errors estimated to fall between -2% and +15%. Variability due to large-scale weather patterns in Z-R
361 parameters in our study was greater than the subgrid spatial variability of rain microstructure.
362 Consequently, the potential for a large improvement in rain estimation when accounting for rain
363 microstructure variability with wind direction is expected to be high. The next research step would
364 be to assess improvements in quantitative estimation of rain by working directly with empirical data
365 of radar-based rain intensity estimates validated by ground observations, and quantifying the
366 accuracy improvements when taking the variability of Z-R parameters with wind directions into
367 account. This is not possible with data from the current study. Disdrometers provide a direct
368 measurement of rain microstructure, and then R and Z are calculated. These values are accurate if we
369 assume an accurate measurement of rain microstructure. Actual radar reflectivity measurements are
370 needed for an appropriate estimation of the improvement associated with using wind direction-
371 specific Z-R relations.

372 5. Conclusions

373 This research demonstrated that rain microstructure varies significantly between weather types
374 in both rain types. Easterly circulations had the highest drop concentration and the smallest drop size
375 while westerly circulations were associated with large drops and low drop concentration. A plausible
376 explanation for these differences is the high humidity content in westerly circulations and high cloud
377 condensation nuclei concentration in easterly circulation. This finding has potential applications for
378 radar-based quantitative precipitation estimates. Z-R parameters vary substantially with synoptic
379 weather patterns that can effectively be summarized by regional wind direction classes. The
380 variability in Z-R parameters with wind direction exceeds their station-to-station spatial variability
381 for stratiform, but not for convective rain. We therefore conclude that building separate Z-R retrieval
382 equation for regional wind direction classes should improve radar-based QPE, especially for
383 stratiform rain events. This approach should be feasible for forecasting on the operational level
384 especially taking into account that daily weather types can be predicted with high accuracy several
385 days in advance.

386

387 **Author Contributions:** Conceptualization, W.G. and A.M.; methodology and formal analysis, W.G.; writing—
388 original draft preparation, W.G.; supervision, A.M.; writing—review and editing, All coauthors.

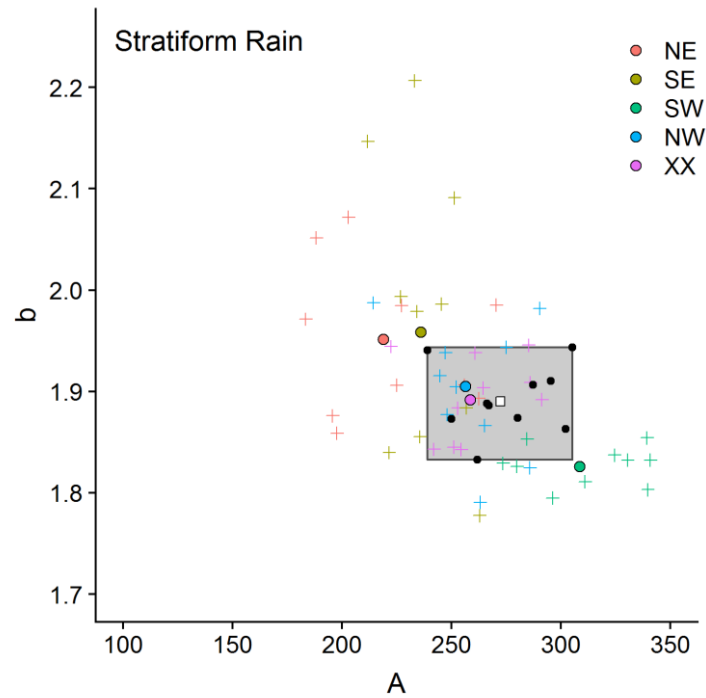
389 **Funding:** J.B. was partly funded by project RTI2018-098693-B-C32 (AEI/FEDER)

390 **Acknowledgments:** We thank the Deutscher Wetterdienst (German Meteorological Service-DWD) for providing
391 the disdrometer data, the classification of weather types, and the cloud observation data. The first author thanks
392 the Deutscher Akademischer Austauschdienst (DAAD) for financial support.

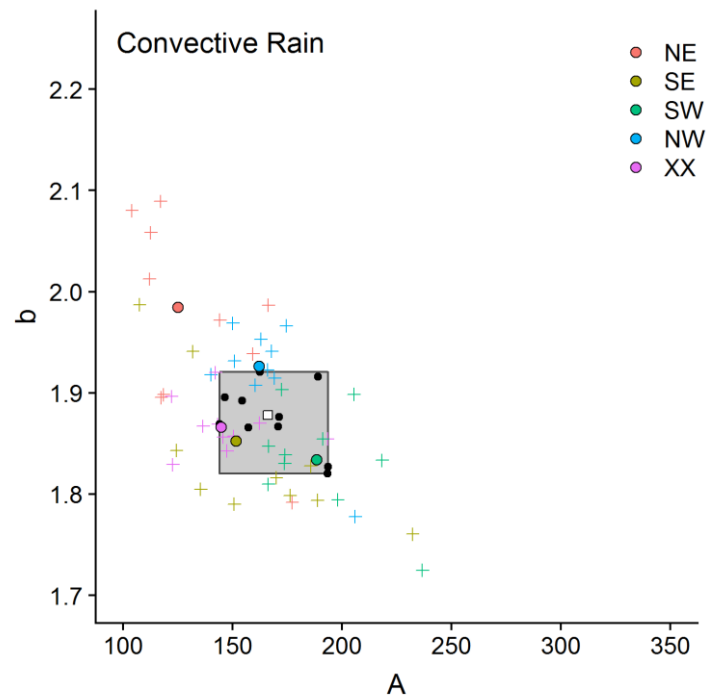
393 **Conflicts of Interest:** The funders had no role in the design of the study; in the collection, analyses, or
394 interpretation of data; in the writing of the manuscript, or in the decision to publish the results.

395 Appendix A

396 Based on the alternative retrieval method [66], Figure A1 shows the prefactor A and the exponent
397 b values corresponding with the four models (see section 2.4.).



(a)



(b)

398
399
400
401
402
403

Figure A1. The parameters of the radar rain intensity retrieval equation ($Z=AR^b$) for the general model (white square), the location model (black dots), the wind direction model (colored circles), and the factorial model (colored crosses) for stratiform rain (a) and convective rain (b). The grey area represents the range of A and b for the location model, where A and b values are calculated using the alternative method (see section 2.4.). The grey area represents the range of A and b for the location model.

404
405
406

References

1. Arulraj, M.; Barros, A.P. Improving quantitative precipitation estimates in mountainous regions by modelling low-level seeder-feeder interactions constrained by Global Precipitation Measurement

- 407 Dual-frequency Precipitation Radar measurements. *Remote Sensing of Environment* **2019**, *231*, 111213,
408 doi:10.1016/j.rse.2019.111213.
- 409 2. Steiner, M.; Smith, J.A.; Uijlenhoet, R. A Microphysical Interpretation of Radar Reflectivity–Rain Rate
410 Relationships. *J. Atmos. Sci.* **2004**, *61*, 1114–1131, doi:10.1175/1520-
411 0469(2004)061<1114:AMIORR>2.0.CO;2.
- 412 3. Thompson, E.J.; Rutledge, S.A.; Dolan, B.; Thurai, M. Drop Size Distributions and Radar Observations
413 of Convective and Stratiform Rain over the Equatorial Indian and West Pacific Oceans. *J. Atmos. Sci.*
414 **2015**, *72*, 4091–4125, doi:10.1175/JAS-D-14-0206.1.
- 415 4. Steiner, M.; Smith, J.A. Convective versus stratiform rainfall: An ice-microphysical and kinematic
416 conceptual model. *Atmospheric Research* **1998**, *47–48*, 317–326, doi:10.1016/S0169-8095(97)00086-0.
- 417 5. Iacobellis, S.F.; McFarquhar, G.M.; Mitchell, D.L.; Somerville, R.C.J. The Sensitivity of Radiative Fluxes
418 to Parameterized Cloud Microphysics. *J. Climate* **2003**, *16*, 2979–2996, doi:10.1175/1520-
419 0442(2003)016<2979:TSORFT>2.0.CO;2.
- 420 6. Jameson, A.R.; Larsen, M.L.; Kostinski, A.B. Disdrometer Network Observations of Finescale Spatial–
421 Temporal Clustering in Rain. *J. Atmos. Sci.* **2015**, *72*, 1648–1666, doi:10.1175/JAS-D-14-0136.1.
- 422 7. Jaffrain, J.; Studzinski, A.; Berne, A. A network of disdrometers to quantify the small-scale variability
423 of the raindrop size distribution. *Water Resour. Res.* **2011**, *47*, 2673, doi:10.1029/2010WR009872.
- 424 8. Das, S.; Maitra, A. Characterization of tropical precipitation using drop size distribution and rain rate-
425 radar reflectivity relation. *Theor Appl Climatol* **2018**, *132*, 275–286, doi:10.1007/s00704-017-2073-1.
- 426 9. Gatlin, P.N.; Thurai, M.; Bringi, V.N.; Petersen, W.; Wolff, D.; Tokay, A.; Carey, L.; Wingo, M. Searching
427 for Large Raindrops: A Global Summary of Two-Dimensional Video Disdrometer Observations. *J.*
428 *Appl. Meteor. Climatol.* **2015**, *54*, 1069–1089, doi:10.1175/JAMC-D-14-0089.1.
- 429 10. Dolan, B.; Fuchs, B.; Rutledge, S.A.; Barnes, E.A.; Thompson, E.J. Primary Modes of Global Drop Size
430 Distributions. *J. Atmos. Sci.* **2018**, *75*, 1453–1476, doi:10.1175/JAS-D-17-0242.1.
- 431 11. Wen, L.; Zhao, K.; Wang, M.; Zhang, G. Seasonal Variations of Observed Raindrop Size Distribution
432 in East China. *Advances in Atmospheric Sciences* **2019**, *36*, 346–362, doi:10.1007/s00376-018-8107-5.
- 433 12. Niu, S.; Jia, X.; Sang, J.; Liu, X.; Lu, C.; Liu, Y. Distributions of Raindrop Sizes and Fall Velocities in a
434 Semiarid Plateau Climate: Convective versus Stratiform Rains. *J. Appl. Meteor. Climatol.* **2010**, *49*, 632–
435 645, doi:10.1175/2009JAMC2208.1.
- 436 13. Fernandez-Raga, M.; Castro, A.; Marcos, E.; Palencia, C.; Fraile, R. Weather types and rainfall
437 microstructure in Leon, Spain. *Int. J. Climatol.* **2017**, *37*, 1834–1842, doi:10.1002/joc.4816.
- 438 14. Hachani, S.; Boudevillain, B.; Delrieu, G.; Bargaoui, Z. Drop Size Distribution Climatology in
439 Cévennes-Vivarais Region, France. *Atmosphere* **2017**, *8*, 233, doi:10.3390/atmos8120233.
- 440 15. Ghada, W.; Buras, A.; Lüpke, M.; Schunk, C.; Menzel, A. Rain Microstructure Parameters Vary with
441 Large-Scale Weather Conditions in Lausanne, Switzerland. *Remote Sensing* **2018**, *10*, 811,
442 doi:10.3390/rs10060811.
- 443 16. Thurai, M.; Gatlin, P.N.; Bringi, V.N. Separating stratiform and convective rain types based on the drop
444 size distribution characteristics using 2D video disdrometer data. *Atmospheric Research* **2016**, *169*, 416–
445 423, doi:10.1016/j.atmosres.2015.04.011.
- 446 17. Cerro, C.; Codina, B.; Bech, J.; Lorente, J. Modeling Raindrop Size Distribution and Z (R) Relations in
447 the Western Mediterranean Area. *J. Appl. Meteor.* **1997**, *36*, 1470–1479, doi:10.1175/1520-
448 0450(1997)036<1470:MRSDAZ>2.0.CO;2.
- 449 18. Munchak, S.J.; Kummerow, C.D.; Elsaesser, G. Relationships between the Raindrop Size Distribution
450 and Properties of the Environment and Clouds Inferred from TRMM. *J. Climate* **2012**, *25*, 2963–2978,
451 doi:10.1175/JCLI-D-11-00274.1.
- 452 19. Villermaux, E.; Bossa, B. Single-drop fragmentation determines size distribution of raindrops. *Nature*
453 *Phys* **2009**, *5*, 697–702, doi:10.1038/nphys1340.
- 454 20. Rosenfeld, D.; Ulbrich, C.W. Cloud Microphysical Properties, Processes, and Rainfall Estimation
455 Opportunities. *Meteorological Monographs* **2003**, *30*, 237, doi:10.1175/0065-
456 9401(2003)030<0237:CMPPAR>2.0.CO;2.
- 457 21. Tokay, A.; Short, D.A. Evidence from Tropical Raindrop Spectra of the Origin of Rain from Stratiform
458 versus Convective Clouds. *J. Appl. Meteor.* **1996**, *35*, 355–371, doi:10.1175/1520-
459 0450(1996)035<0355:EFTRSO>2.0.CO;2.

- 460 22. Caracciolo, C.; Prodi, F.; Battaglia, A.; Porcu', F. Analysis of the moments and parameters of a gamma
461 DSD to infer precipitation properties: A convective stratiform discrimination algorithm. *Atmospheric*
462 *Research* **2006**, *80*, 165–186, doi:10.1016/j.atmosres.2005.07.003.
- 463 23. Caracciolo, C.; Porcu', F.; Prodi, F. Precipitation classification at mid-latitudes in terms of drop size
464 distribution parameters. *Adv. Geosci.* **2008**, *16*, 11–17, doi:10.5194/adgeo-16-11-2008.
- 465 24. Bringi, V.N.; Williams, C.R.; Thurai, M.; May, P.T. Using Dual-Polarized Radar and Dual-Frequency
466 Profiler for DSD Characterization: A Case Study from Darwin, Australia. *J. Atmos. Oceanic Technol.*
467 **2009**, *26*, 2107–2122, doi:10.1175/2009JTECHA1258.1.
- 468 25. Bukovčić, P.; Zrnić, D.; Zhang, G. Convective–stratiform separation using video disdrometer
469 observations in central Oklahoma – the Bayesian approach. *Atmospheric Research* **2015**, *155*, 176–191,
470 doi:10.1016/j.atmosres.2014.12.002.
- 471 26. Ghada, W.; Estrella, N.; Menzel, A. Machine Learning Approach to Classify Rain Type Based on Thies
472 Disdrometers and Cloud Observations. *Atmosphere* **2019**, *10*, 251, doi:10.3390/atmos10050251.
- 473 27. Baur, F.; Hess, P.; Nagel, H. Kalender der grosswetterlagen Europas 1881 - 1939. *Bad Homburg* **1944**,
474 35.
- 475 28. Steirou, E.; Gerlitz, L.; Apel, H.; Merz, B. Links between large-scale circulation patterns and streamflow
476 in Central Europe: A review. *Journal of Hydrology* **2017**, *549*, 484–500, doi:10.1016/j.jhydrol.2017.04.003.
- 477 29. Petrow, T.; Merz, B.; Lindenschmidt, K.-E.; Thieken, A.H. Aspects of seasonality and flood generating
478 circulation patterns in a mountainous catchment in south-eastern Germany. *Hydrol. Earth Syst. Sci.*
479 **2007**, *11*, 1455–1468, doi:10.5194/hess-11-1455-2007.
- 480 30. Nied, M.; Pardowitz, T.; Nissen, K.; Ulbrich, U.; Hundecha, Y.; Merz, B. On the relationship between
481 hydro-meteorological patterns and flood types. *Journal of Hydrology* **2014**, *519*, 3249–3262,
482 doi:10.1016/j.jhydrol.2014.09.089.
- 483 31. Nikolopoulos, E.I.; Borga, M.; Marra, F.; Crema, S.; Marchi, L. Debris flows in the eastern Italian Alps:
484 seasonality and atmospheric circulation patterns. *Nat. Hazards Earth Syst. Sci.* **2015**, *15*, 647–656,
485 doi:10.5194/nhess-15-647-2015.
- 486 32. Wastl, C.; Schunk, C.; Lüpke, M.; Cocca, G.; Conedera, M.; Valsecchi, E.; Menzel, A. Large-scale weather
487 types, forest fire danger, and wildfire occurrence in the Alps. *Agricultural and Forest Meteorology* **2013**,
488 *168*, 15–25, doi:10.1016/j.agrformet.2012.08.011.
- 489 33. Kassomenos, P. Synoptic circulation control on wild fire occurrence. *Physics and Chemistry of the Earth,*
490 *Parts A/B/C* **2010**, *35*, 544–552, doi:10.1016/j.pce.2009.11.008.
- 491 34. Russo, A.; Trigo, R.M.; Martins, H.; Mendes, M.T. NO₂, PM₁₀ and O₃ urban concentrations and its
492 association with circulation weather types in Portugal. *Atmospheric Environment* **2014**, *89*, 768–785,
493 doi:10.1016/j.atmosenv.2014.02.010.
- 494 35. Nidzgorska-Lencewicz, J.; Czarnecka, M. Winter weather conditions vs. air quality in Tricity, Poland.
495 *Theor Appl Climatol* **2015**, *119*, 611–627, doi:10.1007/s00704-014-1129-8.
- 496 36. Grundström, M.; Dahl, Å.; Ou, T.; Chen, D.; Pleijel, H. The relationship between birch pollen, air
497 pollution and weather types and their effect on antihistamine purchase in two Swedish cities.
498 *Aerobiologia* **2017**, *33*, 457–471, doi:10.1007/s10453-017-9478-2.
- 499 37. Ramos, A.M.; Barriopedro, D.; Dutra, E. Circulation weather types as a tool in atmospheric, climate,
500 and environmental research. *Front. Environ. Sci.* **2015**, *3*, doi:10.3389/fenvs.2015.00044.
- 501 38. Huth, R.; Beck, C.; Philipp, A.; Demuzere, M.; Ustrnul, Z.; Cahynová, M.; Kyselý, J.; Tveito, O.E.
502 Classifications of atmospheric circulation patterns: recent advances and applications. *Ann. N. Y. Acad.*
503 *Sci.* **2008**, *1146*, 105–152, doi:10.1196/annals.1446.019.
- 504 39. Buishand, T.A.; Brandsma, T. Comparison of circulation classification schemes for predicting
505 temperature and precipitation in the Netherlands. *Int. J. Climatol.* **1997**, *17*, 875–889,
506 doi:10.1002/(SICI)1097-0088(19970630)17:8<875:AID-JOC164>3.0.CO;2-C.
- 507 40. Vallorani, R.; Bartolini, G.; Betti, G.; Crisci, A.; Gozzini, B.; Grifoni, D.; Iannuccilli, M.; Messeri, A.;
508 Messeri, G.; Morabito, M.; et al. Circulation type classifications for temperature and precipitation
509 stratification in Italy. *Int. J. Climatol.* **2018**, *38*, 915–931, doi:10.1002/joc.5219.
- 510 41. Huth, R.; Beck, C.; Kučerová, M. Synoptic-climatological evaluation of the classifications of
511 atmospheric circulation patterns over Europe. *Int. J. Climatol.* **2016**, *36*, 2710–2726, doi:10.1002/joc.4546.
- 512 42. Broderick, C.; Fealy, R. An analysis of the synoptic and climatological applicability of circulation type
513 classifications for Ireland. *Int. J. Climatol.* **2015**, *35*, 481–505, doi:10.1002/joc.3996.

- 514 43. Cortesi, N.; Trigo, R.M.; Gonzalez-Hidalgo, J.C.; Ramos, A.M. Modelling monthly precipitation with
515 circulation weather types for a dense network of stations over Iberia. *Hydrol. Earth Syst. Sci.* **2013**, *17*,
516 665–678, doi:10.5194/hess-17-665-2013.
- 517 44. Ghada, W.; Yuan, Y.; Wastl, C.; Estrella, N.; Menzel, A. Precipitation Diurnal Cycle in Germany Linked
518 to Large-Scale Weather Circulations. *Atmosphere* **2019**, *10*, 545, doi:10.3390/atmos10090545.
- 519 45. Twardosz, R. A synoptic analysis of the diurnal cycle of thunderstorm precipitation in Kraków
520 (Southern Poland). *Int. J. Climatol.* **2009**, *26*, n/a-n/a, doi:10.1002/joc.1960.
- 521 46. Mandapaka, P.V.; Germann, U.; Panziera, L. Diurnal cycle of precipitation over complex Alpine
522 orography: inferences from high-resolution radar observations. *Q.J.R. Meteorol. Soc.* **2013**, *139*, 1025–
523 1046, doi:10.1002/qj.2013.
- 524 47. Cony, M.; Martin, L. Synoptic patterns that contribute to extremely hot days in Europe.
525 http://www.scielo.org.mx/scielo.php?script=sci_arttext&pid=S0187-62362010000400001. (Accessed on
526 22 January 2020).
- 527 48. Cassano, E.N.; Lynch, A.H.; Cassano, J.J.; Koslow. Classification of synoptic patterns in the western
528 Arctic associated with extreme events at Barrow, Alaska, USA. *Clim. Res.* **2006**, *30*, 83–97,
529 doi:10.3354/cr030083.
- 530 49. Nowosad, J.; Stach, A. Relation between extensive extreme precipitation in Poland and atmospheric
531 circulation. *Quaestiones Geographicae* **2014**, *33*, 115–129, doi:10.2478/quageo-2014-0005.
- 532 50. Maheras, P.; Tolika, K.; Anagnostopoulou, C.; Makra, L.; Szpirosz, K.; Károssy, C. Relationship
533 between mean and extreme precipitation and circulation types over Hungary. *Int. J. Climatol.* **2018**, *38*,
534 4518–4532, doi:10.1002/joc.5684.
- 535 51. Planchon, O.; Quénot, H.; Dupont, N.; Corgne, S. Application of the Hess-Brezowsky classification to
536 the identification of weather patterns causing heavy winter rainfall in Brittany (France). *Nat. Hazards*
537 *Earth Syst. Sci.* **2009**, *9*, 1161–1173, doi:10.5194/nhess-9-1161-2009.
- 538 52. Kirsch, B.; Clemens, M.; Ament, F. Stratiform and convective radar reflectivity–rain rate relationships
539 and their potential to improve radar rainfall estimates. *J. Appl. Meteor. Climatol.* **2019**,
540 doi:10.1175/JAMC-D-19-0077.1.
- 541 53. Friedrich, K.; Kalina, E.A.; Masters, F.J.; Lopez, C.R. Drop-Size Distributions in Thunderstorms
542 Measured by Optical Disdrometers during VORTEX2. *Mon. Wea. Rev.* **2013**, *141*, 1182–1203,
543 doi:10.1175/MWR-D-12-00116.1.
- 544 54. Deutscher Wetterdienst. Description of the method and the weather types.
545 <https://www.dwd.de/EN/ourservices/wetterlagenklassifikation/beschreibung.html;jsessionid=5ED0B>
546 [B104CB32D74A71ADC0C6DE03871.live21064?nn=495490&lsbId=520444](https://www.dwd.de/EN/ourservices/wetterlagenklassifikation/beschreibung.html;jsessionid=5ED0B) (accessed on 27 September
547 2019).
- 548 55. Deutscher Wetterdienst. Weather Type Classification Data.
549 https://www.dwd.de/EN/ourservices/wetterlagenklassifikation/online_wlkdaten.txt?view=nasPublic
550 [ation&nn=495490](https://www.dwd.de/EN/ourservices/wetterlagenklassifikation/online_wlkdaten.txt?view=nasPublic). (Accessed on 22 January 2020).
- 551 56. R Core Team. *R: A Language and Environment for Statistical Computing*; Vienna, Austria, 2019.
552 <https://www.R-project.org/>. (Accessed on 22 January 2020).
- 553 57. RStudio Team. *RStudio: Integrated Development Environment for R*; Boston, MA, 2018.
554 <http://www.rstudio.com/>. (Accessed on 22 January 2020).
- 555 58. Kuhn, M.; Weston, S.; Williams, A.; Keefer, C.; Engelhardt, A.; Cooper, T.; Mayer, Z.; Kenkel, B.; the R
556 Core Team; Benesty, M.; *CARET: Classification and Regression Training*, 2018. [https://CRAN.R-](https://CRAN.R-project.org/package=caret)
557 [project.org/package=caret](https://CRAN.R-project.org/package=caret).
- 558 59. Meyer, D.; Dimitriadou, E.; Hornik, K.; Weingessel, A.; Leisch, F.; *e1071: Misc Functions of the*
559 *Department of Statistics, Probability Theory Group (Formerly: E1071)*, TU Wien, 2018. [https://CRAN.R-](https://CRAN.R-project.org/package=e1071)
560 [project.org/package=e1071](https://CRAN.R-project.org/package=e1071).
- 561 60. Wickham, H.; Reshaping Data with the reshape Package. *Journal of Statistical Software* **2007**, *21*, 1–20.
- 562 61. Hijmans R. J.; *raster: Geographic Data Analysis and Modeling*, 2017. [https://CRAN.R-](https://CRAN.R-project.org/package=raster)
563 [project.org/package=raster](https://CRAN.R-project.org/package=raster).
- 564 62. Hope R. M.; *Rmisc: Rmisc: Ryan Miscellaneous*, 2013. <https://CRAN.R-project.org/package=Rmisc>.
- 565 63. Wickham, H.; *Ggplot2. Elegant graphics for data analysis*, Second edition; Springer: Switzerland, 2016,
566 ISBN 978-3-319-24277-4.

- 567 64. South, A.; *rnaturalearth: World Map Data from Natural Earth*, 2017. [https://CRAN.R-](https://CRAN.R-project.org/package=rnaturalearth)
568 [project.org/package=rnaturalearth](https://CRAN.R-project.org/package=rnaturalearth).
- 569 65. Deutscher Wetterdienst. Historical records of hourly cloud type in Germany.
570 [ftp://opendata.dwd.de/climate_environment/CDC/observations_germany/climate/hourly/cloud_type](ftp://opendata.dwd.de/climate_environment/CDC/observations_germany/climate/hourly/cloud_type/historical/)
571 [/historical/](ftp://opendata.dwd.de/climate_environment/CDC/observations_germany/climate/hourly/cloud_type/historical/) (Accessed on 22 January 2020).
- 572 66. Jaffrain, J.; Berne, A. Influence of the Subgrid Variability of the Raindrop Size Distribution on Radar
573 Rainfall Estimators. *J. Appl. Meteor. Climatol.* **2012**, *51*, 780–785, doi:10.1175/JAMC-D-11-0185.1.
- 574 67. Van der Ent, R.J.; Savenije, H.H.G.; Schaefli, B.; Steele-Dunne, S.C. Origin and fate of atmospheric
575 moisture over continents. *Water Resour. Res.* **2010**, *46*, 61, doi:10.1029/2010WR009127.
- 576 68. Rulfová, Z.; Kyselý, J. Trends of Convective and Stratiform Precipitation in the Czech Republic, 1982–
577 2010. *Advances in Meteorology* **2014**, *2014*, 1–11, doi:10.1155/2014/647938.
- 578 69. Plavcová, E.; Kyselý, J. Projected evolution of circulation types and their temperatures over Central
579 Europe in climate models. *Theor Appl Climatol* **2013**, *114*, 625–634, doi:10.1007/s00704-013-0874-4.
- 580 70. Stryhal, J.; Huth, R. Trends in winter circulation over the British Isles and central Europe in twenty-
581 first century projections by 25 CMIP5 GCMs. *Clim Dyn* **2019**, *52*, 1063–1075, doi:10.1007/s00382-018-
582 4178-3.
- 583 71. Birmili, W.; Wiedensohler, A.; Heintzenberg, J.; Lehmann, K. Atmospheric particle number size
584 distribution in central Europe: Statistical relations to air masses and meteorology. *J. Geophys. Res.* **2001**,
585 *106*, 32005–32018, doi:10.1029/2000JD000220.
- 586 72. Byčenkienė, S.; Plauškaitė, K.; Dudoitis, V.; Ulevicius, V. Urban background levels of particle number
587 concentration and sources in Vilnius, Lithuania. *Atmospheric Research* **2014**, *143*, 279–292,
588 doi:10.1016/j.atmosres.2014.02.019.
- 589 73. Lohmann, U.; Feichter, J. Global indirect aerosol effects: a review. *Atmos. Chem. Phys.* **2005**, *5*, 715–737,
590 doi:10.5194/acp-5-715-2005.
- 591 74. Cecchini, M.A.; Machado, L.A.T.; Artaxo, P. Droplet Size Distributions as a function of rainy system
592 type and Cloud Condensation Nuclei concentrations. *Atmospheric Research* **2014**, *143*, 301–312,
593 doi:10.1016/j.atmosres.2014.02.022.
- 594



© 2020 by the authors. Submitted for possible open access publication under the terms and conditions of the Creative Commons Attribution (CC BY) license (<http://creativecommons.org/licenses/by/4.0/>).